From Self Assembled Monolayers to Clickable Gold Nanoparticles

Inauguraldissertation

Zur

Erlangung der Würde eines Doktors der Philosophie

vorgelegt der

Philosophisch-Naturwissenschaftlichen Fakultät

der Universität Basel

von

Fabian Wilhelm Sander

aus

Illertissen, Deutschland

Basel, 2014

Genehmigt von der Philosphisch-Naturwissenschaftlichen Fakultät der Universität Basel auf Antrag von

Prof. Dr. Marcel Mayor

Prof. Dr. Edwin Constable

Basel, den 26. Februar 2013

Prof. Dr. Jörg Schibler

für Julia und meine Eltern

Alles ist möglich, vorausgesetzt, daß es genügend unvernünftig ist.

Niels Bohr

Acknowledgements

I would like to thank my supervisor Professor Dr. Marcel Mayor. Marcel, I thank you for giving me the opportunity to work on this fascinating topic, and the freedom in my research. I enjoyed our conversations, and I feel honored for having worked with you.

I thank Professor Dr. Edwin Constable for co-refereeing this thesis.

I am grateful to Professor Dr. Michael Zharnikov for co-refereeing this thesis and for the fruitful collaboration and nice discussions.

Moreover, Professor Dr. Dennis Gillingham is acknowledged for chairing my exam.

I would like to thank Dr. Florian von Wrochem for his support at Sony, Stuttgart Technology Center introducing me into XPS and STM techniques and the fruitful collaboration.

Thanks goes to Dr. Hicham Hamoudi for performing and helping to interpret the HRXPS and NEXAFS measurements.

My thanks go to Dr. Jürgen Rotzler for giving me a good start in Basel and having nice discussions.

I would like to thank the golden boys and girls Dr. Torsten Peterle, Dr. Jens Hermes, Dr. Carla Cioffi and Ulrike Fluch for the nice team spirit.

Especially, I thank Jens Hermes for the interesting discussions, fun at conferences and non-chemical topics.

I thank Ulrike Fluch for the nice time as lab neighbor, food supply and fun we had.

I acknowledge Lukas Felix for the hotel service.

Also I want to thank Dr. Federica Reinders and Dr. Jens Tüxen for support and the nice time we enjoyed in the group.

I thank all past and present members of the Mayor group for the nice atmosphere not only for working but also for the coffee breaks. I dedicate a special thanks to all lab mates in Lab

OC 8. The atmosphere was great within the whole department and I thank all past and present coworkers for the nice time during work and beyond that.

I am very grateful for all the support within the department: Dr. Heinz Nadig for performing FAB and EI mass measurements. Werner Kirsch and Sylvie Mittelheiser are acknowledged for performing the elemental analysis. The Werkstatt Team, Roy Lips and Markus Hauri for technical support. The endless support of our secretary staff Brigitte Howald, Marina Mambelli-Johnson and Beatrice Erismann is also gratefully acknowledged.

I thank all past and present colleagues in the department who made the time at the University of Basel that enjoyable.

Furthermore I would like to thank my good friends Andreas, Ralf, Jörg and Mario and my former colleagues form the University of Stuttgart for all fun we had so far.

I thank my parents who made it possible to achieve my goals with their support and love throughout my life.

Especially I thank the most important person in my life, Julia, for her constant support, her patience and her love.

The aim of the present PhD thesis was the investigation of the behavior of gold nanoparticle stabilizing oligo thioether ligands on gold surfaces and further on to develop a protocol for the directed assembly of mono functionalized gold nanoparticle into defined oligomer structures.

Outline

The present cumulative PhD thesis consists of the following parts:

In the **Introduction** the research field of gold nanoparticles is presented with to point out their unique electronic and physical properties. The second focus will be on the controlled interlinking and functionalization of gold nanoparticles using click chemistry and their potential applications, which will be submitted as a review article.

Within **Concept and Strategy** the goals of the research project are introduced and the concepts and outputs of the resulting publications are presented.

The Publications are accumulated with their respective Supporting Information, in the order in which they were prepared:

"*Loops versus Stems: Benzylic Sulfide Oligomers Forming Carpet Type Monolayers"* F. Sander, T. Peterle, N. Ballav, F. Wrochem, M. Zharnikov, M. Mayor *J. Phys. Chem. C*, **2010**, 114, 4118 – 4125.

"*Add a Third Hook: S-Acetyl Protected Oligophenylene Pyridine Dithiols as Advanced Precursors for Self-Assembled Monolayers*" F. Sander, J. P. Hermes, M. Mayor, H. Hamoudi, M. Zharnikov PCCP, **2013**, 15, 2836 – 2846.

"*Dumbbells, Trikes and Quads - Click Gold Nanopartricles together*" F. Sander, U. Fluch, J. P. Hermes and M. Mayor **Small** 2014, *10*, 349 – 359.

"*Click Chemistry with Gold Nanoparticles – A Tool for Functionalization, Interlinking and Labeling*" Fabian Sander and Marcel Mayor, manuscript prepared for submission.

Finally, within **Conclusion and Outlook** the main results are briefly summarized and further potential research is proposed.

Table of Content

1. Introduction

1.1 Molecular Electronics

Electronic devices are an integral component in our daily life and our modern world is hard to imaging working without them. With progress in performance while decreasing the size, electronic devices found their way into our normal course of life. In today's information era we cannot live without computers for communication, economy, medicine, transport and so on. This continuous progress in performance and miniaturization of integrated electronic circuits was predicted by Moore's law in 1965.[1]

Today the miniaturization of current electronic technologies is approaching its limits because of traditional inorganic materials are used and component architectures reaching their theoretical limits of performance. The most employed techniques for mass production to satisfy the worldwide market are silicon based electronic devices. The purification of the waver material is a very energy consuming process as well as the high-energy radiation for pattering and vapor deposition for nanolayers. This makes the fabrication of large chip arrays a very expensive procedure. Another disadvantage of those devices is that most energy to power them is converted to heat rather than to perform their function.

To overcome these problems of a top down approach and the used materials is a great motivation for the development of molecular electronics. While creating new materials with tailor made functions from a bottom up approach the reduction of size, production cost by simple processing steps and the impact to the environment by saving energy while production and operation are main goals. With molecule-based electronics both, new production processes like ink-jet printing and new properties like flexible electronic circuits will benefit.

The concept of using molecules as functional units for electronic circuits provides appealing advantages. With molecules as smallest feature unit, the fundamental understanding of correlation between chemical structure and function and their assembly into devices a new generation of electronic devices can be created. In future custom made electronic circuits gold nanoparticle (Au NPs) will possibly play an important role for example as storage device.

1.2 Gold Nano Particles

Gold Nanoparticles (Au NPs) are a heavily investigated over the last decades because of their usefulness in medicine, catalysis and electronics.[2–4] The first known utilization of Au NPs was far back in the late Greco-Roman times.[5] Freshly precipitated colloidal gold solutions were already known agents to colorize glass. A famous example is the Lycurgus cup that appears green when the light is reflected by the cup and red when you observe the transmitting light. The minute metallic particles of the used gold-silver alloy to colorize the glass have the right size to scatter the blue end of the spectrum more efficiently than the red end, resulting in a red transmission. Faraday was the first in 1857 who discovered the dependence on particle size in color and started to systematical investigate Au NPs.[6] In the mid of the 20th century the development of Au NPs attracted more and more notice. Turkevich et al. demonstrated the synthesis and analysis of citrate stabilized Au NPs and along with this breakthrough more work was performed to synthesize well defined Au NPs.[7] With the discovery of the Schmid-cluster ($Au_{55}(PPh_3)Cl_6$[8] the first steps towards quantum electronics[9] with NPs and applications like labeling[10] were done. In the 80's the developed protocol of Burst et al. for rapid and simple synthesis of thiolate stabilized Au NPs was a milestone.[11,12] In a two phase system of tetrachloroauric acid solved in water, which was transferred into the organic phase (toluene) using tetraoctylammonium bromide (TOAB) as phase transfer agent, the gold salt was reduced by sodium borohydride ($NaBH_4$) in presence of alkanethiols yielding stable Au NPs wither a narrow size distribution around 3 nm.

Since the end of the last century Au NPs moved in the focus of researchers because of their outstanding stability of Au NPs among metal nanoparticles. Their shape and size depended properties made them suitable for various applications.[13] They are used in medicine[14], bio- and macromolecule labeling[15–18] or in chemistry for catalytic applications[19,20]. Also for current and future sensor applications Au NPs are of great interest.[21–24] Au NPs are also of interest for their use in nanoelectronics[25] as potential future storage device.[26]

1.3 Physical and Optical Properties of Au NPs for Molecular Electronics

The most interesting properties of Au NPs are from the molecular electronics point of view the size dependent optical and physical properties (quantum size effect). The ability to interact in the regime of quantum physics gives access to a lot of interesting phenomena. The electronic behavior of Au NPs depends on their size because the distribution of energy states still shows discrete energy levels.[27–31] The Au NPs can provide a size where it is still possible to distinguish different energy levels like in a molecule's orbital. If they are growing in size at certain point no defined transitions can be observed and a continuous spectrum occurs. However, the smaller a nanoparticle is the more defined energy levels are present (Figure 1).

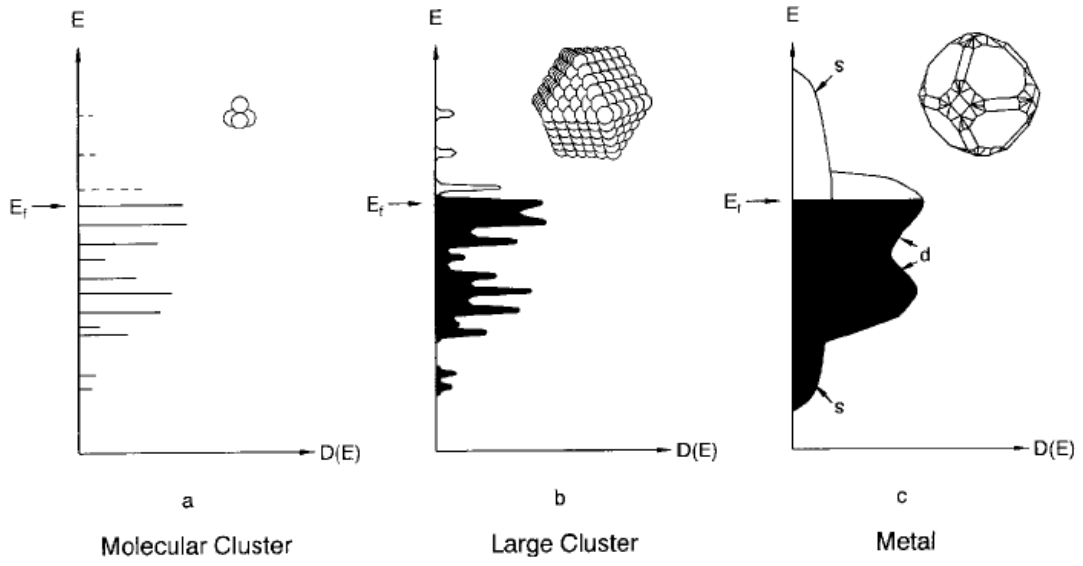

Figure 1. Formation of a metallic band structure. On the way from a molecule a) via nanosized clusters b) the quasi delocalization of valence electrons increases until the bulk state c) is reached. E_F=Fermi energy, D = Density of states. Reprinted from Schmid.[31]

The research of this thesis is focused on assemblies of gold atoms to Au NPs with a certain disparity in size. In literature also the terms 'nanocrystal' and 'colloid' are common but not used in the following text.

Another interesting size depending property of Au NPs is their ability to change color with size due their plasmon resonance.[32] The conducting electrons on the NP's surface are oscillating by the interaction with the electromagnetic field of incoming light. Like a dipol polarized charges around the NP can occur. The resulting force to restore has a unique resonance frequency that match the oscillation of electrons in the nano particles (Figure 2). Depending of the NP's size the force alters and different colors can be observed in the visible spectra.

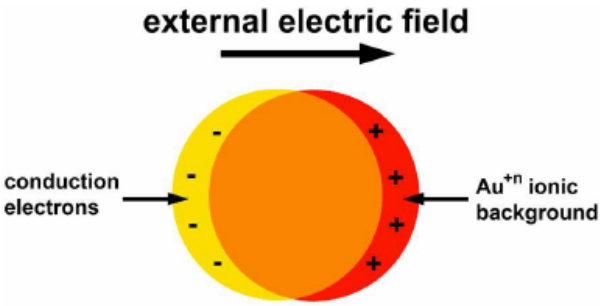

Figure 2. Schematic representation of the charge separation of a gold nanoparticle induced by an external electric field.

The size dependent color of Au NP's make them to an interesting system of sensor application where a direct optical output can be observed when the size of the NPs' changes. The most prominent example in our days is probably the use of Au NPs in pregnancy tests.[14] Au NPs coated with antibody tracing pregnancy are brought in contact to the urine of the test person. If the specific antigen is present the Au NPs start to clump together because of the antibody antigen interactions and trapped in a filter where the occurring plasmonic resonance can be detected by the naked eyes. If the specific antigen is missing no conglomeration occurs and colored aggregates cannot be observed.

To assemble Au NPs in more complicated devices it is crucial that NPs fulfill following requirements: 1) the Au NPs need to be stable with a narrow size distribution with the desired dimension. 2) The surface must have functionality. 3) The Au NPs can be interlinked to other objects in a controlled fashion.

1.4 Click Chemistry as Tool for Au NP Assembly

Over the last decades the development of metal nano particles is a fast growing research field and a considerable interest has arisen in their chemistry and physics.[33] A large variety of functional Au NPs are now known,[33–45] but many families of Au NPs are still resistant to direct synthesis,[34] ligand exchange reactions[37] or functionalization using high-temperature or other incompatible processes. Thus, in view of multiple possible applications, it is essential to reconsider the problem of the efficiency of Au NP functionalization and their assembly. Click chemistry is meanwhile an often-used concept and opened new routes in organic synthesis under mild conditions.

Sharpless and coworkers introduces in 2001 the concept of click chemistry[46] and set their focus not on production of new compounds but on production of new properties. The concept is to provide the whole range of chemical transformations in a set of processes with a high thermodynamic driving force usually higher than 20 kcal mol^{-1}. These "spring-loaded" starting materials allow an easy and efficient transformation into new substances with useful properties. This concept is very appealing to interlink Au NPs to each other or with other molecules in order to create new functional structures.

The exponential increasing number of hits, from 5 in 2004 to 153 in 2012, for term "click nano particle" demonstrates the arising importance of this research field. The concept of click chemistry allows the creation of complex organic shells around NPs and further opens the route to new assembly and labeling strategies exploiting the size dependent physical and electronic properties of these nano objects.

1.5 Composite Materials created by click chemistry

Williams *et al.* introduced in 2006 the concept of functionalization of Au NPs by click chemistry.[47] To avoid the synthesis of individual thiolate ligands for stabilizing Au NPs with special function, click chemistry was used to tailor the stabilizing organic shell. Therefore redox active, fluorescent, and solubilizing species are used to show click chemistry as a facile route toward functionalization of monolayer-protected Au nanoparticles (Figure 3).

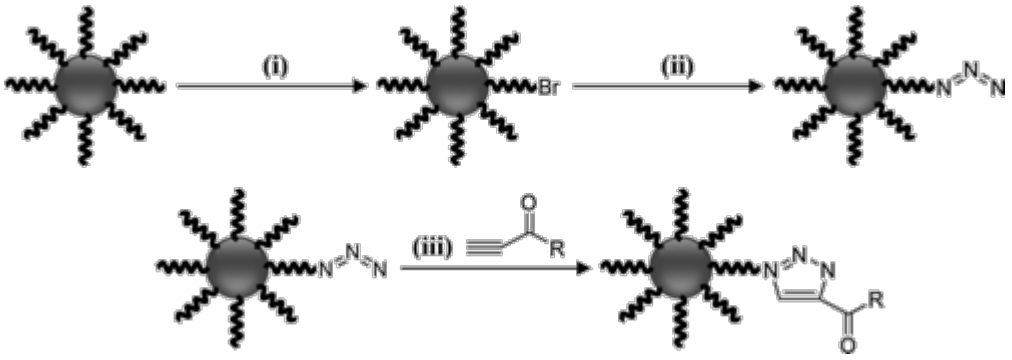

Figure 3. Schematic drawing of Au NPs shell functionalization. (i) ligand exchange: $Br(CH_2)_{11}SH$ in DCM, 60 h at room temperature; (ii) 0.25 M NaN_3 in DCM/DMSO solution, 48 h; (iii) R = propyn-1-one derivatized, 24−96 h in dioxane or 1:1 hexane/dioxane. Reprinted from Williams et al.[47]

After synthesizing thiolate stabilized Au NPs according to the method of Brust et al.[11] and ligand exchange azide groups were established at the Au NPs periphery. Finally the Au NPs

successfully decorated with alkynyl substituted derivatives of ferrocene, nitrobenzene, pyrene, anthracene, poly(ethylene glycol), and aniline. The mild conditions at room temperature allow this protocol to be applied to several other compounds. Also work to optimize this reaction type is done.[48]

Burst and coworkers were one of the first who tried to interlink azide functionalized Au NPs by click chemistry with enzymes.[49] Citrate stabilized Au NPs were treated with thiol terminated ligand bearing an azide group to yield thiol capped, azide functionalized Au NPs. The size of 14 nm remained the same after the ligand exchange. Acetylene labeled lipase (*Thermomyces lanuginosus*) was clicked to the Au NP by incubating an excess of lipase and Cu(I) catalyst with the nanoparticle suspension at room temperature for 3 days. The fact that no by produces occurred while this long incubation time makes this reaction very appealing. This approach to combine biomaterials with metal nano particles is general very independent of the chemical nature of the starting materials. Therefore this reaction set the basis for similar composite materials.

With the increasing focus on bottom up approaches to assemble nano electronic devices DNA is a promising structure due to its well-defined chemical structure and the multitude of electrostatic and chemical binding sites utilizable for modification with molecules, metal ions or metal nanoparticles.

However, the fabrication of DNA-based circuit elements requires the spatially defined immobilization of chemical building blocks to the DNA strand that, because of their electronic structure, are capable of electrical switching or charge storage. The use of metal nanoparticles with diameters below 2 nm, which allow the exploitation of single electron tunneling effects, appears very promising in this context. Therefore Simon et al. demonstrated the DNA template chain like assembly of glutathione functionalized Au NPs to artificial alkyne modified DNA duplexes by Cu(I) catalyzed Huisgen cycloaddition.[50] This approach to covalently immobilize Au NPs on a highly customizable template holds great potential for a controlled assembly of Au NPs in a defined spatial arrangement.

The previous concepts to add functions by click chemistry to azide functionalized Au NPs can be used to build up responsive nanocomposite materials. Peng and coworkers modified Au NPs by click chemistry to yield pH and temperature responsive nanocomposites.[51] Via a ligand exchange procedure mono-azide poly(ethylene glycol) (SS-PEG-N_3) functionalized Au NPs were synthesized. By subsequent coupling with alkyl-terminated poly(4-vinylpyridine) under click conditions pH responsive Au NPs were yielded (Figure 5).

With a pH blow 4 the pyridyl groups are protonated and the repulsing electrostatic forces prevent the particles from agglomeration resulting in a transparent solution. If the pH is higher than 5 the pyridyl groups are deprotonated and the particles start to agglomerate resulting in a intransparent solution. The whole process was shown to be reversible.

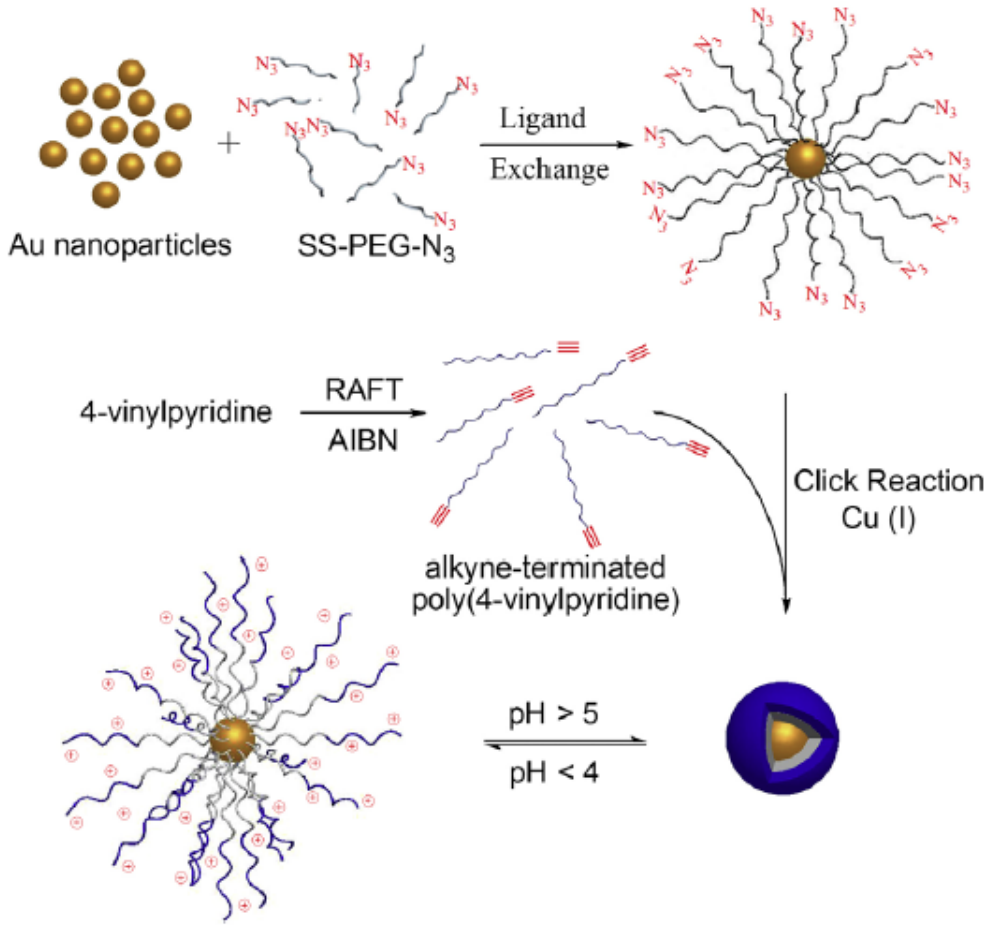

Figure 4. Synthesis of pH responsive Au NP nanocomposits. Reprinted from Peng et al.[51]

With altered polymers clicked to the Au NPs ligand shell also thermoresponsive behavior could be achieved.[52] With alkyne-terminated poly(N-isopropylacrylamide) clicked to the (SS-PEG-N_3) stabilized Au NPs also the transparency of the Au NP solution changed. This time the change was induced by temperature resulting in an intransparent solution at temperatures higher than 40 ºC and transparent solutions at lower temperatures. The whole process was again reversible (Figure 6).

Also for medicine applications click chemistry protocols to modify Au NPs are used.[53] Recently a new prostate cancer treatment is under development where bio compatible

polyethylene glycol stabilized Au NPs are used as carrier for antigens causing cancer cells death and tumor label.

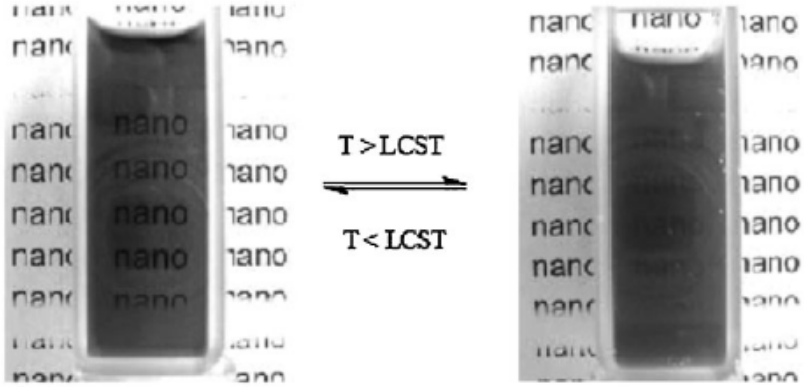

Figure 5. Picture of transparency change at the lower critical solution temperature (LCST). Reprinted from Peng et al.[52]

Also the assembly of different metal NPs utilizing click chemistry was demonstrated. For example the assembly of small alkynyl Au NPs with the size of about 20 nm as satellites around 70 nm azide functionalized Au NPs.[54] However, gold nano rods and silver nano particles could be interlinked by click chemistry as well.[55]

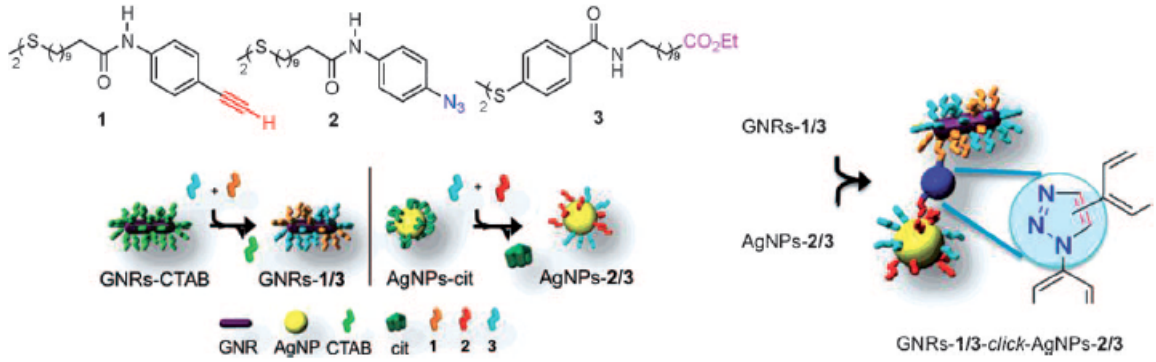

Figure 6. Left: schematic presentation of ligand exchange for Au NP and Ag NP functionalization. Right: assembly of Au NP and Ag NP after click reaction. Reprinted from Franchini et al.[55]

Therefore the gold nanorods were functionalized with terminal alkines and the Ag NPs with terminal azides (Figure 4). After applying click conditions to a solution of both reactants the desired assembly could be observed.[55] Such nanoassemblies can find important applications in numerous biomedical applications including biosensing and bioimaging.[56,57] Facile fabrication of such complex assemblies can be easily extended to different shape-controlled plasmonic nanostructures and other functional inorganic nanostructures such as magnetic nanoparticles, semi-conducting quantum dots and up-conversion nanocrystals.

1.6 Au NP Enhanced Metal Ion Sensing by Click Chemistry

Au NPs are very interesting for any kind of sensor application because of their size dependent color. In any system were the size of Au NPs can be change by agglomeration or interlinking with other structures an optical read out is possible. In 2008 mixed alkine / azide functionalized Au NPs were used for colorimetric copper(II) detection.[21] The concept is as simple as effective. The fact that the extinction coefficient of 13 nm diameter nano particles is by several magnitudes of order higher than those of traditional chromophores[58] allows the naked eye to observer color in nanomolar concentrations. Since copper is used as catalyst in azide alkine click chemistry based on the Huisgen's reaction low concentrations of copper allows completing this reaction. Therefore terminal azide and alkyne functionalized thiols were used to functionalize Au NPs. In a ligand exchange citrate stabilized Au NPs were mixed with the respective thiols (Figure 7). The yielded functionalized Au NPs showed a reddish purple color.

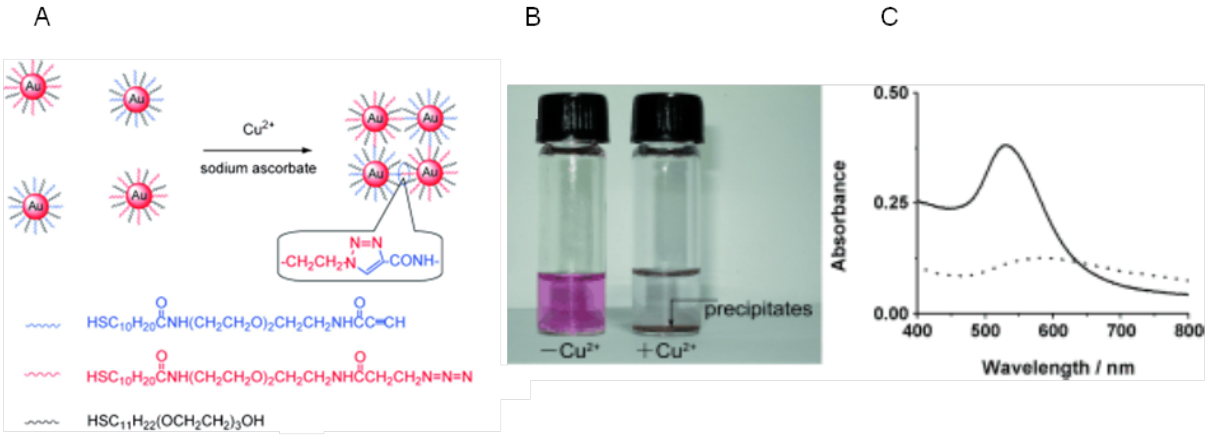

Figure 7. A) The detection of Cu^{2+} ions using click chemistry between two types of gold NPs, each modified with thiols terminated in an alkyne or an azide functional group; B) Color change after cross-linked visible by the naked eye; C) UV/Vis spectra before (black line) and after (dotted line). Reprinted from Jiang et al.[21]

In presence of Cu(II) and a reducing agent, here sodium ascorbate is used, the nano particles start to agglomerate and the color is fading. This process can be monitored by the naked eye without any instruments.

Based on this work several new systems for an optical copper detection based on Au NPs as signal reporter were developed. In a very similar system the generation of Cu(I) out of Cu(II)acetate by bulk electrolysis to promote the click reaction turned out to be very efficient.[59]

As most examples used mixed azide alkyne functionalize particles Gooding *et al*.[60] used 3-azidopropylamie functionalized Au NPs that undergoes the click reaction with 1,4-diethynylbenzene. An advantage of this protocol is the minimal synthetic work to prepare the interface for Cu(II) detection

DNA functionalized Au NPs showed a faster click reaction and provides the additional advantage of an quantitative Cu(II) detection due to the dependence of the DNAs melting points to the degree of cross linking.[61] The more copper found in the sample the more cross linked DNA strands were received resulting in a higher melting point direct correlating the Cu(II) concentration. This method hits the Environmental Protecting Agency-defined limits for the maximum Cu(II) contamination limit of 20 μM in drinking water making it relevant for testing drinking water.

Also unmodified Au NPs were recently used to establish a colorimetric copper detection.[62] By a Cu(I) induced azide-alkyne click ligation caused structural change of single-stranded DNA to double-stranded DNA. This structural change of probe can be monitored by the unmodified AuNPs via mediating their aggregation with a red-to-blue colorimetric read-out because of the differential ability of ssDNA and dsDNA to protect AuNPs against salt-induced aggregation. Under the optimum conditions, this biosensor can sensitively and specifically detect Cu^{2+} with a low detection limit of 250 nM and a linear range of 0.5–10 μM.[62] In contrast to the previous sensing systems this bio sensors do not rely on inter particle cross linking but on the novel design using noncrosslinking aggregation mediated by electrostatic stabilization.

Beside copper, lead is also a very toxic transition metal that cause a lot of environmental pollution because of it's use in batteries, gasoline and paints. Propargylamin functionalized Au NPs where further reacted by click chemistry with azide terminated triethylene glycol in order to detect Pb^{2+} ions.[63] The achieved ligand shell can than act as chelating substrate able to trap Pb^{2+}. The selective response to Pb^{2+} is attributed to the size-fitting effect of the pseudo-crown ethers. The Au NPs are interlinked by the Pb^{2+} due to the coordination process and change color because auf the aggregations (Figure 8).

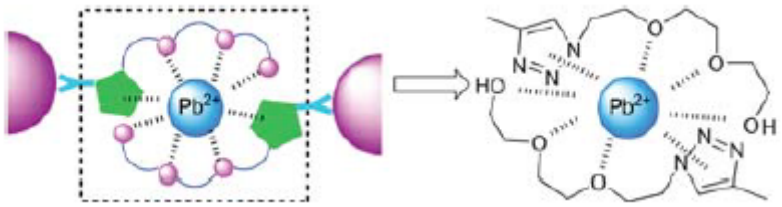

Figure 8. Schematic drawing of the chelating interaction of the functionalized Au NPs to detect lead ions. Reprinted from Han et al.[63]

Not only the detection of metal ions is realized by click reactions with Au NPs also a system for the detection of ascorbic acid is established using azide and alkyne functionalized particles in present of Cu(II).[64] In presence of ascorbic acid Cu(I) is generated hat catalyzes the click reaction resulting in interlinked particles that change color. This method has been proven to be robust against the presence of other reducing organic compounds such as glucose, cysteine, dopamine, uric acide and thiamine.

Proteins can be detected as well using the Cu(I) catalyzed click reaction.[65] Basically the classical Biuret test is combined with the enhanced optical readout by Au NPs. The Biuret reagent is an aqueous mix of potassium hydroxide and a Cu(II) salt. The formed solution proteins are capable to reduce Cu(II) to Cu(I). The change in color by the crosslinked Au NPs enhance the sensitivity of the protein detection dramatically.

In an extended system also the improved detection of toxic organophosphate pesticides (OPs) could be realized.[66] Detection of OPs based on the direct stimulation of Au NPs aggregation or growth by the acetylcholineesterase – acetylthiocholine system (AChE–ATCl) has been reported. However, high amounts of OPs are usually required to initiate detectable color change of Au NPs because of the direct dependence of nanoparticle aggregation on the AChE–ATCl system, limiting the colorimetric sensitivity. Therefore a click reaction as an intermediate colorimetric signal amplification process has been used.

All this concepts are using the superior extinction coefficient of Au NPs to enhance the optical detection of targets like metal ions, ascorbic acid, proteins or organophosphate pesticides.

1.7 Outlook

The various concepts to interlink Au NPs by click chemistry and the potential applications in medicine, labeling and sensing demonstrate the importance of this research field. The replacement of coloring agents for sensing applications by Au NPs will set new standards for detections limits by the naked eye or in lab on a chip devices. The ongoing development of Au NPs click reactions as signal amplifier for conventional sensing systems show the high potential of these applications. Also the possibility to add molecules to Au NPs by simple click reactions to tailor their functionality holds a big future potential for applications. Thermo- and pH responsive probes could be achieved via click chemistry functionalized Au NPs. Also the assembly by DNA templating as bottom up approach for future nano electronic applications is possible.

One drawback is still the control over the number of functional groups around a particle. For a controlled assembly without aggregation into huge networks it is necessary to synthesize Au NPs with only one available moiety for click reaction. Recently the synthesis of a dendritic ligand and subsequent stabilization of Au NPs fulfilling this requirement is reported in literature.[67] These Au NPs will give access many new approaches for labeling, surface functionalization, sensors and future molecular electronic devices.

1.8 References

1. G. Moore, *Electronics*, 1965, **38**, 114–116.
2. R. Sardar, A. M. Funston, P. Mulvaney, and R. W. Murray, *Langmuir*, 2009, **25**, 13840–13851.
3. M. Homberger and U. Simon, *Phil. Trans. R. Soc. A*, 2010, **368**, 1405–1453.
4. M.-C. Daniel and D. Astruc, *Chem. Rev.*, 2004, **104**, 293–346.
5. H. Goesmann and C. Feldmann, *Angew. Chem. Int. Ed.*, 2010, **49**, 1362–1395.
6. M. Faraday, *Phil. Trans. R. Soc. Lond.*, 1857, **147**, 145–181.
7. J. Turkevich, P. C. Stevenson, and J. Hillier, *Discuss. Faraday Soc.*, 1951, **11**, 55.
8. G. Schmid, R. Pfeil, R. Boese, F. Bandermann, S. Meyer, G. H. M. Calis, and J. W. A. van der Velden, *Chem. Ber.*, 1981, **114**, 3634–3642.
9. G. Schmid, *Chem. Rev.*, 1992, **92**, 1709–1727.
10. J. F. Hainfeld and F. R. Furuya, *J. Histochem. Cytochem.*, 1992, **40**, 177–184.
11. M. Brust, M. Walker, D. Bethell, D. J. Schiffrin, and R. Whyman, *J. Chem. Soc., Chem. Commun.*, 1994, 801–802.
12. M. Brust, D. J. Schiffrin, D. Bethell, and C. J. Kiely, *Adv. Mater.*, 1995, **7**, 795–797.
13. H. Häkkinen, *Chem. Soc. Rev.*, 2008, **37**, 1847–1859.
14. L. B. Bangs, *Pure Appl. Chem.*, 1996, **68**, 1873–1879.
15. I. Willner and B. Willner, *Nano Lett.*, 2010, **10**, 3805–3815.
16. R. D. Powell and J. F. Hainfeld, *Micron*, 2011, **42**, 163–174.
17. J. I. Cutler, E. Auyeung, and C. A. Mirkin, *J. Am. Chem. Soc.*, 2012, **134**, 1376–1391.
18. L. Dykman and N. Khlebtsov, *Chem. Soc. Rev.*, 2012, **41**, 2256.
19. C. Della Pina, E. Falletta, L. Prati, and M. Rossi, *Chem. Soc. Rev.*, 2008, **37**, 2077–2095.
20. A. Corma and H. Garcia, *Chem. Soc. Rev.*, 2008, **37**, 2096–2126.
21. Y. Zhou, S. Wang, K. Zhang, and X. Jiang, *Angew. Chem. Int. Ed.*, 2008, **47**, 7454–7456.
22. R. Wilson, *Chem. Soc. Rev.*, 2008, **37**, 2028–2045.
23. Z. Wang and Y. Lu, *J. Mater. Chem.*, 2009, **19**, 1788.
24. X. Zhang, Q. Guo, and D. Cui, *Sensors*, 2009, **9**, 1033–1053.
25. G. Schmid, *Chem. Soc. Rev.*, 2008, **37**, 1909–1930.
26. S.-J. Kim and J.-S. Lee, *Nano Lett.*, 2010, **10**, 2884–2890.

27. R. P. Andres, T. Bein, M. Dorogi, S. Feng, J. I. Henderson, C. P. Kubiak, W. Mahoney, R. G. Osifchin, and R. Reifenberger, *Science*, 1996, **272**, 1323–1325.
28. S. Chen, *Science*, 1998, **280**, 2098–2101.
29. T. Laaksonen, V. Ruiz, P. Liljeroth, and B. M. Quinn, *Chem. Soc. Rev.*, 2008, **37**, 1836–1846.
30. F. Remacle and R. D. Levine, *ChemPhysChem*, 2001, **2**, 20–36.
31. G. Schmid, *Adv. Eng. Mater.*, 2001, **3**, 737–743.
32. L. M. Liz-Marzán, *Langmuir*, 2006, **22**, 32–41.
33. M.-C. Daniel and D. Astruc, *Chem. Rev.*, 2004, **104**, 293–346.
34. M. Brust, M. Walker, D. Bethell, D. J. Schiffrin, and R. Whyman, *J. Chem. Soc., Chem. Commun.*, 1994, 801–802.
35. P. Mulvaney, *Langmuir*, 1996, **12**, 788–800.
36. R. Elghanian, J. J. Storhoff, R. C. Mucic, R. L. Letsinger, and C. A. Mirkin, *Science*, 1997, **277**, 1078–1081.
37. A. C. Templeton, W. P. Wuelfing, and R. W. Murray, *Acc. Chem. Res.*, 2000, **33**, 27–36.
38. R. M. Crooks, M. Zhao, L. Sun, V. Chechik, and L. K. Yeung, *Acc. Chem. Res.*, 2001, **34**, 181–190.
39. R. W. J. Scott, O. M. Wilson, and R. M. Crooks, *J. Phys. Chem. B*, 2005, **109**, 692–704.
40. J. Kim, S. Park, J. E. Lee, S. M. Jin, J. H. Lee, I. S. Lee, I. Yang, J.-S. Kim, S. K. Kim, M.-H. Cho, and T. Hyeon, *Angew. Chm. Int. Ed.*, 2006, **45**, 7754–7758.
41. C. L. Johnson, E. Snoeck, M. Ezcurdia, B. Rodríguez-González, I. Pastoriza-Santos, L. M. Liz-Marzán, and M. J. Hÿtch, *Nature Mater.*, 2007, **7**, 120–124.
42. G. Han, P. Ghosh, and V. M. Rotello, *Nanomedicine*, 2007, **2**, 113–123.
43. S. J. Son, X. Bai, and S. B. Lee, *Drug Discov. Today*, 2007, **12**, 657–663.
44. S. E. Skrabalak, L. Au, X. Lu, X. Li, and Y. Xia, *Nanomedicine*, 2007, **2**, 657–668.
45. S.-Y. Shim, D.-K. Lim, and J.-M. Nam, *Nanomedicine*, 2008, **3**, 215–232.
46. H. C. Kolb, M. G. Finn, and K. B. Sharpless, *Angew. Chem. Int. Ed.*, 2001, **40**, 2004–2021.
47. D. A. Fleming, C. J. Thode, and M. E. Williams, *Chem. Mater.*, 2006, **18**, 2327–2334.
48. E. Boisselier, L. Salmon, J. Ruiz, and D. Astruc, *Chem. Commun.*, 2008, 5788–5790.

49. J. L. Brennan, N. S. Hatzakis, T. R. Tshikhudo, V. Razumas, S. Patkar, J. Vind, A. Svendsen, R. J. M. Nolte, A. E. Rowan, and M. Brust, *Bioconjugate Chem.*, 2006, **17**, 1373–1375.
50. M. Fischler, A. Sologubenko, J. Mayer, G. Clever, G. Burley, J. Gierlich, T. Carell, and U. Simon, *Chem. Commun.*, 2007, 169–171.
51. T. Zhang, Y. Wu, X. Pan, Z. Zheng, X. Ding, and Y. Peng, *Eur. Polym. J.*, 2009, **45**, 1625–1633.
52. T. Zhang, Z. Zheng, X. Ding, and Y. Peng, *Macromol. Rapid Commun.*, 2008, **29**, 1716–1720.
53. E. C. Dreaden, B. E. Gryder, L. A. Austin, B. A. Tene Defo, S. C. Hayden, M. Pi, L. D. Quarles, A. K. Oyelere, and M. A. El-Sayed, *Bioconjugate Chem.*, 2012, **23**, 1507–1512.
54. N. Gandra and S. Singamaneni, *Chem. Commun.*, 2012, **48**, 11540–11542.
55. E. Locatelli, G. Ori, M. Fournelle, R. Lemor, M. Montorsi, and M. Comes Franchini, *Chemistry*, 2011, **17**, 9052–9056.
56. T. Vo-Dinh, H.-N. Wang, and J. Scaffidi, *J. Biophotonics*, 2010, **3**, 89–102.
57. D. M. Beal and L. H. Jones, *Angew. Chem. Int. Ed.*, 2012, **51**, 6320–6326.
58. R. Jin, G. Wu, Z. Li, C. A. Mirkin, and G. C. Schatz, *J. Am. Chem. Soc.*, 2003, **125**, 1643–1654.
59. Z. Lin, S. Gao, J. Lin, W. Lin, S. Qiu, L. Guo, B. Qiu, and G. Chen, *Anal. Methods*, 2012, **4**, 612–615.
60. C. Hua, W. H. Zhang, S. R. M. D. Almeida, S. Ciampi, D. Gloria, G. Liu, J. B. Harper, and J. J. Gooding, *Analyst*, 2011, **137**, 82–86.
61. X. Xu, W. L. Daniel, W. Wei, and C. A. Mirkin, *Small*, 2010, **6**, 623–626.
62. Q. Shen, W. Li, S. Tang, Y. Hu, Z. Nie, Y. Huang, and S. Yao, *Biosens. Bioelectron.*, 2013, **41**, 663–668.
63. H. Li, Q. Zheng, and C. Han, *Analyst*, 2010, **135**, 1360–1364.
64. Y. Zhang, B. Li, and C. Xu, *Analyst*, 2010, **135**, 1579–1584.
65. K. Zhu, Y. Zhang, S. He, W. Chen, J. Shen, Z. Wang, and X. Jiang, *Anal. Chem.*, 2012, **84**, 4267–4270.
66. G. Fu, W. Chen, X. Yue, and X. Jiang, *Talanta*, 2013, **103**, 110–115.
67. J. P. Hermes, F. Sander, U. Fluch, T. Peterle, D. Thompson, R. Urbani, T. Pfohl, and M. Mayor, *J. Am. Chem. Soc.*, 2012.

2 Concept and Strategy

2.1 Previous Work

Since 2008 our research group introduced a new concept to synthesize Au NPs stabilized by oligo thioether ligands. Macromolecular octadentate thioether ligands turned out to be suitable to stabilize Au NPs of a narrow size distribution around 1.3 nm.[1] The new developed ligands show two key features: To stabilize the Au NPs benzylic thioether moieties were used, which are flexible enough to enwrap the gold nano particles, *tert*-butyl decorated bridging phenyl rings used to shield the Au NPs from agglomeration and further growing by establishing a sterical demanding organic shell around the particle (Figure 9). With a number of eight thioether moieties the ligand – gold interaction is strong enough to form long term stable Au NPs that are enwrapped by two ligands.

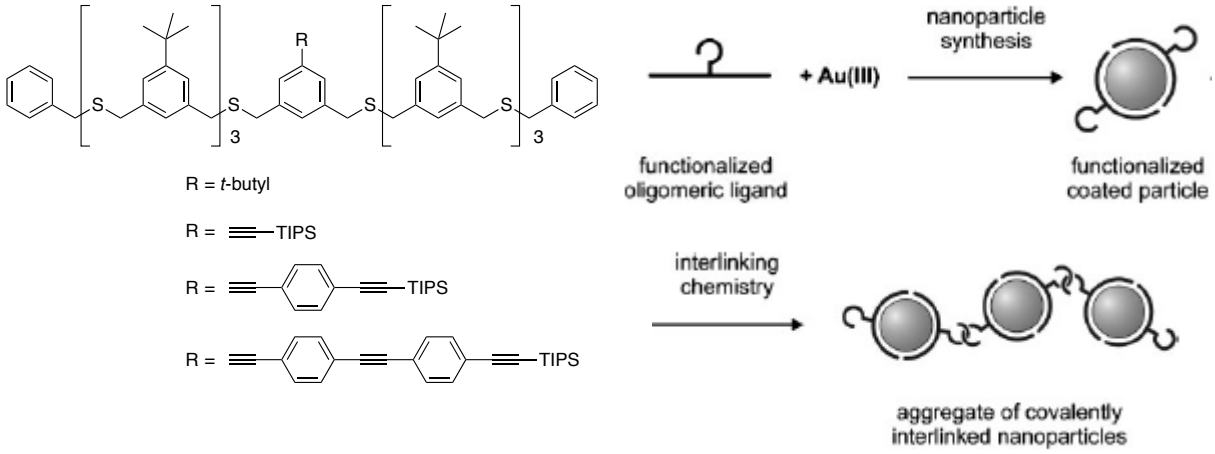

Figure 9. Left**:** Linear ligand for stabilizing Au NPs including a functional OPE rod. Right: Schematic drawing of the oxidative particle coupling exploiting the TIPS masked acetylene. Reprinted from Mayor et al.

To add function to the synthesized Au NPs the linear ligand was modified. At the center unit the *tert*-butyl moiety was exchanged by an oligophenylene ethylene (OPE) rod with a tri-*iso*-propylsilyl group (TIPS) protecting the terminal acetylene. Using these second generation linear ligands, Au NPs with functional moieties were available. After deprotection of the acetylene, followed by a wet chemical oxidative coupling protocol it was possible to build up covalent interlinked oligomer Au NP structures.[2]

With perspective of a more rigid arrangement of the OPE rod in the NPs periphery the phenyl ring next to the Au NPs surface for the center unit was substituted by an pyridine. The nitrogen's lone pair should provide an additional coordination center to the Au NPs surface

and bring the OPE rod in a fixed arrangement. Also the lack of the hydrogen atom pointing to the Au NP causing sterical repulsion should improve the fixed arrangement.[3]

These advanced Au NPs were also coupled to oligomers in the same manner as described before. The interparticle distances of the benzyl ligands and pyridine ligands were compared. The distance between the coupled Au NPs stabilized by pyridine derivatives matched the calculated lengths of the linking structures. The Au NPs stabilized with benzyl derivatives showed shorter interparticle distances. It was suggested that the OPE structure of the benzyl ligands is forced into a tilt geometry by the hydrogen atom pointing to the Au NP's surface causing sterical repulsion (Figure 10). For pyridine ligands the lone pair of the pyridine do not cause any repulsion and even offers an additional coordination side to fix the OPE in a perpendicular arrangement to the Au NPs surface. This hypothesis could not be supported by theoretical calculations.[4]

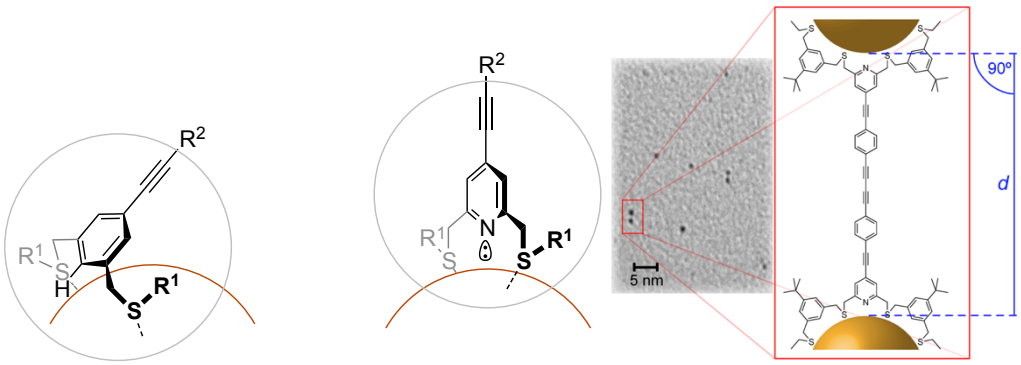

Figure 10. The proposed arrangement of the functional anchors on the NP surface. Representative TEM picture with sketch displaying the proposed ligand arrangement. Reprinted from Mayor et. al.[3]

To gain full control over the spatial arrangement of the Au NPs it is important to control the number of functional moieties installed around the NP. Therefore a new dendritic ligand design was established to build ligands that are capable to stabilize one Au NP per ligand.[5] It is shown that a dendritic ligand design can stabilize one particle per ligand. By implementing one OPE rod into the dendritic design it is possible to synthesis mono functionalized Au NPs (Figure 10).[6]

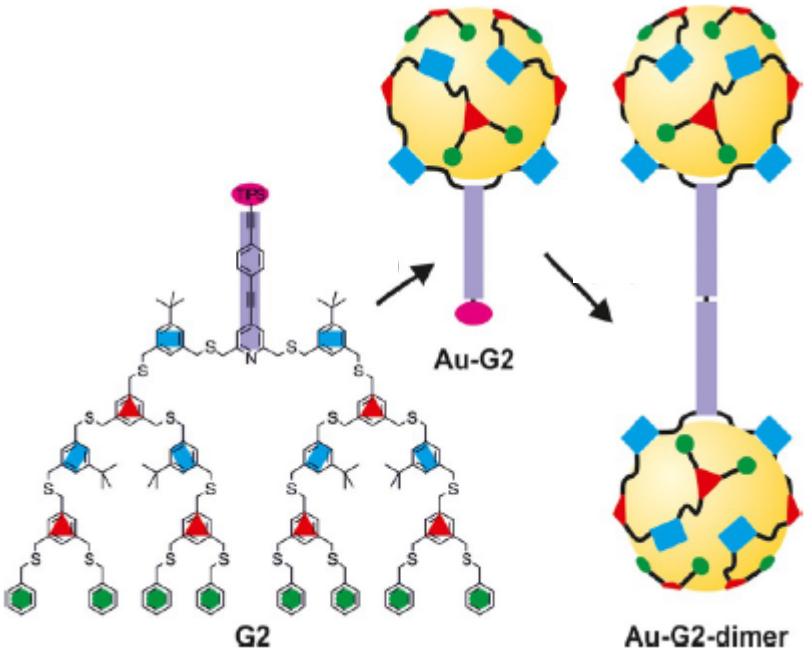

Figure 11. General concept of forming ligand-stabilized monofunctional Au NPs and NP dimers. Reprinted from Mayor et al.[6]

Experiments to form dimers by oxidative coupling supported the proposed monofunctional nature of the **G2** stabilized Au NPs (Figure 11).

2.2 Goals and Results

The goals of the present thesis are: 1) to investigate the binding of the synthesized linear thioether ligands to Au NPs and proof the advantage of the introduced pyridine moiety to increase the control of the spatial arrangement of the coupled Au NPs.

2) to develop new concepts to interlink mono functionalized Au NPs into organic / inorganic hybrid structures that make them suitable for future assembling into molecular electronic devices or for labeling applications.

To investigate the interactions of the linear thioether ligands on a gold surface we designed model compounds with free thiol groups to create self assembled monolayers on a Au 111 surface. Three different binding modes were proposed: (i) the ligand bind with the free thiols and the thioethers to the gold surface forming a striped phase, (ii) only the free thiols bind to the surface forming a bridge phase or (iii) only one thiol is binding to the gold substrate forming a SAM like standing phase (Figure 12).

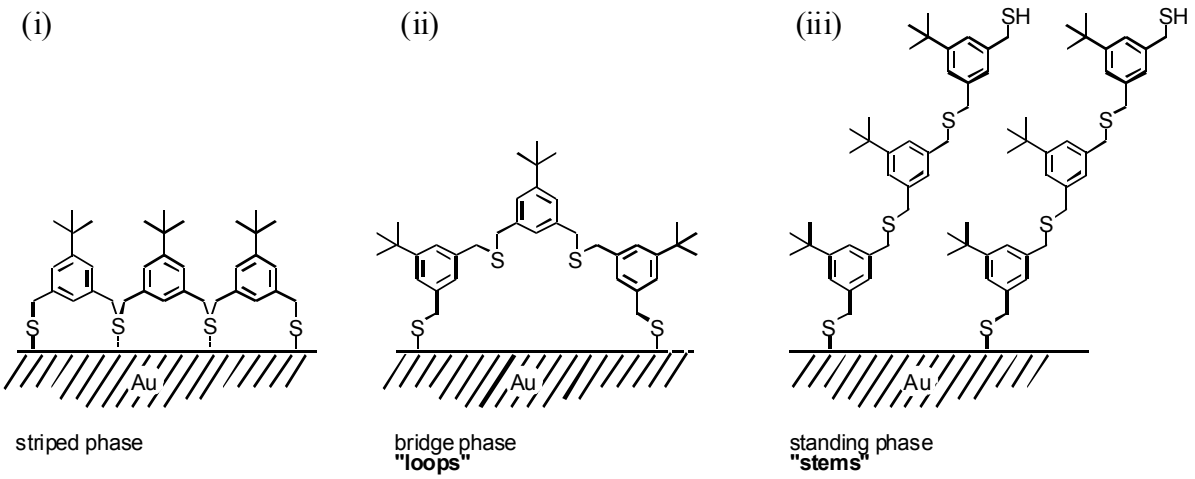

Figure 12. The proposed arrangements of the designed model compounds on a Au 111 surface.

The formed SAMs are analyzed by high resolution x-ray photoelectron spectroscopy (HRXPS), near edge X-ray absorption fine structure (NEXAFS) and scanning tunneling microscopy (STM). The model compounds are found to form bridge phase with a minor amount of molecules standing upright on the surface. This research was published in *Journal of Physical Chemistry C*.[7]

We also wanted to proof the advantage of the pyridine substituted central united that showed superior results in terms spatial arrangement of coupled Au NPs. Therefore we created two

series of model compounds, oligophenylene benzyl (OPB) and oligophenylene pyridine (OPP) derivatives. The model compounds were deposited on an Au 111 surface to build an interface that could be analyzed by HRXPS and NEXAFS.

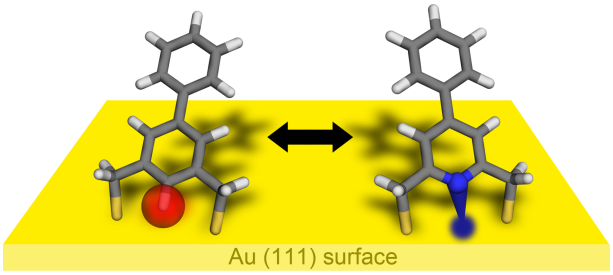

Figure 13. Schematic drawing of the proposed arrangements of OPB and OPP on a gold surface.

The recorded HRXPS data showed that the OPPs were able to form cleaner and more ordered SAMs than the OPBs. With NEXAFS it was also possible to measure the tilt angle of the molecules respective to the surface where the OPPs also show a more upright arrangement than the OPBs. Finally it was possible to prove by C K-edge NEXAFS spectra the nitrogen atom of the pyridine is coordinating to the surface. With this results we proof the need of pyridine based OPEs as functional groups in Au NP stabilizing ligands to achieve full spatial control after coupling them in to oligomers. This work was published in *Physical Chemistry Chemical Physics*.[8]

The second goal was approached using the mono functionalized dendritic ligand **G2** (Figure 4) to stabilize Au NPs and further interlink them into a defined arrangement. So far only homo coupling between Au NPs into dimers or linear oligomers was performed that already shows interesting results. To broaden the variety of future application of these nano particles we wanted to find a wet chemistry protocol that allows connecting the Au NPs to other molecules. The acetylene moiety already installed in the periphery of the **G2** stabilized Au NPs' give access to azide – acetylene click chemistry. This copper(I) catalyzed (2+3)-cycloaddition is a well understood reaction that works under mild conditions and all used reagents can be easily removed by washing with water. That make this reactions conditions perfectly suitable to interlink Au NPs. In order to perform click chemistry azide functionalized linker molecules have to be synthesized. *Bis*-1,4, *tris*-1,3,5 and *tetrakis*-*1,2,4,5*-(azidomethyl)benzenes were selected as linker molecules because they provide azide groups in a defined geometric arrangement (Figure 14).

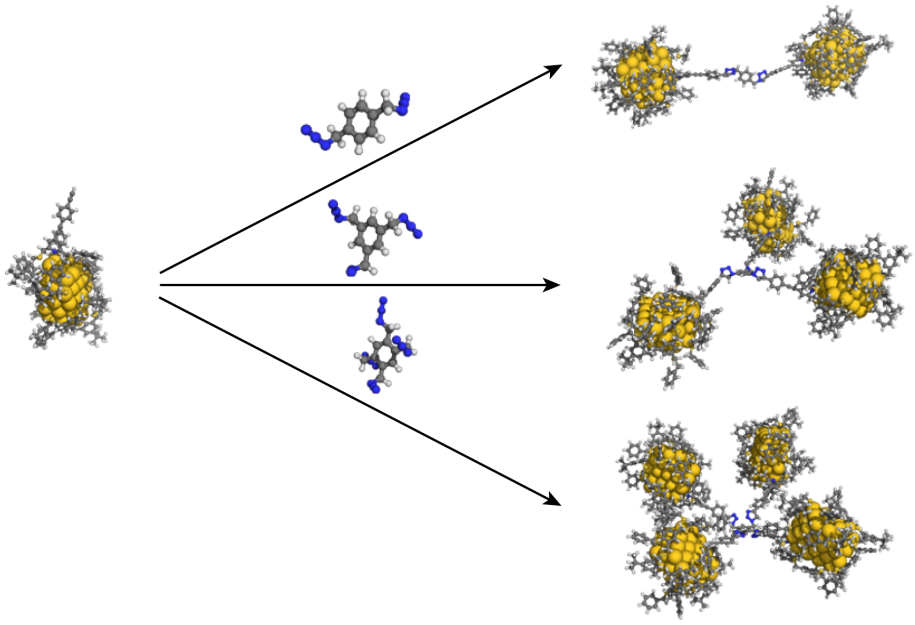

Figure 14. 3D sketch of the click reaction and the resulting oligomers. G2 stabilized Au NPs (left)

All linker molecules showed the formation of the desired oligomers that matches the calculated length for the interlinking structures with a perpendicular arrangement of the OPE. The oligomers were obtained in yields close to 50 %. However, the formation of the desired oligomers final proves the monofunctionalized nature of the **G2** stabilized Au NPs.

The research was published in *Small*.

2.3 References

1. T. Peterle, A. Leifert, J. Timper, A. Sologubenko, U. Simon, and M. Mayor, *Chem. Commun.*, 2008, 3438–3440.

2. T. Peterle, P. Ringler, and M. Mayor, *Advanced Functional Materials*, 2009, **19**, 3497–3506.

3. J. P. Hermes, F. Sander, T. Peterle, C. Cioffi, P. Ringler, T. Pfohl, and M. Mayor, *Small*, 2011, **7**, 920–929.

4. D. Thompson, J. P. Hermes, A. J. Quinn, and M. Mayor, *ACS Nano*, 2012, **6**, 3007–3017.

5. J. P. Hermes, F. Sander, T. Peterle, R. Urbani, T. Pfohl, D. Thompson, and M. Mayor, *Chemistry - A European Journal*, 2011, **17**, 13473–13481.

6. J. P. Hermes, F. Sander, U. Fluch, T. Peterle, D. Thompson, R. Urbani, T. Pfohl, and M. Mayor, *J. Am. Chem. Soc.*, 2012.

7. F. Sander, T. Peterle, N. Ballav, F. von Wrochem, M. Zharnikov, and M. Mayor, *J. Phys. Chem. C*, 2010, **114**, 4118–4125.

8. F. Sander, J. P. Hermes, M. Mayor, H. Hamoudi, and M. Zharnikov, *Phys. Chem. Chem. Phys.*, 2013, **15**, 2836–2846.

3 Publications

Loops vs. Stems: Benzylic Sulfide Oligomers Forming Carpet Type Monolayers

Fabian Sander[†], Torsten Peterle [†¥], Nirmalya Ballav[‡§], Florian von Wrochem[$], Michael Zharnikov [‡], Marcel Mayor [†,£]**

[†]Department of Chemistry, University of Basel, St. Johanns-Ring 19, 4056 Basel, Switzerland;

[‡]Angewandte Physikalische Chemie, Universität Heidelberg, Im Neuenheimer Feld 253, 69120 Heidelberg, Germany; [$]Material Science Laboratory, Sony Deutschland GmbH, Materials Science Laboratory, Hedelfinger Strasse 61, 70327 Stuttgart, Germany; [£]Institute of Nanotechnology, Karlsruhe Institute of Technology, P. O. Box 3640, 76021 Karlsruhe, Germany.

[§] Present address: Laboratory for Micro and Nanotechnology, Paul Scherrer Institut, 5232 Villigen, Switzerland

[¥] Present address: Creavis Technologies & Innovation, Evonik Degussa GmbH, Paul-Baumann-Straße 1, 45772 Marl, Germany

* Corresponding authors: marcel.mayor@unibas.ch (M. Mayor) and Michael.Zharnikov@urz.uni-heidelberg.de (M. Zharnikov).

Reprinted with permission from *J. Phys. Chem. C*, **2010**, *114*, 4118 – 4125. Copyright 2010 American Chemical Society.

Abstract

Chain-like oligomers consisting of several in *meta* position interlinked benzylic sulfides and terminal benzylic thiols were synthesized and the nature of the molecular monolayers formed by their self-assembly on gold (111) substrates was investigated. The fabricated films were characterized by high-resolution X-ray photoelectron spectroscopy and near-edge X-ray absorption fine structure spectroscopy. In the case of the short oligomers, the spectroscopic studies were additionally supported by scanning tunneling microscopy experiments. The target molecules were found to form dense and contamination-free SAM-like "carpet" films on gold (111). In spite of the multidentate nature of the benzylic sulfides oligomers, the predominant molecular conformation in these films were bridges ("loops") formed by the covalent attachment of both terminal thiols with a minor amount of molecules which were bound by only one thiol group as upright standing "stems" protruding the SAM. The films exhibited only a limited degree of order, with a slight preference of the perpendicular-to-the-surface orientation of the individual phenyl rings of the oligomer chains.

1. Introduction

Self-assembled monolayers (SAMs) of organic molecules provide a flexible and relatively simple tool to tailor the interfacial properties of metal, semiconductor, and oxide surfaces.[1] SAM-forming molecules comprise a chemical functionality with a high affinity for the target surface that provides the anchoring of the molecule to the surface and chain-like spacer that drives molecular assembly and allows the spontaneous formation of 2D crystalline structures. In addition, a specific functional (tail) group can be attached to the spacer, determining, after the self-assembly, new chemical and physical identity of the functionalized substrate. Due to the high affinity of thiols for the surfaces of coinage metals, the most extensively studied SAM systems are based on the strong chemisorption of organic thiols onto gold, silver and copper. Especially with *n*-alkanethiols on gold surfaces, highly-ordered and stable SAMs were obtained.[1] Parallel, it has been shown that also a much weaker interaction between dialkylsulfides and gold surfaces can provide ordered SAMs.[2] However, in contrast to alkanethiol-derived SAMs, dialkylsulfide SAMs on gold were reported to be much less robust and also not as well ordered.[3-7] Initial indications of cleavage of one of the two C-S bonds in dialkylsulfides on gold surfaces[8] were later found to be related to minor (~0.1%) alkylthiol impurities in the target compounds; due to the higher affinity for gold, these impurities were overrepresented in the resulted "dialkylsulfide" films.[9] More stable and better packed monolayers based on sulfides were obtained by using oligodentate thioether ligands such as a tetradentate calix-(4)-arene derived thioether ligand by Reinhoudt *et al.*[10-12] and other tridentate thioether ligands.[13-14] The interaction between thioethers and gold surfaces gained recent attention by the group of C. H. Sykes. They studied single molecule motion of dialkyl sulfides on Au(111) surfaces by low-temperature scanning tunneling microscopy (STM), by which it was shown that the rotation of single molecules around the central sulfur atom can be actuated both thermally and mechanically.[15] The behavior of alkanedithiols on gold surfaces was also recently investigated by de Boer *et al.* who showed that, dependent on their concentration, long alkanedithiols can form loops on gold surfaces.[16]

Within this context, we became interested in mixed thiol-thioether model compounds to investigate their surface binding properties on gold substrates in view of formation of SAM-like films. This is of particular interest as benzylic sulfides based oligomers display promising gold particle stabilizing properties.[17] The stability of these oligomers coated particles even gave access to an integer number of functional groups per particle using tailor made oligomers.[18] An important question in this regard is (i) whether such oligomeres comprising

terminal thiol groups bind to gold substrates by both thiol and sulfide groups forming a striped phase or (ii) they are linked with both terminal thiol groups forming loops (bridge phase) or (iii) they are anchored by only one of the thiol groups resulting in a conventional SAM-like arrangement (standing phase) (see Figure 1).

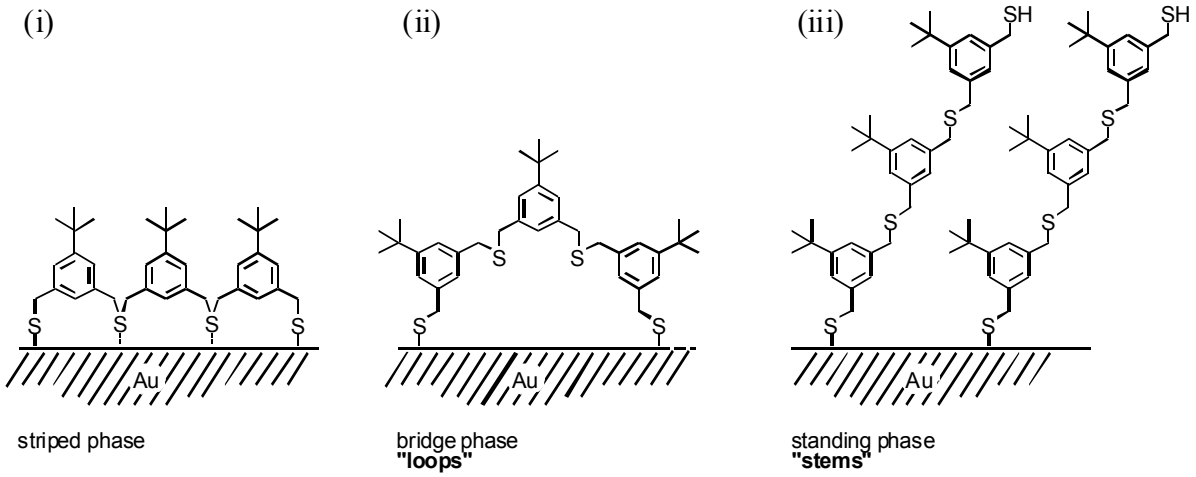

Figure 1. Schematic representation of possible binding modes of the thiol-thioether oligomer **2** (see Figure 2) to the gold substrate.

To answer this question the linear thiol terminated oligomers **1**-**4** (Figure 2) were synthesized and their monolayer forming properties were investigated by synchrotron-based high-resolution X-ray photoelectron spectroscopy (HRXPS), near-edge X-ray absorption fine structure (NEXAFS) spectroscopy and, in the case of molecules **1** and **2,** also by scanning tunneling microscopy (STM).

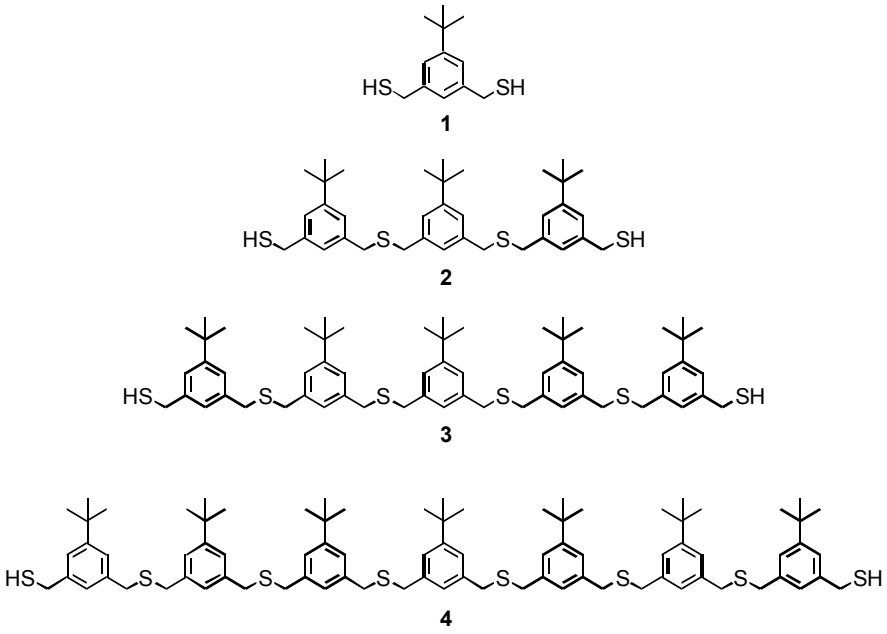

Figure 2. Molecular structures of the thiol/thioether oligomers **1** - **4**.

2. Experimental Section

2.1. Synthesis and Characterization. The model structures were originally optimized to stabilize gold nanoparticles and their synthesis and characterization were already reported.[17] The *tert*-butyl groups were introduced to enhance the solubility of the molecules and to inhibit the agglomeration of nanoparticles by steric repulsion. The monomere **1** was synthesized by a two step reaction sequence from the 5-*tert*-butyl-*m*-xylene (**5)** in good yields. In the first step 1,3-bis(bromomethyl)-5-*tert*-butylbenzne (**6)** was obtained in reasonable yields by a radical bromination reaction. Subsequent treatment of the dibromide **6** with thiourea followed by hydrolysis of the intermediate provided the dithiol **1**. The bifunctional compound **7** comprising one benzylic bromine as leaving group and a triphenylmethyl protected benzylic thiol is an ideal building block for the assembly of the longer oligomers **2-4** by a stepwise elongation strategy. The key building block **7** was obtained by treating the dibromide **6** with the stericaly demanding sulfur nucleophile Triphenylmethanethiol (TrtSH) in refluxing tetrahydrofurane (THF) in the presence of potassium carbonate (K_2CO_3) as base. By applying the elongation/deprotection reaction sequence with the building block **7**, the monomer **1** was transformed to the trimer **2**. Thus, the dithiol **1** was treated with 2 equivalents of the benzylic bromide **7** in dry THF and sodium hydride (NaH) as base at room temperature. After work up and purification by column chromatography the doubly tritylprotected trimer **9** was obtained in good yields. Subsequent deprotection with trifluoroacetic acid (TFA) and triethylsilane (Et_3SiH) as cation scavenger provided quantitatively the trimeric dithiol **2**. The same elongation/deprotection reaction sequence was applied to **2** and **3** in order to assemble the pentamer **3** and the heptamer **4** (Scheme 1). All synthesized compounds were purified by column chromatography or distillation and were fully characterized by ^{1}H- and ^{13}C-NMR spectroscopy, MALDI-ToF mass spectroscopy and elemental analysis.

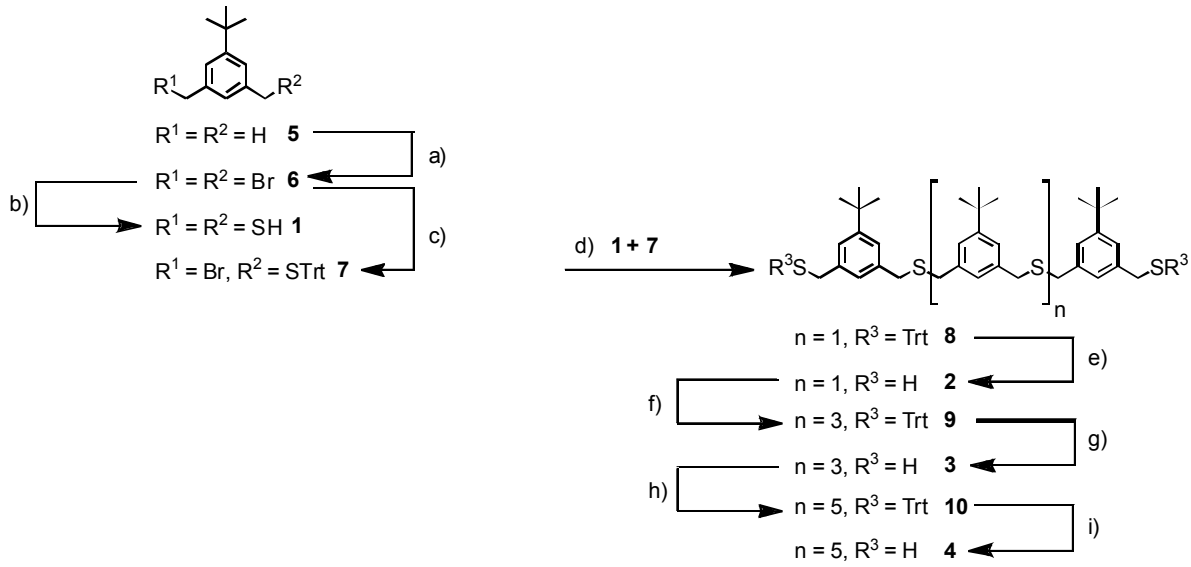

Scheme 1. Synthesis of model compounds **1**-**4**: a) N-bromosuccinimide, azo-*bis*-(isobutyronitrile), $CHOOCH_3$, hv, 3 h, 70%; b) thiourea, dimethylsulfoxide, 12 h, NaOH, 64%; c) TrtSH, K_2CO_3, THF, reflux, 12 h, 51%; d) NaH, THF, rt, 1 h, 96%; e) Et_3SiH, TFA, CH_2Cl_2, rt, 15 min, 99% f) NaH, THF, rt, 1 h, 96%; g) Et_3SiH, TFA, CH_2Cl_2, rt, 15 min, 99%; h) NaH, THF, rt, 1 h, 91%; i) Et_3SiH, TFA, CH_2Cl_2, rt, 15 min, 99%.

2.2. SAM Preparation. The gold substrates for the spectroscopic experiments (see below) were prepared by thermal evaporation of 200 nm of gold onto polished single crystal silicon (100) wafers (Silicon Sense) primed with a 5 nm titanium adhesion layer; such evaporated films are frequently used as standard substrates for SAM formation. The films were polycrystalline, with a grain size of 20-50 nm as observed by atomic force microscopy and STM. The grains predominantly possess a (111) orientation.[19-20] The gold substrates for the STM experiments (see below) were prepared by evaporation of Au on freshly cleaved mica (pressure: 5×10^{-6} mbar, 100 nm thickness) and subsequent flame annealing of the substrates in a butane flame, resulting in polycrystalline Au(111) surfaces with large (100-200 nm) atomically flat terraces.

The SAMs were formed by immersion of freshly prepared substrates into a 10 μM solution of the target compounds in absolute ethanol at room temperature for 24 h. Due to the low solubility of the compounds in ethanol, they were preliminary dissolved in toluene as 1 mM solutions. After immersion, the samples were carefully rinsed with pure ethanol, blown dry with argon, and kept, if necessary, for several days in argon-filled glass containers until the characterization. For the preparation of the STM samples the solubility issue was removed by immersion of the freshly prepared substrates into a 10 μM solution of the target compounds in dichloromethane at room temperature for 24 h.

As direct references to the target systems of this study, SAMs of non-substituted alkanethiols, viz. octanethiolate (OT), dodecanethiolate (DDT) and octadecanethiolate (ODT) were fabricated using the same film preparation procedure as for the target compounds of this study except for the preliminary dissolving in toluene.

2.3 Spectroscopic characterization of the SAMs. The fabricated films were characterized by X-ray photoelectron spectroscopy (XPS – the spectra are not shown, since HRXPS is superior), high-resolution XPS (HRXPS), and angle-resolved NEXAFS spectroscopy. All experiments were performed at room temperature. The XPS, HRXPS, and NEXAFS measurements were carried out under UHV conditions at a base pressure lower than 1.5×10^{-9} mbar. The spectra acquisition time was selected in such a way that no noticeable damage by the primary X-rays occurred during the measurements.[21-24]

HRXPS experiments were performed at the bending magnet beamline D1011 at the MAX II storage ring of the MAX-lab synchrotron radiation facility in Lund, Sweden. For these measurements, only the films on mica were used. The spectra were collected using a normal emission geometry at a photon energy of 350 eV for the S 2p range and 350 and 580 eV for the C 1s range. In addition, Au 4f spectra were acquired and the O 1s range was monitored. The binding energy (BE) scale of every spectrum was individually calibrated using the Au $4f_{7/2}$ emission line of AT-covered Au substrate at 83.95 eV.[25] The energy resolution was greater than 100 meV, which is noticeably smaller than the full widths at half maximum (fwhm) of the photoemission peaks addressed in this study.

XPS measurements were performed using a Mg Ka X-ray source and a LHS 11 analyzer. The spectra acquisition was carried out in normal emission geometry with an energy resolution of ≈0.9 eV. The X-ray source was operated at a power of 260 W and positioned ≈1.5 cm away from the samples. The fitting of the XPS spectra was performed in the same way as the HRXPS spectra. Since the spectra quality of the latter technique was superior, XPS spectra are not shown. XPS data were mostly used to determine the portions of the different sulfur-derived species and the effective thickness of the target SAMs.

HRXPS and XPS spectra were fitted by symmetric Voigt functions using either a Shirley-type or a linear background, depending on the spectral range and primary photon energy. To fit the S $2p_{3/2,1/2}$ doublets we used a pair of such peaks with the same fwhms, a branching ratio of 2 ($2p_{3/2}/2p_{1/2}$) and a spin-orbit splitting (verified by fit) of ≈1.18 eV.[26] The fits were carried out self-consistently: the same peak parameters were used for identical spectral regions. The accuracy of the resulting BE/fwhm values in the case of HRXPS is 0.02-0.03 eV.

The thickness of the target films was determined on the basis of the I_{C1s}/I_{Au4f} intensity ratios, assuming a standard exponential attenuation of the photoelectron signal and using the attenuation lengths reported by Wilkes *et al.*.[27] As calibration references, the DDT/Au and ODT/Au samples of known thickness were used, assuming that these samples have comparable packing densities as the target films.

NEXAFS spectroscopy measurements were performed at the HE-SGM beamline of the synchrotron storage ring BESSY II in Berlin, Germany. The spectra acquisition was carried out at the C K-edge in the partial electron yield mode with a retarding voltage of -150 V. Linear polarized synchrotron light with a polarization factor of ≈82% was used. The energy resolution was ≈0.40 eV. The incidence angle of the light was varied from 90° (***E***-vector in surface plane) to 20° (***E***-vector near surface normal) in steps of 10-20° to determine the orientational order in the SAMs. This approach is based on the dependence of the cross-section of the resonant photoexcitation process on the orientation of the electric field vector of the synchrotron light with respect to the molecular orbital of interest (so-called linear dichroism in X-ray absorption).[28] Raw NEXAFS spectra were normalized to the incident photon flux by division through a spectrum of a clean, freshly sputtered gold sample. The photon energy (PE) scale was referenced to the pronounced π* resonance of highly oriented pyrolytic graphite at 285.38 eV.[29]

The structural properties of the monolayers were characterized at ambient conditions using a scanning tunneling microscope (Multimode Nanoscope IIIa, Digital Instruments) equipped with a low current amplifier. Self-cut Pt/Ir (80/20) tips were used as a probe, and the quality of the tips was verified by obtaining molecular resolution images on reference OT monolayers. The STM scans were recorded in constant current mode. The tunneling conditions were selected in order to obtain perturbation-free images even for the long thioether trimers. For this purpose, a bias voltage of 500 mV (tip positive) and a tunneling current of 2 pA was employed, resulting in a tunneling impedance of 2.5×10^{11} Ω.

DFT calculations were done to compare the feature sizes obtained from STM images with the physical size of molecules **1** and **2**. These calculations were performed at the VWN theory level[30] with a DNP polarized basis set using the program Dmol^3. Further computational details and the relaxed structures of **1** and **2** can be found in the Supporting Information.

3. Results and Discussion

3.1. XPS and HRXPS. Normalized C 1s and S 2p HRXPS spectra of **1**, **2**, **3** and **4** on Au acquired at a photon energy of 350 eV are presented in Figures 3 and 5, respectively, along with the corresponding fits by several individual components and a background.

The C 1s HRXPS spectra of the target films exhibit a single emission peak at a BE of 284.4-284.8 eV assigned to the backbone of the target molecules. No features related to oxygen-containing functional groups are observed. This correlates with the O 1s XPS spectra (not shown), in which no oxygen signal was observed for **2**/Au, **3**/Au, and **4**/Au and only a low intense signal was exhibited for **1**/Au. This indicates that all contaminants were removed from the substrate surface upon the adsorption of the target compounds, by the so called process of self-cleaning, typical for high quality thiol-derived SAMs.

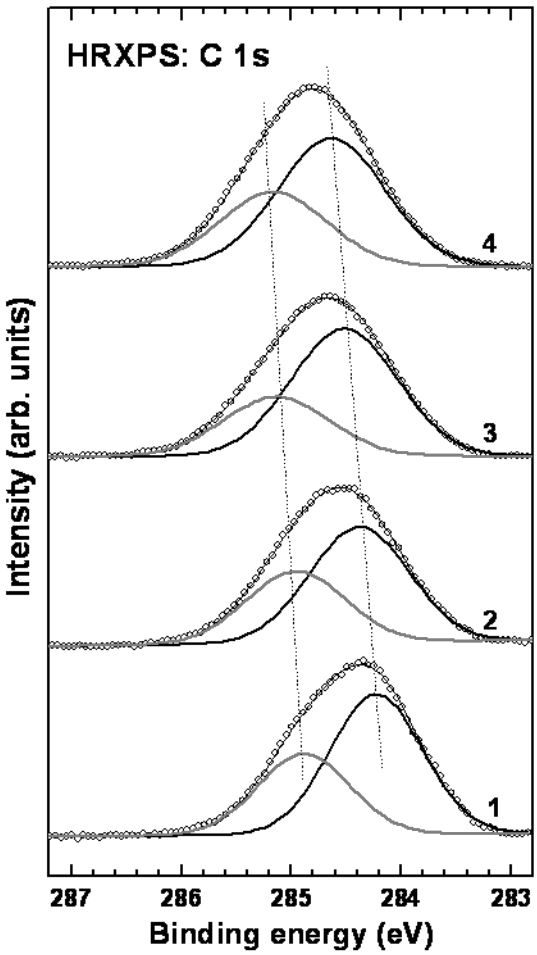

Figure 3. C 1s HRXPS spectra of **1**/Au – **4**/Au.

The observed emission peak is asymmetric, which is especially obvious for **1**/Au, and can be split into two components as shown in Figure 3. The low BE component is assigned to the carbon atoms in the phenyl rings, whereas the high BE component is assigned to the aliphatic side groups. The BE of the joint emission peak and those of both components exhibit a gradual shift to higher values with increasing length of the molecular chain. Such a shift could be related to a weaker screening of the C 1s photoemission hole by the substrate electrons. This suggests a larger average spacing between the respective carbon atoms and the substrate for the long-chain molecules as compared to the short-chain ones. This finding disagrees with the striped phase model (see Figure 1), which assumes a horizontal arrangement of the target molecules on the substrate. In this model the average spacing between the carbon atoms in the molecular chains and the substrate should be independent of the chain length.

Further evidence that the striped phase model is not correct in the present case is provided by the evaluation of the effective thickness of the target films. As seen in Figure 4, where the effective thicknesses derived from both HRXPS and XPS data are presented, this parameter increases with increasing length of the target molecule. This is not consistent with the striped phase model, which assumes chain-length-independent effective thickness associated with the complete coverage of the substrate by a monolayer of the target molecules in the stripe geometry.

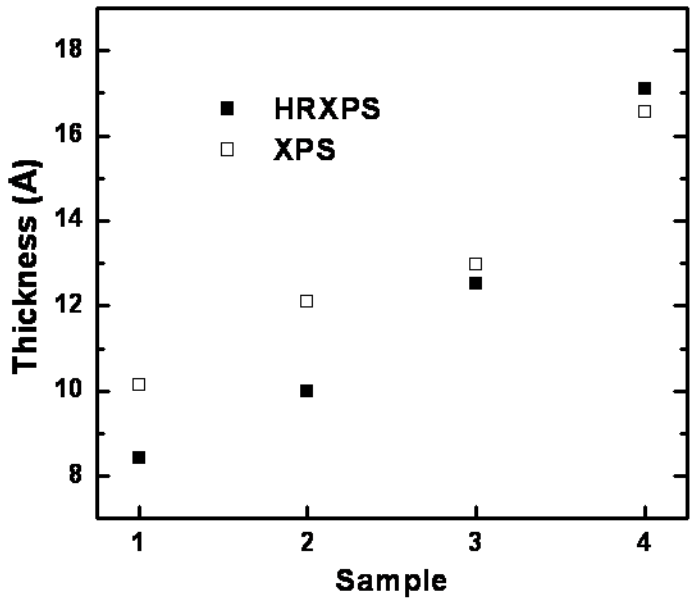

Figure 4. Effective thickness of **1**/Au – **4**/Au.

Otherwise, the observed increase of the effective thickness by going from **1**/Au to **4**/Au over **2**/Au and **3**/Au does not correlate exactly with the change in the length of the molecular chain. This is not expected for the standing phase model (Figure 1) which assumes a vertical arrangement of the target molecules. Indeed, in this case the molecular packing density, given by the identity of the molecular chain, should be similar for all target molecules, so that their thickness should directly correlate with the chain length. Thus, we are only left with the bridge phase model (Figure 1), with only a small portion of alternative adsorption geometries. The bridge-type adsorption should be mediated by both terminal thiol groups which can easily transform to strongly bonding thiolate moieties after the substrate-mediated abstraction of hydrogen.

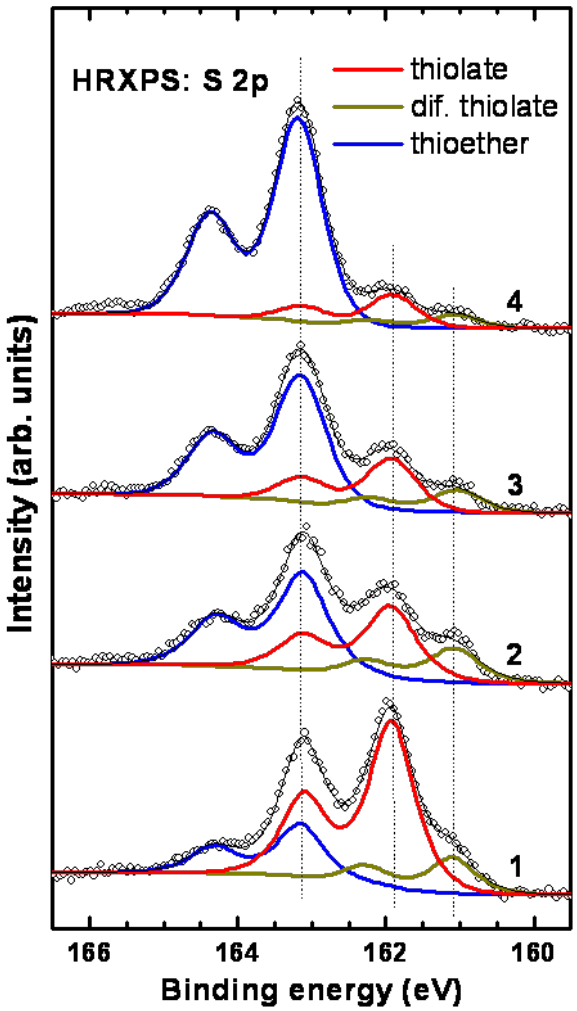

Figure 5. S 2p HRXPS spectra of **1**/Au – **4**/Au.

The hypothesized adsorption model is further corroborated by the analysis of the S 2p HRXPS spectra of the target compounds (Figure 5). These spectra exhibit three distinct S

$2p_{3/2,1/2}$ doublets at a BE of ≈161.0, ≈161.9, and 163.1-163.2 eV (S $2p_{3/2}$). No features at higher BE (165.5 – 169.8 eV), characteristic of oxidized sulfur (from SO^- to SO_4^-)[31] were observed. The doublet at 161.9 eV is common of thiolate species bound to metal surfaces.[20,32-33] The doublet at ca. 161.0 eV is frequently observed in the HRXPS spectra of thiol-derived SAMs[33-34] and can be tentatively assigned to a differently (than thiolate) chemisorbed SAM constituent.[34-37] Alternatively this doublet can be assigned to atomic sulphur as pointed by Yang *et al.*[38] and as discussed by Shaporenko *et al.*,[34] but we find this assignment to be less applicable in the present case. The doublet at 163.1-163.2 eV can be ascribed to unbound or weakly bound coordination-type S in the thioether groups of the target films.[9,39-40] There is a small and gradual upward shift in the BE position of the respective doublet when moving from **1** to **4** which assumes a weaker mean interaction with the substrate for the thioether moieties compared to the longer target molecules. Similar to the C 1s case (see above), this can be related to weaker screening of the S 2p photoemission hole by the conduction electrons in the substrate with increasing spacing between the thioether moiety and substrate.

Fitting the experimental spectra in Figure 5 and taking the intensities of the individual S 2p doublets, we can determine the relative contributions of the strongly bound ("161.0 eV" + "161.9 eV") sulphur species on one side and weakly bound or unbound moieties ("163.1-161.3 eV") on the other side. The derived portions are plotted in Figure 6, along with the analogous values determined on the basis of the XPS spectra (not shown). The HRXPS and XPS derived values are in good agreement, despite the observation of some minor differences.

The data in Figure 6 should be considered in reference to the different models for adsorption of the target molecules onto the Au substrate as shown in Figure 1. Assuming that no molecular decomposition occurs and bonding to the substrate is mediated by one thiol-derived thiolate group (standing phase - similar to the SAMs di- and terphenyl-based dithiol),[41-43] the portion of the strongly bound sulfur in **1**/Au, **2**/Au, **3**/Au, and **4**/Au should be 50%, 25%, 16.6%, and 12.5%, respectively, as long as the stronger (as compared to thioethers) attenuation of the respective signal by the hydrocarbon overlayer is not taken into account. Such a correction will result in a noticeable reduction of the above values, especially for the long-chain target compounds. The alternative bridge model postulates the bonding of the target molecules by both thiol-derived thiolate groups (see Figure 1). In this case the portion of the strongly bound sulfur in **1**/Au, **2**/Au, **3**/Au, and **4**/Au should be 100%, 50%, 33%, and 25%, respectively, with comparably smaller effect of the attenuation as the effective

thickness of the target films within this bridge phase model is at least half than that for the case of the standing phase model. Comparing the experimental values in Figure 6 with the prediction from both models, one finds that the parameters of **1**/Au, and especially of **2**/Au, **3**/Au, and **4**/Au are very close to those of the bridge phase model, which suggests, in agreement with the C 1s data (see above), that this bonding configuration dominates in the target films. Compared to the bridge phase model, the observed deviations are most pronounced for **1**/Au and quite small for the other target films. This is believed to be related to a definite amount of monodentate bonding species (standing phase) embedded into the matrix of bidentate bound molecules (bridge phase).

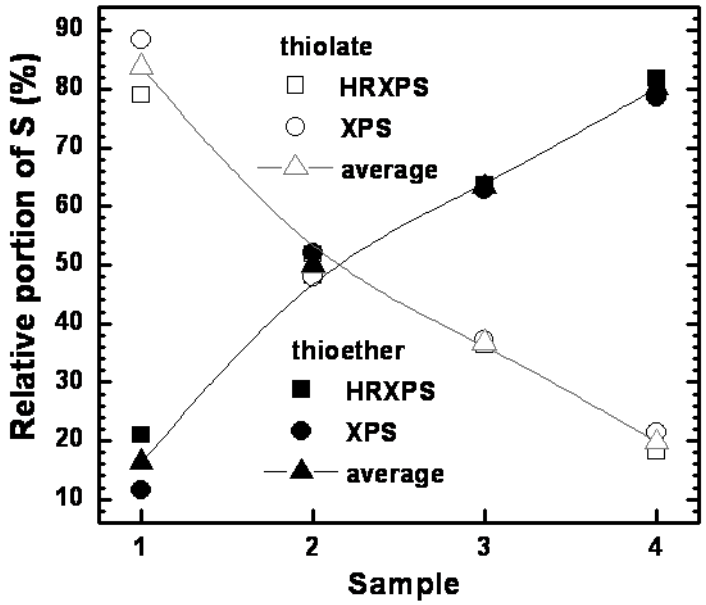

Figure 6. Relative portions of thiolate and thioether moieties measured by XPS and HRXPS in **1**/Au - **4**/Au.

3.3. NEXAFS spectroscopy. Complementary information on the composition and chemical identity of the target films is provided by the NEXAFS data. Generally, NEXAFS spectra give an insight into the electronic structure of target films, sampling the electronic structure of the unoccupied molecular orbitals of the film constituents.[28] The C K-edge spectra of the target films recorded at the magic angle of X-ray incidence (51° - after a correction for the polarization factor;[28] at this orientation the spectrum is independent of the molecular orientation) are presented in Figure 7. These spectra exhibit a C 1s absorption edge ascribed to the C 1s → continuum excitations and a series of absorption resonances characteristic of the target molecules. A signature of contamination, usually represented by a strong and sharp

π* (COOH) resonance at 288.5-288.7 eV[40,44] is absent, which suggests, in accordance with the C 1s and O 1s XPS data (see previous section), a high quality of the target films.

The NEXAFS spectra in Figure 7 are dominated by a pronounced π_1* resonance of the phenyl rings at 285.2 eV.[28, 45-50] The relative intensity of this resonance is comparable with that of phenylthiolate SAMs on Au but noticeably less that that for the biphenylthiolate or terphenylthiolate SAMs.[24,48]

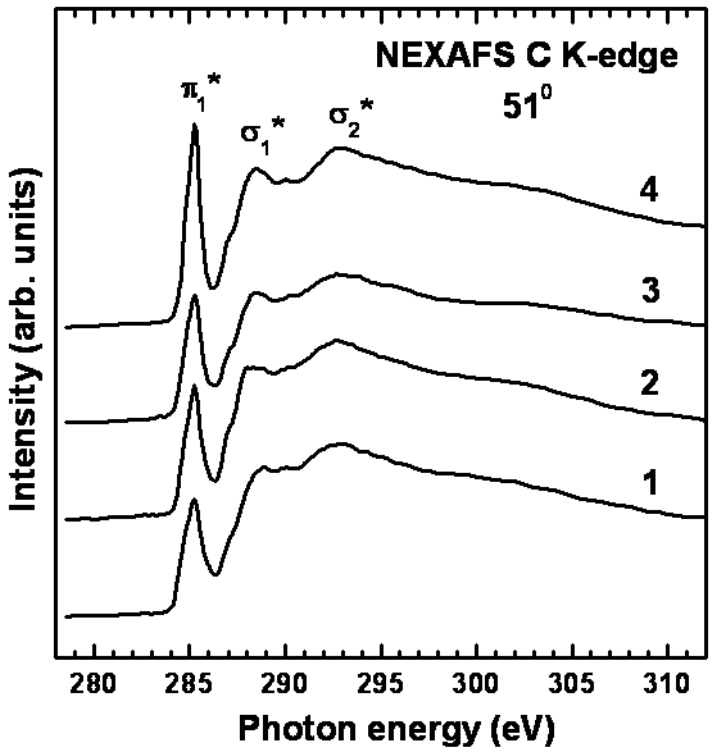

Figure 7. C K-edge NEXAFS spectra of **1**/Au – **4**/Au recorded at an angle of X-ray incidence of 51°.

The reduced intensity in the case of phenylthiolate SAMs can be related to a partial quenching of the π_1* resonance due to the interaction with the substrate – the respective SAMs are disordered and the molecules are inclined. This can occur to the same extent in the target films of this study as well. Significantly, the intensity of the π_1* resonance increases with increasing length of the molecular chain, which suggests, in accordance with the bridge phase model (see Figure 1), a smaller effect of the substrate in the case of the films comprised of long-chain molecules.

Another interesting effect is the asymmetry of the π_1* resonance in the spectra of **1**/Au – **4**/Au. Such asymmetry is not observed for oligophenyl-based SAMs.[49-50] In the present case,

this asymmetry is presumably related to a partial splitting of the π_1* resonance because of the substitution groups at the phenyl rings in the target molecules.

In addition to the insight into the electronic structure of the target systems, NEXAFS data provides valuable information on the orientation of the film constituents due to the linear dichroism effects (see Section 2). For ordered molecular films, the intensity of the absorption resonances changes at a variation of the incidence angle of the synchrotron light. A convenient way to monitor these changes is the difference between the spectra acquired at normal (90°) and grazing (20°) incidence. Such C K-edge difference spectra for target films of this study are displayed in Figure 8. All these spectra exhibit a weak positive peak at the position of the π_1* resonance, with increasing amplitude of this peak at going from **1** to **4** over **2** and **3**. This suggests the presence of some orientational order in the target film, with preferential orientation of the individual rings. Considering that the transition dipole moment of the π* orbitals is oriented perpendicular to the plane of the phenyl rings, we can conclude that the rings in the target films are preferably oriented perpendicular to the substrate, with enhancement of this effect with the increasing chain length.

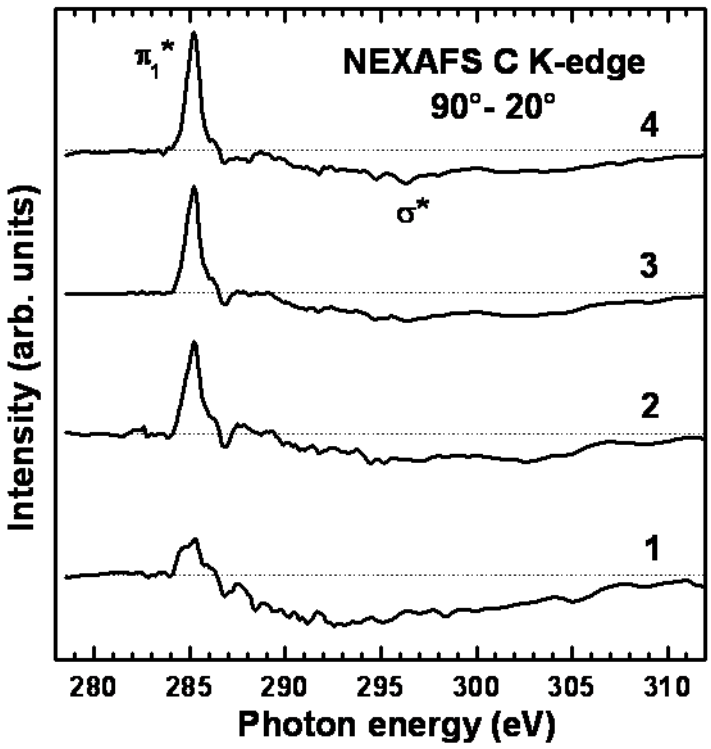

Figure 8. C K-edge NEXAFS difference spectra of **1**/Au – **4**/Au.

3.4. STM. Scanning probe methods are the only available tools for high-resolution real-space imaging of metal and semiconductor surfaces. The arrangement and periodicity of molecular layers at surfaces can be detected with high accuracy by this means, in particular using STM.[51-52] In the present study, the thioether oligomers represented a challenge for STM imaging since the tunneling resistance through the long oligomer chains could easily exceed the maximum impedance given by the STM setup. Therefore, we restricted our STM experiments to the systems **1**/Au and **2**/Au, with the target molecules possessing no more than three thioether units. At the same time, in order to scan above the monolayer with the STM tip, we used tunneling impedances in the TΩ range.

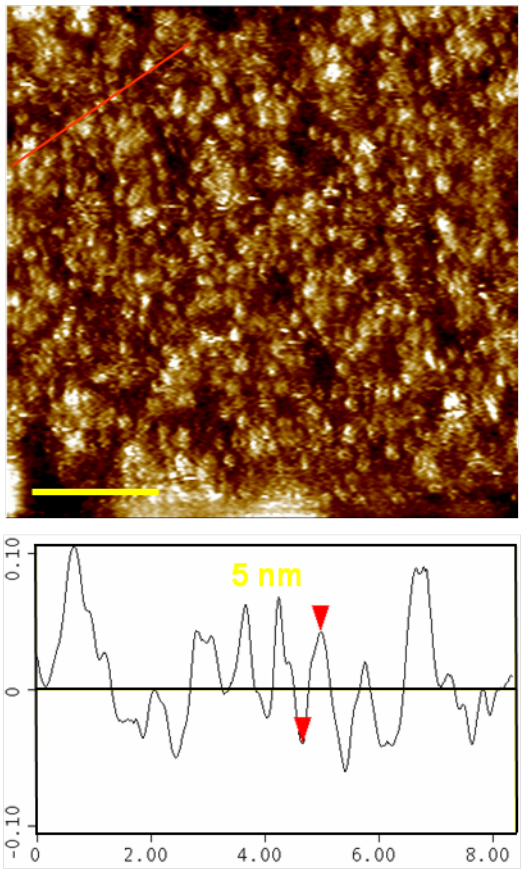

Figure 9: Top panel: STM constant-current image of **1**/Au (scan range: 20 x 20 nm^2). The average next neighbor distance between the features is ≈0.7 nm. Bottom panel: A representative height profile along the red line shown in the STM image. The apparent STM height resulting from this section is ≈0.08 nm. The image is acquired at I_t = 2 pA and U_g = 500 mV.

Figure 9 shows a high resolution STM image of **1** /Au. Even though a long-range 2D lattice cannot be recognized, the short thioether monomers form a densely packed and regularly spaced molecular arrangement on Au(111). The average distance between next neighbor (NN)

features is ≈0.7 nm, in excellent agreement with the lateral size of structure **1** as determined from a DFT-relaxed model (relaxation in the gas phase, Figure S1 in the Supplementary Information), whereas the average STM apparent height (h_{STM}) of the protrusions is ≈0.1 ± 0.015 nm. Even though the present STM images cannot answer the question whether **1** binds to Au as a bidentate or a monodentate, the lack of scan instabilities in the STM image and the confined shape of the molecular protrusions indicate a robust molecular anchoring of **1** to the Au substrate, provided presumably by a bidentate configuration.

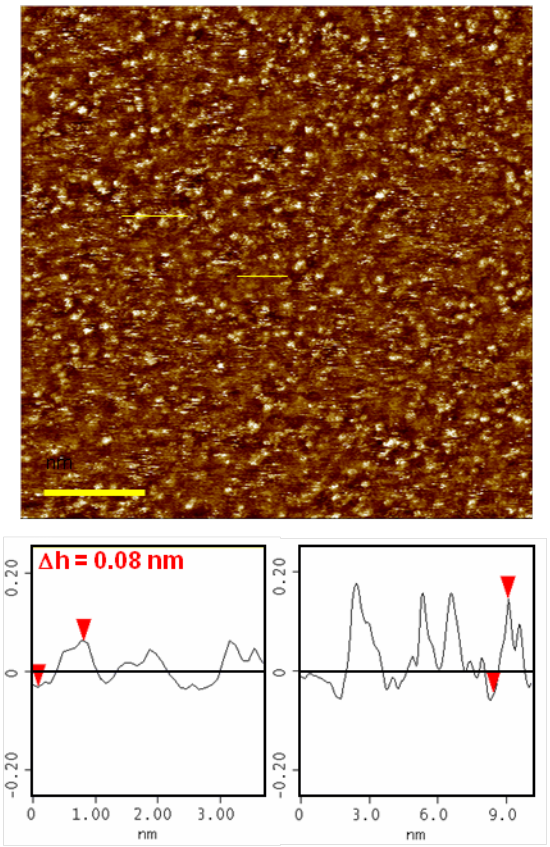

Figure 10. Top panel: STM constant-current image of **2**/Au (scan range: 50 x 50 nm^2)**;** a disordered film is observed. Bottom panel: Two representative height profiles along a row of either dark or bright features, as indicated by the yellow lines in the image. The apparent STM heights are ≈0.09 nm and ≈0.19 nm for the dark and bright features, respectively. The image is acquired at I_t = 2 pA and U_g = 500 mV.

The situation is more complex when the trimer **2** is considered. As shown in Figure 10, the surface shows a disordered film structure with a homogeneous distribution of dark and bright features. The approximate NN distance between the protrusions is now ≈1.1 nm, in good agreement with the lateral size of the relaxed, folded trimer structure **2** (see Figure S2 in the Supplementary Information). The dark features in the STM image, with an apparent height of ≈0.09 ± 0.01 nm (see Figures 10 and S4), show a height profile that is close to that of the

features observed for monomer **1**. Thus, these features correspond most probably to folded or looped trimers linked as a bidentate to the substrate, as the physical height of such structures is close to that of compound **1** (see models S1 and S2 in the Supplementary Information). However, the bright features in Figure 10 reach STM heights of up to h_{STM} ≈0.18 ± 0.015nm, which is about twice the height of the dark features for the same film. These bright features are not well resolved (Figure 10), which is often the case as far as the tilt angle of a molecular wire is not constrained, leaving the backbone free to move while the STM tip scans the surface.[53]

These observations suggest that a small fraction of **2** in the respective monolayer is standing upright (model in Figure S3) and being linked to Au only with a single thiolate anchor group. Thus, the hypothesized monolayer consists of a matrix of bridge-like trimers **2** with a few standing trimers protruding from the surrounding matrix. Based on the STM results, a rough estimation assuming a molecular area of 1.5 nm^2 for trimer **2** results in a fraction of 10-20% of standing molecules in the monolayer (Figure 10). This conclusion is consistent with the HRXPS results which, based on the ratio of bound and unbound sulfur species, provide an evidence that a smaller fraction of monodentate bonding configurations (standing phase) exists within the matrix of looped molecules (bridge phase).

4. Conclusions

A series of chain-like oligomeric model compounds **1**-**4** containing in-chain benzylic sulfides and terminal benzylic thiols as potential anchor groups for bonding to coinage metal surfaces were synthesized and used for the preparation of SAM-like films on Au(111) substrates. Several complementary experimental techniques, viz. XPS, HRXPS, NEXAFS spectroscopy, and STM were used to characterize the fabricated films. A considerable stronger binding affinity of benzylic thiols to gold compared to benzylic sulfides was found to be the major factor determining the character of the molecular assembly on the target substrates. In spite of the multidentate nature of the oligomers **2**-**4**, a striped phase associated with the bonding of both benzylic thiols and benzylic sulfides to the gold surface was not observed. In contrast, the acquired data suggest the formation of SAM-like, “carpet” films with the majority of the molecules bound to the gold surface in a “bridge” fashion by both terminal thiols and a few molecules bound by only one thiol group and protruding out the “carpet” as sketched in Figure 11.

Even though these films were found to be contamination-free and densely packed, they exhibited only a very limited degree of orientational order associated with a partial alignment of the phenyl rings perpendicular to the substrate. The bulky *tert* butyl group providing excellent process ability even of long oligomers probably handicaps the formation of ordered SAMs.

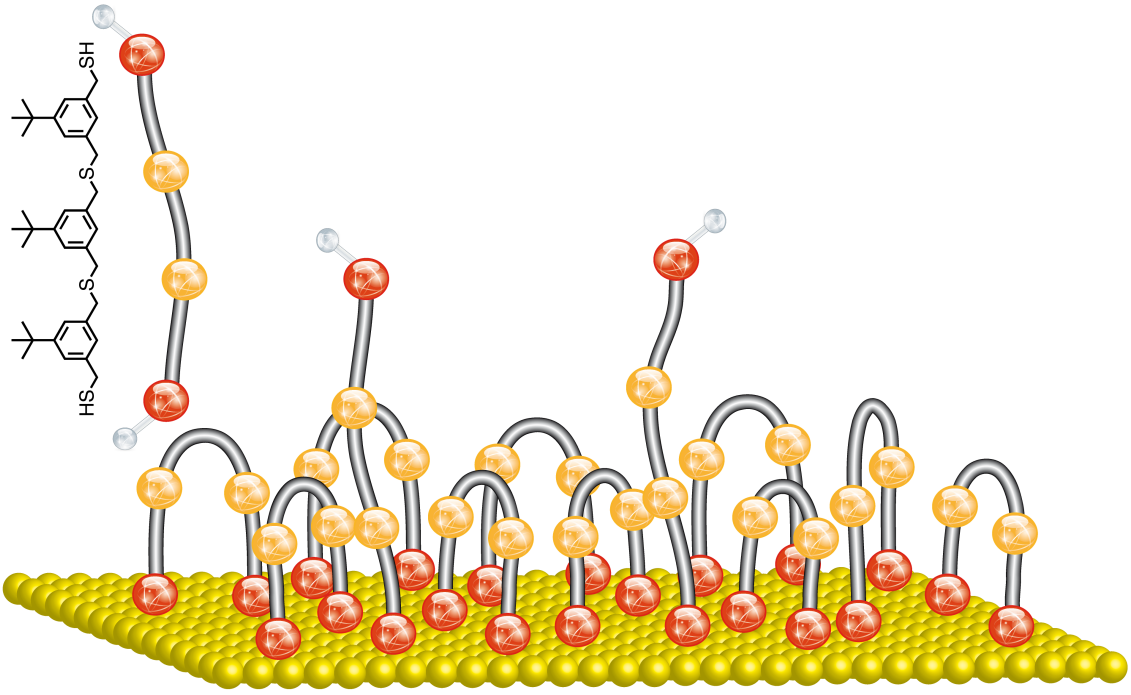

Figure 11. Sketch of the molecular arrangement in **2**/Au, representative of the entire series **1**/Au – **4**/Au, with the majority of the molecules covalently attached to the substrate by both terminal thiol groups and forming loops and a fraction of the molecules bonded to the substrate by one terminal thiol group only.

While benzylic sulfides displayed very interesting size steering and stabilizing features for gold nanoparticles, their interaction with flat gold surfaces cannot compete with terminal thiols. We are currently exploring macrocyclic benzylic sulfides as potential model compounds to further investigate their interactions with gold surfaces.

Acknowledgement. NB and MZ thank M. Grunze for the support of this work, A. Nefedov and Ch. Wöll for technical cooperation at BESSY II, and the BESSY II and MAX-lab staff for the assistance during the experiments. This work has been supported by DFG (ZH 63/9-3). We would like to acknowledge support from the European Community - Research

Infrastructure Action under the FP6 "Structuring the European Research Area" Programme (through the Integrated Infrastructure Initiative "Integrating Activity on Synchrotron and Free Electron Laser Science"). FS, TP and MM are grateful for financial support of the Swiss National Science Foundation, the Gebert Rüf Foundation and the EU through the project FUNMOL (number 213382).

Supporting Information Available: Results of NMR-spectroscopic characterization and elemental analyses of **1**-**4** are presented in the Supporting Information, along with additional information on the DFT calculations and their results and additional STM data. This information is available free of charge via the Internet at http://pubs.acs.org.

References

(1) Love, J. C.; Estroff, L. A.; Kriebel, J. K.; Nuzzo, R. G.; Whitesides, G. M. *Chem. Rev.* **2005**, *105*, 1103.

(2) Troughton, E. B.; Bain, C. D.; Whitesides, G. M.; Nuzzo, R. G.; Allara, D. L.; Porter, M. D. *Langmuir* **1988**, *4*, 365.

(3) Jung, C.; Dannenberger, O.; Xu, Y.; Buck, M.; Grunze, M. *Langmuir* **1998**, *14*, 1103.

(4) Lavrich, D. J.; Wetterer, S. M.; Bernasek, S. L.; Scoles, G. *J. Phys. Chem. B* **1998**, *102*, 3456.

(5) Noh, J.; Murase, T.; Nakajima, K.; Lee, H.; Hara, M. *J. Phys. Chem. B* **2000**, *104*, 7411.

(6) Noh, J.; Nakamura, F.; Kim, J.; Lee, H.; Hara, M. *Mol. Cryst. Liquid Cryst.* **2002**, *377*, 165.

(7) Noh, J.; Kato, H. S.; Kawai, M.; Hara, M. *J. Phys. Chem. B* **2002**, *106*, 13268.

(8) Zhong, C.-J.; Porter, M. D. *J. Am. Chem. Soc.* **1994**, *116*, 11616.

(9) Zhong, C.-J.; Brush, R. C.; Anderegg, J.; Porter, M. D. *Langmuir* **1999**, *15*, 518.

(10) van Velzen, E. U. T.; Engbersen, J. F. J.; Reinhoudt, D. N. *J. Am. Chem. Soc.* **1994**, *116*, 3597.

(11) Huisman, B.-H.; Rudkevich, D. M.; Van Veggel, F. C. J. M.; Reinhoudt, D. N. *J. Am. Chem. Soc.* **1996**, *118*, 3523.

(12) Schonherr, H.; Vancso, G. J.; Huisman, B.-H.; Van Veggel, F. C. J. M.; Reinhoudt, D. N. *Langmuir* **1999**, *15*, 5541.

(13) Kittredge, K. W.; Minton, M. A.; Fox, M. A.; Whitesell, J. K. *Helvetica Chim. Acta* **2002**, *85*, 788.

(14) Weidner, T.; Krämer, A.; Bruhn, C.; Zharnikov, M.; Shaporenko, A.; Siemeling, U.; Trager, F. *Dalton Transact.* **2006**, 2767.

(15) Baber, A. E.; Tierney, H. L.; Sykes, E. C. H. *ACS Nano* **2008**, *2*, 2385.

(16) Akkerman, H. B.; Kronemeijer, A. J.; Van Hal, P. A.; De Leeuw, D. M.; Blom, P. W. M.; De Boer, B. *Small* **2008**, *4*, 100.

(17) Peterle, T.; Leifert, A.; Timper, J.; Sologubenko, A.; Simon, U.; Mayor, M. *Chem. Comm.* **2008**, 3438.

(18) Peterle, T.; Mayor, M.; Ringler, P. *Adv. Func. Mat.* **2009**, *19*, 3497.

(19) Köhn, F. *Diploma Thesis*, Universität Heidelberg, Heidelberg, Germany, 1998.

(20) Heister, K.; Zharnikov, M.; Grunze, M.; Johansson, L. S. O. *J. Phys. Chem. B* **2001**, *105*, 4058.

(21) Wirde, M.; Gelius, U.; Dunbar, T.; Allara, D. L. Nucl. Inst. Meth. Phys. Res. Section B: Beam Interactions with Materials and Atoms **1997**, 131, 245.

(22) Jäger, B.; Schürmann, H.; Müller, H. U.; Himmel, H. J.; Neumann, M.; Grunze, M.; Woll, C. *Z. Phys. Chem.* **1997**, *202*, 263.

(23) Heister, K.; Zharnikov, M.; Grunze, M.; Johansson, L. S. O.; Ulman, A. *Langmuir* **2001**, *17*, 8.

(24) Zharnikov, M.; Grunze, M. *J. Vac. Sci. Technol. B: Microelectronics and Nanometer Structures* **2002**, *20*, 1793.

(25) *Surface chemical analysis – X-ray photoelectron spectrometers – Calibration of the energy scales*, ISO 15472:2001.

(26) Moulder, J. F.; Stickle, W. E.; Sobol, P. E.; Bomben, K. D. *Handbook of X-ray Photoelectron Spectroscopy,* Chastian, J. Ed.; Perkin-Elmer Corp.: Eden Prairie, MN, 1992.

(27) Lamont, C. L. A.; Wilkes, J. *Langmuir* **1999**, *15*, 2037.

(28) Stöhr, J. *NEXAFS Spectroscopy*; Springer Series in Surface Sience 25; Springer-Verlag: Berlin, 1992.

(29) Batson, P. E. *Phys. Rev. B* **1993**, *48*, 2608.

(30) Vosko, S. H.; Wilk, L.; Nusair, M. *Can. J. Phys.* **1980**, *58*, 1200

(31) Wang, M.-C.; Liao, J.-D.; Weng, C.-C.; Klauser, R.; Shaporenko, A.; Grunze, M.; Zharnikov, M. *Langmuir* **2003**, *19*, 9774.

(32) Laibinis, P. E.; Whitesides, G. M.; Allara, D. L.; Tao, Y. T.; Parikh, A. N.; Nuzzo, R. G. *J. Am. Chem. Soc.* **1991**, *113*, 7152.

(33) Zharnikov, M. *J. El. Spec. Rel. Phenom.*, in press, doi: 10.1016/j.elspec.2009.05.008.

(34) Shaporenko, A.; Terfort, A.; Grunze, M.; Zharnikov, M. *J. El. Spec. Rel. Phenom.* **2006**, *151*, 45.

(35) Himmelhaus, M.; Gauss, I.; Buck, M.; Eisert, F.; Wöll, C.; Grunze, M. *J. El. Spec. Rel. Phenom.* **1998**, *92*, 139.

(36) Ishida, T.; Hara, M.; Kojima, I.; Tsuneda, S.; Nishida, N.; Sasabe, H.; Knoll, W. *Langmuir* **1998**, *14*, 2092.

(37) Ishida, T.; Choi, N.; Mizutani, W.; Tokumoto, H.; Kojima, I.; Azehara, H.; Hokari, H.; Akiba, U.; Fujihira, M. *Langmuir* **1999**, *15*, 6799.

(38) Yang, Y. W.; Fan, L. J. *Langmuir* **2002**, *18*, 1157.

(39) Trevor, J. L.; Lykke, K. R.; Pellin, M. J.; Hanley, L. *Langmuir* **1998**, *14*, 1664.

(40) Weidner, T.; Ballav, N.; Zharnikov, M.; Priebe, A.; Long, N. J.; Maurer, J.; Winter, R.; Rothenberger, A.; Fenske, D.; Rother, D.; Bruhn, C.; Fink, H.; Siemeling, U. *Chem. - Europ. J.* **2008**, *14*, 4346.

(41) Azzam, W.; Wehner, B. I.; Fischer, R. A.; Terfort, A.; Woll, C. *Langmuir* **2002**, *18*, 7766.

(42) Tai, Y.; Shaporenko, A.; Rong, H.-T.; Buck, M.; Eck, W.; Grunze, M.; Zharnikov, M. *J. Phys. Chem. B* **2004**, *108*, 16806.

(43) Shaporenko, A.; Elbing, M.; Blaszczyk, A.; Von Hanisch, C.; Mayor, M.; Zharnikov, M. *J. Phys. Chem. B* **2006**, *110*, 4307.

(44) Shaporenko, A.; Adlkofer, K.; Johansson, L. S. O.; Tanaka, M.; Zharnikov, M. *Langmuir* **2003**, *19*, 4992.

(45) Horsley, J. A.; Stöhr, J.; Hitchcock, A. P.; Newbury, D. C.; Johnson, A. L.; Sette, F. *J. Chem. Phys.* **1985**, *83*, 6099.

(46) Yokoyama, T.; Seki, K.; Morisada, I.; Edamatsu, K.; Ohta, T. *Phys. Scripta* **1990**, *41*, 189.

(47) Solomon, J. L.; Madix, R. J.; Stöhr, J. *Surf. Sci.***1991**, *255*, 12.

(48) Frey, S.; Stadler, V.; Heister, K.; Eck, W.; Zharnikov, M.; Grunze, M.; Zeysing, B.; Terfort, A. *Langmuir* **2001**, *17*, 2408.

(49) Shaporenko, A.; Heister, K.; Ulman, A.; Grunze, M.; Zharnikov, M. *J. Phys. Chem. B* **2005**, *109*, 4096.

(50) Shaporenko, A.; Rößler, K.; Lang, H.; Zharnikov, M. *J. Phys. Chem. B* **2006**, *110*, 24621.

(51) Poirier, G. E. *Chem. Rev.* **1997**, *97*, 1117.

(52) Schreiber, F. *Prog. Surf. Sci.* **2000**, *65*, 151.

(53) Donhauser, Z. J.; Mantooth, B. A.; Kelly, K. F.; Bumm, L. A.; Monnell, J. D.; Stapleton, J. J.; Price, D. W.; Rawlett, A. M.; Allara, D. L.; Tour, J. M.; Weiss, P. S. *Science* **2001**, *292*, 2303.

3.1.1 Supporting Information:

DFT calculations

The structures **1** and **2** (Figure S1 and S2) are relaxed in the gas phase by means of DFT calculations performed within the local density approximation using the VWN functional. A double numerical basis set with polarization functions (DNP) is employed. The DFT algorithm is provided by the program Dmol (Accelrys, San Diego).

From the relaxed geometry of **1**, the molecular dimensions, i.e. the thiol-thiol distance (width) and the molecular height, roughly corresponding to the distance between the central hydrogen on the phenyl and the hydrogen on the methylene, are determined. Including the atomic radius, we obtain a width of 8.23 Å and a height of 8.74 Å. Note that molecule **1** is smaller in size in the direction perpendicular to the plane of the phenyl ring, and this could affect the overall monolayer structure. However, either an asymmetry in the shape of the molecular features or a lateral stacking behavior within the monolayer could not be observed in the STM micrographs.

Upon relaxation, **2** forms a folded structure whose molecular dimensions, due to the different possible conformational isomers, are not as clearly defined as in case of structure **1**. At the surface, the molecule is assumed to coordinate mostly with the two terminal thiol groups to Au (bidentate). Since the interaction with the Au surface will have an impact on the molecular structure, the calculated distances represent a first approximation to the real structure of the adsorbed molecule. The average molecular size from this calculation (including H-radius) is ~12 Å (Figure S2). In the stretched form, compound **2** forms a stable structure (Figure S3), whose length is 21.5 Å (including H-radius). Thus, in the monolayer it would protrude by a length of ~10 Å from the matrix consisting of looped trimers.

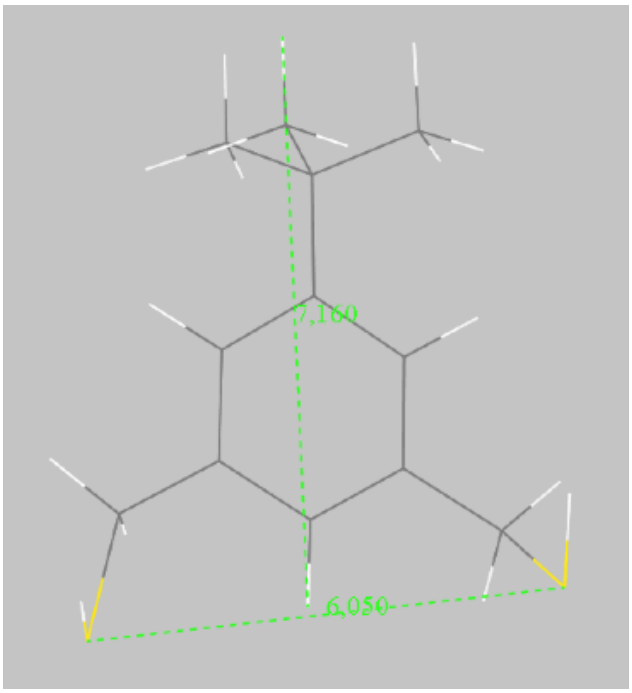

Figure S1. Molecular structure of **1** as determined from DFT calculations in the gas phase. The distances represent the lateral and vertical molecular dimensions in Å.

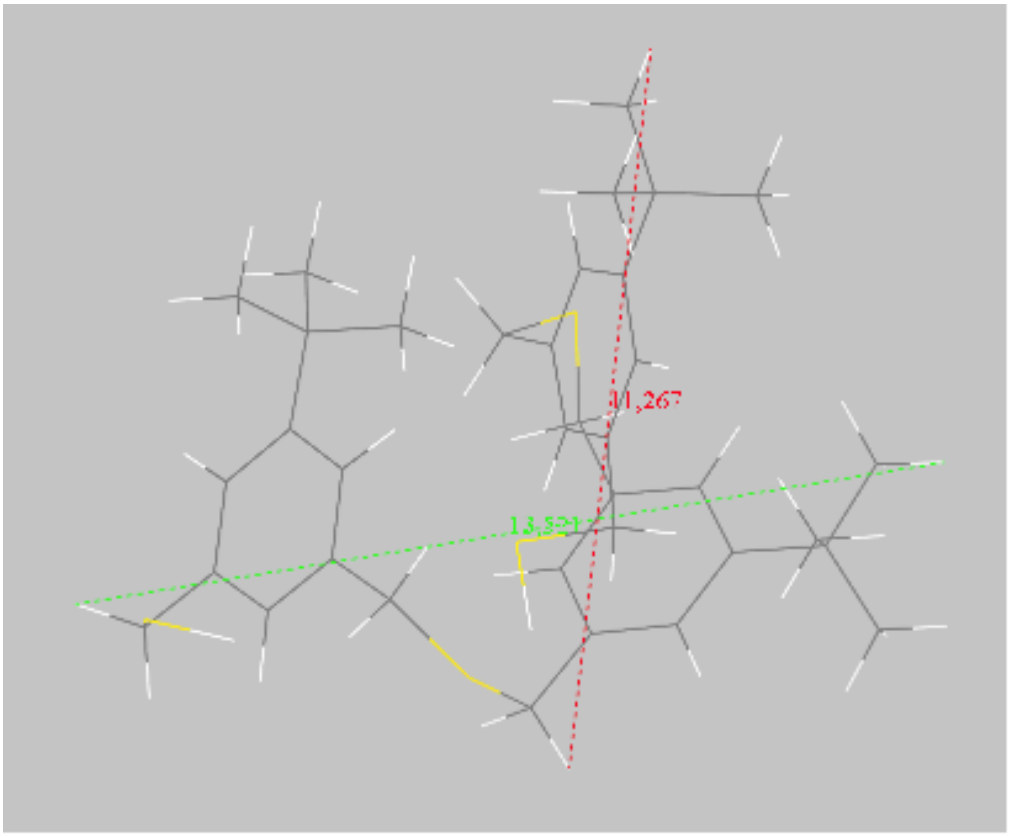

Figure S2. Folded molecular structure of **2** as determined from DFT calculations in the gas phase. The distances represent the lateral and vertical molecular size in Å. The molecular dimensions along the three Cartesian axes are 11.26 Å, 13.52 Å and 7.8 Å (perpendicular to the plane).

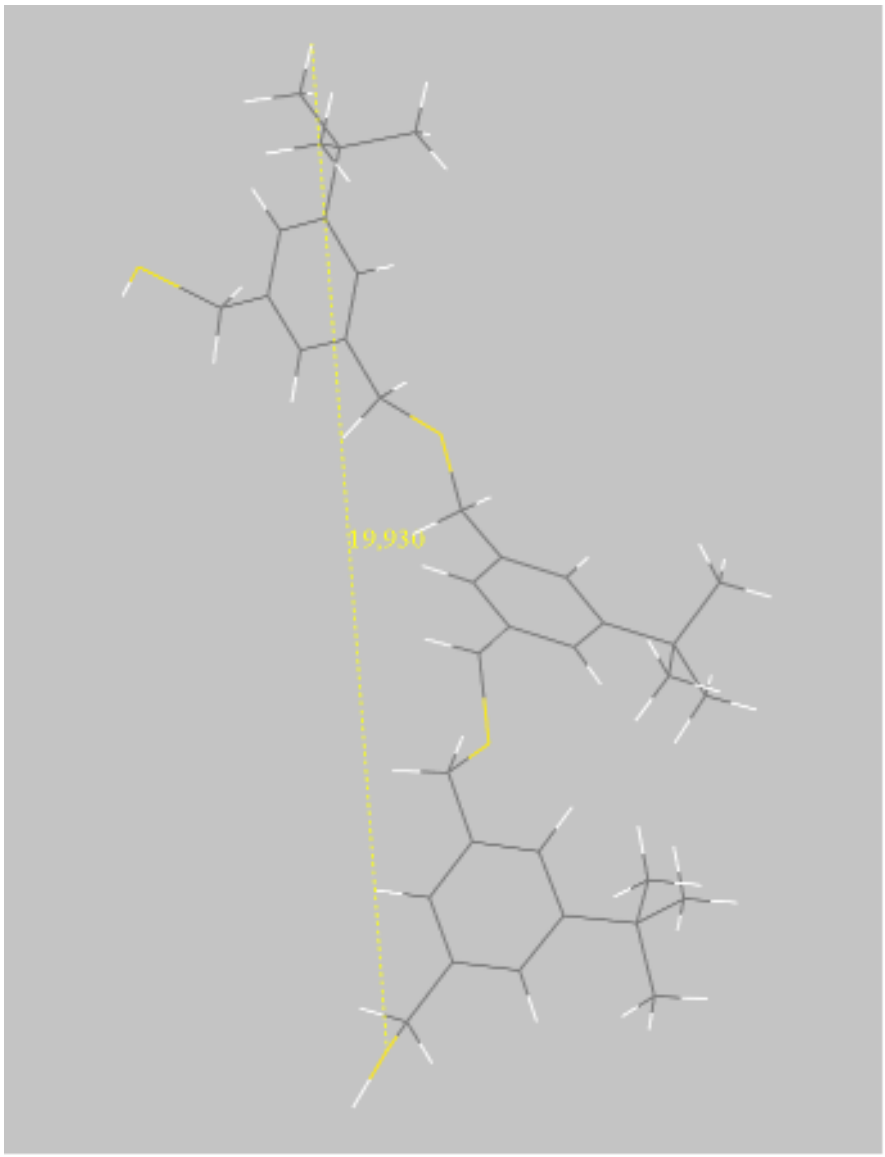

Figure S3. Unfolded molecular structure of **2** as determined from DFT calculations in the gas phase. The length of the relaxed extended structure (from the S atom of the first thiolate to the H atom at the opposite end of **2**) is 19.9 Å.

Sample preparation

Polycrystalline Au substrates are realized by thermal evaporation (pressure: 5×10^{-6} mbar) of 100 nm Au on freshly cleaved mica substrates. Atomically flat Au(111) surfaces are obtained by flame annealing of the substrates in a butane flame followed by quenching in methanol. The monolayers are prepared in argon environment with the immersion of the Au(111) surfaces into a solution of **1** in ethanol and **2** in dichloromethane for 24 h at room temperature. Subsequently, the quality of the resulting SAMs is verified by XPS analysis upon direct transfer (in a sealed box) from the Glove-box into the UHV measurement chamber.

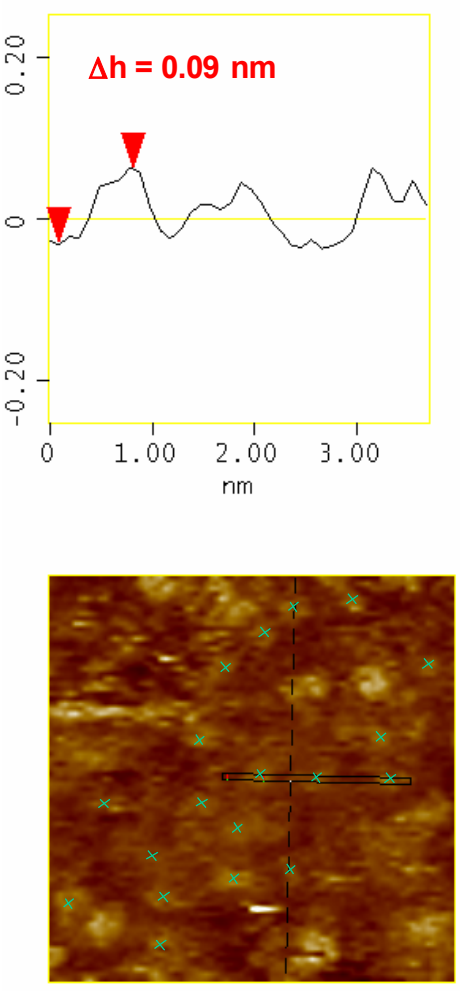

Figure S4. Zoom image from the STM scan in Figure 8 showing monolayers of compound **2** (range: 8×8 nm^2). The dark features observed in the monolayers are indicated by green crosses. The graph shows a section along three of these features, as indicated by the black rectangle in the image (the section is an average of several scan lines). The scans are acquired at $I_t = 2$ pA and $U_g = 500$ mV.

Wrochem, F.; Scholz, F.; Schreiber, A.; Nothofer, H.-G.; Ford, W. E.; Morf, P.; Jung, T.; Yasuda, A.; Wessels, J. M. *Langmuir* **2008**, *24*, 6910-6917.

Materials and reagents

Solvents and reagents

Reagents were used as received from *Fluka AG* (Buchs, Switzerland), *Acros AG* (Basel, Switzerland), *Merck* (Darmstadt, Germany) and *Aldrich* (Buchs, Switzerland). Solvents for chromatography and extractions were of technical grade and were distilled prior to use. Dry solvents used for reactions corresponded to the quality *puriss p. a., abs., over Molecular Sieves* from *Fluka AG*. For an inert atmosphere *Argon 4.8* from *PanGas AG* (Dagmersellen, Switzerland) was used.

NMR spectroscopy

Nuclear magnetic resonance (NMR) spectra were recorded using a *Bruker* DPX-NMR (400 MHz for ^{1}H and 100 MHz for ^{13}C) at ambient temperature in the solvents indicated. Solvents for NMR were obtained from *Cambridge Isotope Laboratories* (Andover, MA, USA). Chemical shifts are given in ppm relative to tetramethylsilane (TMS). The spectra are referenced to the residual proton signal of the deuterated solvent ($CDCl_3$: 7.26 ppm) for 1H spectra or the carbon signal of the solvent ($CDCl_3$: 77.0 ppm, CD_2Cl_2: 55.8 ppm, DMSO-d_6: 39.5 ppm) for ^{13}C spectra. The coupling constants (J) are given in Hertz (Hz), the multiplicities are denoted as: *s* (singlet), *d* (duplet), *t* (triplet), *q* (quartet), *m* (multiplet) and *br* (broad).

Matrix-assisted laser desorption/ionization-time of flight (MALDI-ToF)

Mass spectra were performed on a *Applied Bio Systems Voyager-De™ Pro* mass spectrometer using 1,8,9-anthracenetriol or α-cyano-4-hydroxycinnamic acid as matrix. Important signals are given in mass units per charge (*m/z*), the fragments and intensities are given in brackets.

Elemental analysis (EA)

Elemental analyses were carried out by W. Kirsch on a *Perkin-Elmer Analysator 240.* The values are given in mass percent.

Melting points (MP)

Melting points (MP) were determined in °C using a *Stuart SMP3* apparatus and are uncorrected.

Column Chromatography

For preparative separations by column chromatography, silica gel 60 from *Fluka* (0.043-0.06 mm) was used.

(5-*tert*-Butyl-1,3-phenylene)dimethanethiol (1)

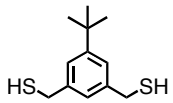

$C_{12}H_{18}S_2$

226.40 g/mol

A solution of 1,3-bis(bromomethyl)-5-*tert*-butylbenzene (**6**) (3.00 g, 9.3 mmol, 1 eq) and thiourea (1.77 g, 23.3 mmol, 2.5 eq) in dry dimethyl sulfoxide (40 ml) under an atmosphere of argon was left stirring for 15 h at room temperature. The mixture was poured into an ice cooled aqueous sodium hydroxide solution (1m, 50 ml), which was then acidified with 1m hydrochloric acid. The mixture was extracted with dichloromethane three times and the combined organic fractions were washed once with water. The crude product was obtained after drying over magnesium sulfate, filtration and evaporation to dryness. After purification by kugelrohr distillation (2×10^{-1} mbar, 195°C), the pure title compound **1** was obtained as a colorless solid. 1.34 g, 6.0 mmol, 64%.

^{1}H NMR (400 MHz, $CDCl_3$): ∂ = 7.22 (*br*, 2H, Aryl-*H*), 7.14 (*br*, 1H, Aryl-*H*), 3.74 (*d*, J = 7.5 Hz, 4H, C*H*$_2$), 1.79 (*t*, J = 7.5 Hz, 2H, S*H*), 1.33 (*s*, 9H, C(C*H*$_3$)$_3$).

^{13}C NMR (100 MHz, $CDCl_3$): ∂ = 152.1, 141.1, 124.8, 123.8, 34.7, 31.3, 29.1.

5,5'-(5-*tert*-Butyl-1,3-phenylene)bis(methylene)bis(sulfanediyl)bis(methylene)bis(3-*tert*-butyl-5,1-phenylene)dimethanethiol (2)

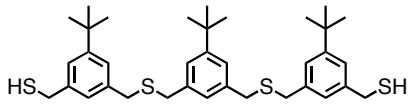

$C_{36}H_{50}S_4$

611.04 g/mol

The trityl protected trimer **8** (557 mg, 0.51 mmol, 1 eq) was dissolved in 8 ml dichloromethane. Triethylsilane (220 µl, 160.6 mg, 1.38 mmol, 2.7 eq) was added, followed by trifluoroacetic acid (320 µl, 4% of the dichloromethane volume). The mixture turned yellow and became colorless again after approx. 2 minutes. Stirring was continued for a further 10 minutes before the reaction was quenched with a saturated sodium bicarbonate solution. The two phases were separated and the aqueous phase was extracted twice with dichloromethane. The combined organic fractions were dried over magnesium sulfate, filtrated and evaporated to dryness. The product was purified by column chromatography hexane/dichloromethane 1:2), to give the dithiol trimer **2** as a colorless solid. 312 mg, 0.51 mmol, quant.

EA: found: C 70.44%, H 8.33%

required: C 70.76%, H 8.25%

^{1}H NMR (400 MHz, $CDCl_3$): ∂ = 7.20 (*br*, 6H, Aryl-*H*), 7.08 (*br*, 3 H, Aryl-*H*), 3.72 (*d*, J = 7.5 Hz, 4H, C*H*$_2$), 3.62 – 3.60 (*m*, 8H, C*H*$_2$), 1.72 (*t*, J = 7.5, 2H, S*H*), 1.33 (*s*, 9H, C(C*H*$_3$)$_3$), 1.31 (*s*, 18H, C(C*H*$_3$)$_3$).

^{13}C NMR (100 MHz, $CDCl_3$): ∂ = 151.86, 151.62, 140.89, 138.19, 137.94, 126.80, 125.83, 124.80, 124.73, 123.77, 35.97, 35.88, 34.69, 34.65, 31.39, 31.35, 29.11.

MS (MALDI-ToF, *m/z*): 633.6 [*M*+Na]$^+$.

MP: 73.9°C.

5,5'-(5,5'-(5-*tert*-Butyl-1,3-phenylene)bis(methylene)bis(sulfanediyl)bis(methylene)bis(3-*tert*-butyl-5,1-phenylene)bis(methylene)bis(sulfanediyl)bis(methylene))bis(3-*tert*-butyl-5,1-phenylene)dimethanethiol (3)

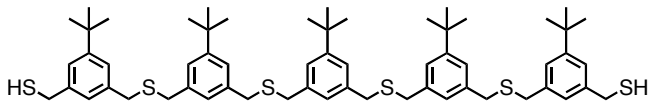

$C_{60}H_{82}S_6$

995.68 g/mol

The trityl protected pentamer **9** (563.9 mg, 0.38 mmol, 1 eq) was dissolved in 6 ml dichloromethane. Triethylsilane (160 µl, 115.2 mg, 1.00 mmol, 2.6 eq) was added, followed by trifluoroacetic acid (240 µl, 4% of the dichloromethane volume). The mixture turned yellow and became colorless again after approx. 2 minutes. Stirring was continued for a further 10 minutes before the reaction was quenched with a saturated sodium bicarbonate solution. The two phases were separated and the aqueous phase was extracted twice with dichloromethane. The combined organic fractions were dried over magnesium sulfate, filtered and evaporated to dryness. The product was purified by column chromatography (hexane/dichloromethane 1:2), to give the dithiol pentamer **3** as a colorless solid. 375.5 mg, 0.38 mmol, 99%.

EA: found: C 72.24%, H 8.34%

required: C 72.38%, H 8.30%

^{1}H NMR (400 MHz, $CDCl_3$): ∂ = 7.21 – 7.18 (*m*, 10H, Aryl-*H*), 7.11 – 7.06 (*m*, 5H, Aryl-*H*), 3.71 (*d*, J = 7.5 Hz, 4H, CH_2), 3.63 – 3.57 (*m*, 16H, CH_2), 1.76 (*t*, J = 7.5, 2H, S*H*), 1.33 – 1.29 (*m*, 45H, C(CH_3)$_3$).

^{13}C NMR (100 MHz, $CDCl_3$): ∂ = 151.8, 151.6, 140.9, 138.2, 138.0, 126.8, 125.8, 124.8, 124.7, 123.8, 36.0 (2×), 35.9, 34.7, 34.6, 31.4 (2×), 29.1.

MS (MALDI-ToF, *m/z*): 1017.9 [*M*+Na]$^+$.

MP: 107.5 °C.

5,5'-(5,5'-(5,5'-(5-*tert*-Butyl-1,3-phenylene)bis(methylene)bis(sulfanediyl)bis(methylene)-bis(3-*tert*-butyl-5,1-phenylene)bis(methylene)bis(sulfanediyl)bis(methylene))bis(3-*tert*butyl-5,1-phenylene)bis(methylene)bis(sulfanediyl)bis(methylene))bis(3-*tert*-butyl-5,1-phenylene)dimethanethiol (4)

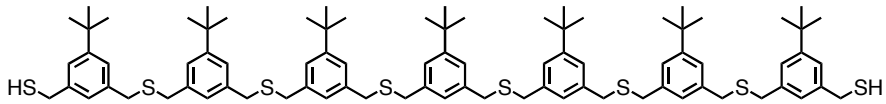

$C_{84}H_{114}S_8$

1380.32 g/mol

The trityl protected heptamer **9** (295.7 mg, 0.16 mmol, 1 eq) was dissolved in 4 ml dichloromethane. Triethylsilane (101 µl, 73.5 mg, 0.63 mmol, 4 eq) was added, followed by trifluoroacetic acid (160 µl, 4% of the dichloromethane volume). The mixture turned yellow and became colorless again after approx. 2 minutes. Stirring was continued for a further 10 min, before the reaction was quenched with a saturated sodium bicarbonate solution. The two phases were separated and the aqueous phase was extracted twice with dichloromethane. The combined organic fractions were dried over magnesium sulfate, filtrated and evaporated to dryness. The product was purified by column chromatography (hexane/dichloromethane 1:1), to give the dithiol heptamer **4** as a colorless solid. 215.9 mg, 0.16 mmol, 99%.

EA: found: C 73.00%, H 8.31%

required: C 73.09%, H 8.32%

^{1}H NMR (400 MHz, $CDCl_3$): ∂ = 7.21 – 7.17 (*m*, 14H, Aryl-*H*), 7.11 – 7.06 (*m*, 7H, Aryl-*H*), 3.71 (*d*, J = 7.5 Hz, 4H, CH_2), 3.62 – 3.57 (*m*, 24H, CH_2), 1.76 (*t*, J = 7.5, 2H, S*H*), 1.33 – 1.29 (*m*, 63H, C(CH_3)$_3$).

^{13}C NMR (100 MHz, $CDCl_3$): ∂ = 151.8, 151.6, 140.9, 138.2, 138.0, 126.8, 125.8, 124.8, 124.7, 123.8, 36.0, 35.9, 34.7, 34.6, 31.4 (2×), 29.1.

MS (MALDI-ToF, *m/z*)): 1401.1 [*M*+Na]$^+$.

MP: 131.0°C.

1,3-Bis(bromomethyl)-5-*tert*-butylbenzene (6)

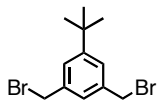

$C_{12}H_{16}Br_2$

320.06 g/mol

N-Bromosuccinimide (30.17 g, 170 mmol, 2.1 eq) and 5-*tert*-butyl-*m*-xylene (15.0 ml, 12.98 g, 80 mmol, 1 eq) were dissolved in methyl formate (150 ml). 2,2'-Azobis(2-methylpropionitrile) (75 mg) was then added and the reaction mixture was illuminated by a 500 W halogen lamp for 3 hours. The solvent was evaporated under reduced pressure and the residue was redissolved in dichloromethane. The organic solution was washed twice with a saturated aqueous solution of sodium hydrogen carbonate and then once with water. After drying over magnesium sulfate, the solvent was removed by evaporation. The residue was recrystallized from dichloromethane/hexane twice to give 1,3-bis(bromomethyl)-5-*tert*-butylbenzene (**6**) as colorless crystals. 18.02 g, 56.3 mmol, 70%.

^{1}H NMR (400 MHz, $CDCl_3$): ∂ = 7.34 (*br*, 2H, Aryl-*H*), 7.27 (*br*, 1H, Aryl-*H*), 4.49 (*s*, 4H, C*H*$_2$), 1.34 (*s*, 9H, C(C*H*$_3$)$_3$).

^{13}C NMR (100 MHz, $CDCl_3$): ∂ = 153.0, 138.4, 127.3, 126.7, 35.2, 33.9, 31.6.

(3-(Bromomethyl)-5-*tert*-butylbenzyl)(trityl)sulfane (7)

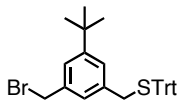

$C_{31}H_{31}BrS$

515.55 g/mol

1,3-Bis(bromomethyl)-5-*tert*-butylbenzene (**6**) (1.00 g, 3.1 mmol, 1 eq) and triphenylmethanethiol (863 mg, 3.1 mmol, 1 eq) were dissolved in 20 ml dry tetrahydrofuran under an atmosphere of argon. Potassium carbonate (650 mg, 4.7 mmol, 1.5 eq) was added and the mixture was heated to reflux for 20 hours. After cooling to room temperature, 100 ml water was added and the mixture was extracted three times with 50 ml MTBE. The combined organic fractions were washed with brine, dried over magnesium sulfate and evaporated to dryness. After purification by column chromatography (hexane/dichloromethane 4:1), the product **7** was obtained as colorless solid. 818 mg, 1.6 mmol, 51%.

EA: found: C 71.92%, H 6.20%

required: C 72.22%, H 6.06%

^{1}H NMR (400 MHz, $CDCl_3$): ∂ = 7.49 – 7.44 (*m*, 6H, Aryl-*H*, Trt-*H*), 7.35 – 7.20 (*m*, 10H, Trt-*H*), 7.03 (*s*, 1H, Aryl-*H*), 6.95 (*s*, 1H, Aryl-*H*), 4.43 (*s*, 2H, CH_2), 3.33 (*s*, 2H, CH_2), 1.27 (*s*, 9H, C(CH_3)$_3$).

^{13}C NMR (100 MHz, CDCl3): ∂ = 151.97, 144.65, 137.50, 137.46, 129.65, 127.94, 126.82, 126.72, 126.30, 124.81, 67.60, 36.95, 34.65, 33.95, 31.23.

MS (MALDI-ToF, *m/z*): 537.0 [*M*+Na]$^+$.

MP: 140.1°C.

(5-*tert*-Butyl-1,3-phenylene)bis(methylene)bis((3-*tert*-butyl-5-(tritylthiomethyl)benzyl)sulfane) (8)

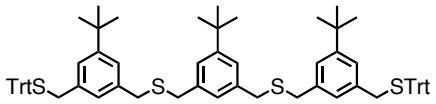

$C_{76}H_{78}S_4$

1095.67 g/mol

(5-*tert*-Butyl-1,3-phenylene)dimethanethiol (**1**) (154 mg, 0.68 mmol, 1 eq) and (3-(bromomethyl)-5-*tert*-butylbenzyl)(trityl)sulfane (**7**) (700 mg, 1.36 mmol, 2 eq) were dissolved in 40 ml dry tetrahydrofuran under an atmosphere of argon. Sodium hydride (60% in mineral oil, 135 mg, 3.3 mmol, 5 eq) was added and the mixture was stirred for 2 hours at room temperature. The reaction was quenched with water and extracted with MTBE three times. The combined organic fractions were washed with brine, dried over magnesium sulfate and evaporated to dryness. Purification of the crude product was achieved by column chromatography (hexane/dichloromethane 3:2) to yield the trityl protected trimer as colorless foam.

708 mg, 0.65 mmol, 96 %.

EA: found: C 81.10%, H 7.25%

required: C 81.12%, H 7.18%

^{1}H NMR (400 MHz, $CDCl_3$): ∂ = 7.49 – 7.44 (*m*, 12H, Trt-*H*), 7.32 – 7.27 (*m*, 12 H, Trt-*H*), 7.24 – 7.19 (*m*, 6H, Trt-*H*), 7.16 (*br*, 2H, Aryl-*H*), 7.13 (*br*, 2H, Aryl-*H*), 7.04 (*br*, 1H, Aryl-*H*), 6.98 (*br*, 2H, Aryl-*H*), 6.90 (*br*, 2H, Aryl-*H*), 3.55 (*s*, 4H, CH_2), 3.54 (*s*, 4H, CH_2), 3.30 (*s*, 4H, CH_2), 1.29 (*s*, 9H, C(CH_3)$_3$), 1.26 (*s*, 18H, C(CH_3)$_3$).

^{13}C NMR (100 MHz, $CDCl_3$): ∂ = 151.5, 144.7, 138.0, 137.9, 137.0, 129.7, 128.0, 126.8, 126.7, 124.8, 124.7, 67.5, 37.2, 35.9, 34.6 (2×), 31.4, 31.3.

MS (MALDI-ToF, *m/z*): 1033.3 $[M+K]^+$.

MP: 70.0°C.

(5-*tert*-Butyl-1,3-phenylene)bis(methylene)bis((3-*tert*-butyl-5-((3-*tert*-butyl-5-(tritylthiomethyl)benzylthio)methyl)benzyl)sulfane) (9)

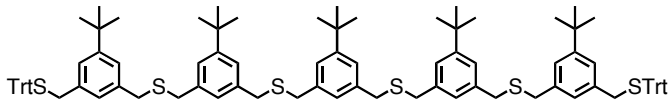

$C_{98}H_{110}S_6$

1480.31 g/mol

The dithiol trimer **2** (227.0 mg, 0.37 mmol, 1 eq) and (3-(bromomethyl)-5-*tert*-butylbenzyl)(trityl)sulfane (**7**) (421.4 mg, 0.82 mmol, 2.2 eq) were dissolved in 20 ml dry tetrahydrofuran under an atmosphere of argon. Sodium hydride (60% in mineral oil, 60 mg, 1.5 mmol, 4 eq) was added and the mixture was stirred for 1.5 hours at room temperature. The reaction was quenched with water and extracted three times with MTBE. The combined organic fractions were washed with brine, dried over magnesium sulfate and evaporated to dryness. Purification of the crude product was achieved by column chromatography (hexane/dichloromethane 3:2) to yield the trityl protected pentamer **9** as a colorless foam. 525.5 mg, 0.36 mmol, 97 %.

EA: found: C 79.57%, H 7.64%

required: C 79.52%, H 7.49%

^{1}H NMR (400 MHz, $CDCl_3$): ∂ = 7.50 – 7.44 (*m*, 12H, Trt-*H*), 7.33 – 7.27 (*m*, 12H, Trt-*H*), 7.24 – 7.19 (*m*, 6H, Trt-*H*), 7.18 – 7.05 (*m*, 11H, Aryl-*H*), 6.98 (*br*, 2H, Aryl-*H*), 6.90 (*br*, 2H, Aryl-*H*), 3.60 – 3.54 (*m*, 16H, CH_2), 3.31 (*s*, 4H, CH_2), 1.32 – 1.24 (*m*, 45H, C(CH_3)$_3$).

^{13}C NMR (100 MHz, $CDCl_3$): ∂ = .151.5, 144.7, 138.0, 137.9, 137.0, 129.7,127.9. 126.8, 126.7, 126.6, 124.8, 124.7, 67.5, 37.2, 36.0, 35.9, 34.6 (2∂), 31.3 (2×).

MS (MALDI-ToF, *m/z*): 1017.9 [M – (2×Trt) + Na]$^+$, 1518.2 [M+K]$^+$.

MP: 71.2°C.

(5-*tert*-Butyl-1,3-phenylene)bis(methylene)bis((3-*tert*-butyl-5-((3-*tert*-butyl-5-((3-*tert*butyl-5-(tritylthiomethyl)benzylthio)methyl)benzylthio)methyl)benzyl)sulfane) (10)

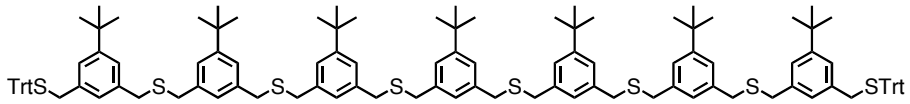

$C_{122}H1_{42}S_8$

1864.95 g/mol

The dithiol pentamer **3** (365.0 mg, 0.37 mmol, 1 eq) and 1(3-(bromomethyl)-5-*tert*-butylbenzyl)(trityl)sulfane (**7**) (416.1 mg, 0.81 mmol, 2.2 eq) were dissolved in 20 ml dry tetrahydrofuran under an atmosphere of argon. Sodium hydride (60% in mineral oil, 140 mg, 3.5 mmol, 9.5 eq) was added and the mixture was stirred for 2.5 hours at room temperature. The reaction was quenched with water and extracted with MTBE three times. The combined organic fractions were washed with brine, dried over magnesium sulfate and evaporated to dryness. Purification of the crude product was achieved by column chromatography (hexane/dichloromethane 2:3) to yield the trityl protected heptamer **10** as a colorless solid. 624.3 mg, 0.34 mmol, 92 %.

EA: found: C 78.50%, H 7.80%

required: C 78.57%, H 7.67%

^{1}H NMR (400 MHz, $CDCl_3$): ∂ = 7.50 – 7.44 (*m*, 12H, Trt-*H*), 7.33 – 7.27 (*m*, 12H, Trt-*H*), 7.25 – 7.06 (*m*, 23 H, Aryl-*H*, Trt-*H*), 6.99 (*br*, 2H, Aryl-*H*), 6.91 (*br*, 2H, Aryl-*H*), 3.62 – 3.54 (*m*, 24H, CH_2), 3.31 (*s*, 4H, CH_2), 1.34 – 1.26 (*m*, 63H, C(CH_3)$_3$).

^{13}C NMR (100 MHz, $CDCl_3$): ∂ = .151.5, 144.72, 138.0, 137.9, 137.0, 129.7, 127.9, 126.8, 126.7, 124.8, 124.7, 67.5, 37.2, 36.0, 35.9, 34.6 (2×), 31.4, 31.3.

MS (MALDI-ToF, *m/z*): 1901.8 $[M+K]^+$.

MP: 71.5°C.

Add a Third Hook: S-Acetyl Protected Oligophenylene Pyridine Dithiols as Advanced Precursors for Self-Assembled Monolayers

Fabian Sander,[a] Jens Peter Hermes,[a] Marcel Mayor[a,b], Hicham Hamoudi[c] and Michael Zharnikov*[c]*

Self-assembled monolayers (SAMs) of thiols on gold substrates are potentially important systems for future technologies such as molecular electronics and sensing. Especially in molecular electronics a strong interaction and coupling between the "device" molecules and substrate is crucial. In this context, we present here two series of novel SAM precursors, viz. bidentate oligophenylenes with either 1,3-phenylenedimethanethiol or pyridine-2,6-diyldimethanethiol anchoring group. Both series are shown to form densely packed monolayers with a low level of contamination and a high orientational order that are additionally promoted by the interaction between the terminal pyridine moiety and the substrate in the second series. At the same time, most of the SAM constituents do not exhibit a strictly bidentate bonding to the substrate – whereas one anchor group has a thiolate-type bonding, the other is weakly coordinated, unbound, or participating in a disulfide bridge with the adjacent molecules. We believe that such a bonding heterogeneity stems from the fundamental problems of molecular self-assembly in the given case.

1 Introduction

Preparation of self-assembled monolayers (SAMs) is a powerful and relatively simple way to arrange molecules on surfaces in a well-controlled fashion. The molecules have to feature a chemical functionality with a high affinity towards the target surface that provides the anchoring of the molecule to the substrate and a geometry that drives molecular assembly and allows the spontaneous formation of two dimensional (2D) crystalline structures. Because of the high affinity of thiols towards the surfaces of coinage metals, the most extensively studied SAM systems are based on the strong chemisorption of organic thiols onto gold,

silver, and copper. Molecules carrying a functional tail group give access to functional SAMs that provide a broad range of applications like electrode modification,[1] biosensors,[2] molecular machines[3] as well as molecular electronic components and devices.[4]

With increasing complexity of the SAM constituents, which is frequently required in view of specific applications, the problem occurs that these species demand too much space and are not able to pack into dense 2D monolayers. One way to overcome this difficulty is to use statistical mixtures of short non-substituted molecules and longer SAM constituents bearing a bulky functional tail group; by this way the latter species can be imbedded into the "background" comprised of the former ones so that the sterical constraints are released.[5] Another approach to solve this issue is to use multidentate anchor groups that cover more space on the surface than a single anchor group typical of most of the SAM precursors. This architecture provides more space for sterically demanding functional tail groups and has, potentially, the additional advantage of a more stable connection to the surface by multiple binding sites. Therefore bi-, tripods[6–8] and more complex[9,10] precursors were synthesized, including benzyl dithiols and dimethanethiols,[11–17] and used to form SAMs. Unfortunately, the results on these systems are quite controversial and, in most cases, these molecules were not able to pack in homogeneous fashion and/or as dense and highly orientated on the surface as desired. However, as reviewed recently there is still a high potential for design and application of SAM systems with multidentate anchor groups.[18] As SAMs on gold are also suitable model systems to study the binding properties of model compounds to the surface, they can also be used for a better understanding of molecules stabilizing metal nanoparticles (NPs). With this goal in mind and in view of particular interest in pyridine subunits as a building block of NP stabilizers,[19,20] we focus here on the binding and self assembly of bidentate oligophenylene benzyl (OPB) and oligophenylene pyridine (OPP) derivatives on gold substrates (Figure 1).

As SAMs on gold are also suitable model systems to study the binding properties of model compounds to the surface, they can also be used for a better understanding of molecules stabilizing metal nanoparticles (NPs). With this goal in mind and in view of particular interest in pyridine subunits as a building block of NP stabilizers,[19,20] we focus here on the binding and self assembly of bidentate oligophenylene benzyl (OPB) and oligophenylene pyridine (OPP) derivatives on gold substrates (Figure 1). Both series of model compounds are expected to form SAMs with different packing densities and molecular orientations on a gold surface. In particular, due to the hydrogen atom of the benzyl pointing

direct to the substrate, sterical repulsion can force the molecules to a distinctly tilted arrangement. In contrast, the pyridine derivatives comprising an additional binding site, the lone pair of nitrogen, should promote an upright orientation of the molecules or at least result in formation of better packed monolayers because of the lack of the disturbing sterical effects compared to the benzyl derivatives.

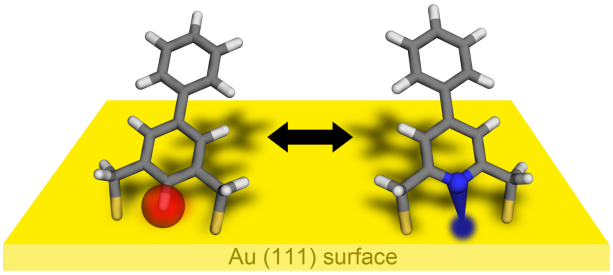

Figure 15. Sketch of possible binding modes of the bidentate phenyl- (left) and pyridine derivatives (right) on a gold substrate. OPBs are tilted due sterical repulsion of the hydrogen atom pointing to the surface. OPPs should bind in a more upright arrangement.

To prove this hypothesis a new series of oligophenylenes and their pyridine derivatives were synthesized (Figure 2) and their SAM forming properties analyzed by two complementary techniques, high resolution X-ray photoelectron spectroscopy (HRXPS) and near-edge X-ray absorption fine structure (NEXAFS) spectroscopy.

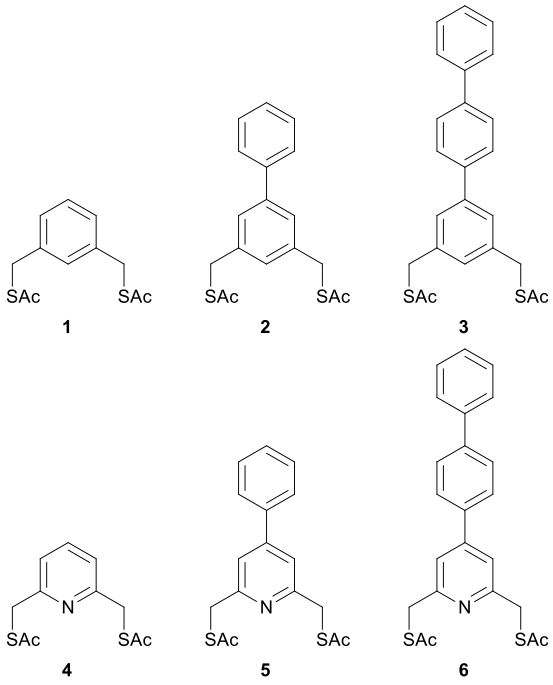

Figure 16. Model compounds of benzyl (**1** – **3**) and pyridine (**4** – **6**) derivatives.

These structures were chosen because oligophenylene provide good stacking properties and should form well-ordered SAMs.

The 1,3 (*meta*) substitution pattern of the benzene and pyridine rings was used since, in contrast to the 1,4 (*para*) or 1,2 (*ortho*) substitutions, it can force an upright geometry of the adjacent ring upon adsorption on coinage metal substrates.[11,13] Also, the introduction of the methylene unit between the anchor groups and the ring was intentional since it gives a better conformational flexibility upon adsorption which is rather restricted if the anchor groups are bonded directly to the ring. In the latter case, no self-assembly is observed.[13,14] The conformational flexibility is necessary to adapt to the substrate and to avoid additional constrains imposed by the most probable sp^3 bonding configuration of the anchor group's sulfur. In particular, the configuration can be preserved if both bound anchor groups have anti conformations with respect to the plane of the "bottom" phenyl ring in the upright standing molecule.[15] So far only the molecules **1** and **3**, even though with the thiol anchor group instead of thioacetates, were tried as SAM precursors. For **1** (with the thiol anchor group), SAM formation with an upright ring orientation was reported on Au and Ag, but the results regarding the exact bonding mode are quite controversial.[11–14,16] For **3** (with the thiol anchor group), formation of densely packed SAMs on Au was reported as well, with both thiol anchor groups bound to the substrate in the thiolate fashion.[15,17]

2 Experimental part

2.1 Synthesis of SAM precursors

To compound **1** commercial available 1,3-bis(bromomethyl)benzene **7** was reacted with potassium thioacetate in tetrahydrofuran (THF) to yield compound **1** as a colorless solid in excellent yields. Compounds **2** and **3** were build up from 1-bromo-3,5-dimethylbenzene **8** (Scheme 1) that was first brominated in a radical reaction with N-bromosuccinimide (NBS) and azobisisobutyronitrile (AIBN) as radical starter in methylformate to the dibromine **9**[21] followed by a S_N2 reaction with potassium thioacetate in THF to get compound **10** in excellent yields.[22] Both oligophenylenes **2** and **3** are Suzuki coupling products from **10** with the corresponding phenyl- and biphenyl boronic acid. For the coupling the Buchwald ligand 2-dicyclohexylphosphino-2',6'-dimethoxybiphenyl (S-Phos) was used with palladium acetate ($Pd(OAc)_2$) and potassium phosphate as base in toluene. To overcome the low reactivity of the starting material the reaction was performed under microwave irradiation at 160 ºC in toluene. Both desired compounds **2** and **3** were obtained as colorless solids in acceptable yields.[23,24] To synthesize compound **4** the commercial available 2,6-bis(bromomethyl)

pyridine **11** was reacted with potassium thioacetate in the same manner as for **1** to obtain the product as a white solid in excellent yield. For the structures **5** and **6** the synthesis was started from chelidamic acid **12** (Scheme 1) that was brominated with phosphorus pentabromide and then quenched with ethanol to yield the diethyl 4-bromopyridine-2,6-dicarboxylate **13**.[25] Subsequent reduction with sodium borohydride in methanol to the diol **14**, followed by bromination with hydrogen bromine and sulfuric acid to the dibromide **15**[26] and conversion with potassium thioacetate in THF gave the dithioacetate **16** in good yields. Again the optimized Buchwald protocol for Suzuki coupling was applied under microwave irradiation with the corresponding phenyl and biphenyl boronic acid to form the final structures **5** and **6** as white solids in acceptable yields. Note that compounds **1**, **3**, and **4** have been synthesized previously by others[24,27,28] but we selected new synthesis routes which appear to be more simple and efficient.

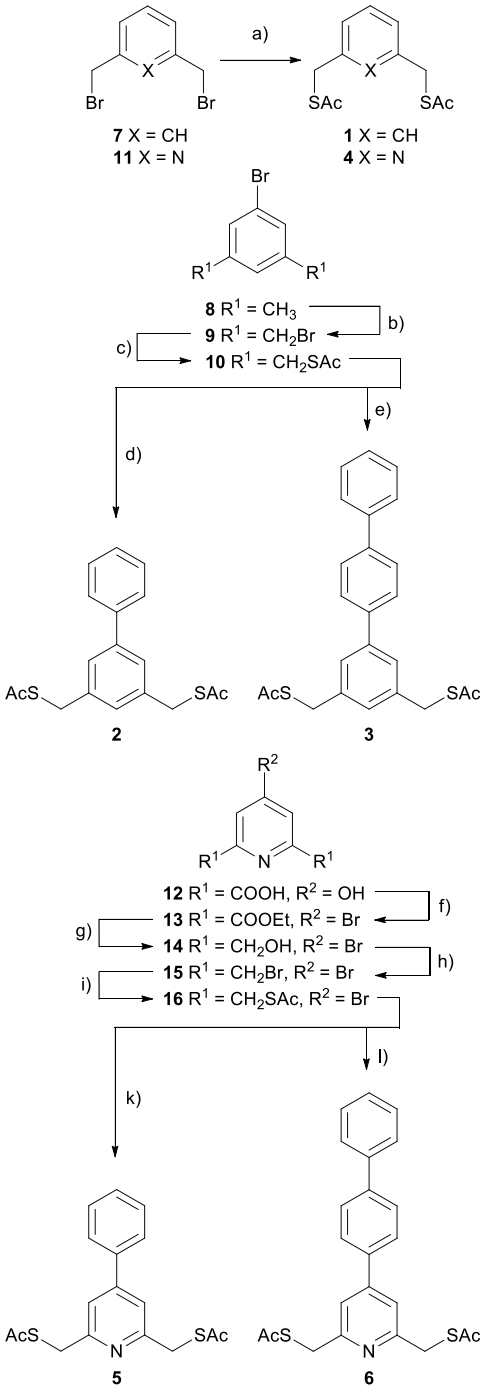

Scheme 1. Synthesis of **1** - **6**; a) KSAc, THF, rt, 18 h, 96 %; b) AIBN, NBS, methylformate, hν, reflux, 18 h, 48 %; c) KSAc, THF, rt, 16 h, 96 %; d) PhB(OH)2, Pd(OAc)2, S-Phos, K3PO4, toluene, microwave, 1 h, 160 ºC, 51 %; e) 4-PhPhB(OH)2, Pd(OAc)2, S-Phos, K3PO4, toluene, microwave, 1 h, 160 ºC, 53 %; f) 1) PBr5, 110 ºC, 1,5 h 2) EtOH, 0 ºC, 79 %; g) NaBH4, EtOH, reflux, 12 h, quant.; h) HBr, H2SO4, reflux, 12 h, 96 %; i) KSAc, THF, rt, 16 h, 96 %; k) PhB(OH)2, Pd(OAc)2, S-Phos, K3PO4, toluene, microwave, 1 h, 160 ºC, 54 %; l) 4-PhPhB(OH)2, Pd(OAc)2, S-Phos, K3PO4, toluene, microwave, 1 h, 160 ºC, 51 %.

2.2 Preparation of SAMs

For SAM formation gold substrates were prepared by thermal evaporation of 200 nm of gold onto polished single crystal silicon (100) wafers (Silicon Sense) primed with a 5 nm titanium adhesion layer. The films were polycrystalline, with a grain size of 20-50 nm as observed by atomic force microscopy and scanning tunneling microscope (STM). The grains predominantly possessed a (111) orientation.[29]

Table 1. Conditions used for in situ deprotection of the acetyl group.

Solvent	Temperature	Deprotection agent
DMF	RT	KOH
EtOH	50 ºC	KOH
CH_2Cl_2	RT	---
DMF	RT	Et_3N
DMF	RT	NH_4OH

The SAMs were formed by immersion of freshly prepared substrates into a 1 mM solution of the target compounds **1** - **6** in absolute dimethylformamide (DMF) at room temperature for 24 h with 3 equivalents of potassium hydroxide (KOH) as base to deprotect the acetyl groups in situ. After immersion, the samples were carefully rinsed with pure DMF, blown dry with nitrogen, and kept, if necessary, for several days in nitrogen filled glass containers until the characterization. Other conditions to form the SAM on the gold surface were tested with varying solvent, temperature, base (Table 1), and immersion time (up to 48 h) but no noticeable improvement in the SAM quality was achieved. Therefore the recorded spectra of those experiments, performed both at the synchrotron and in the home laboratory (see below), are not presented.

As direct references to the target systems of this study, SAMs of non-substituted alkanethiols, viz. dodecanethiolate (DDT) and hexadecanethiolate (HDT) were fabricated. These SAMs were formed by immersion of freshly prepared substrates into 1 mM solution of the target compounds in ethanol for 24 h at room temperature. After immersion, the samples were carefully rinsed with pure ethanol and blown dry with argon.

2.3 Characterization of SAMs

The fabricated films were characterized by synchrotron-based HRXPS and angle-resolved NEXAFS spectroscopy. All experiments were performed at room temperature. Both HRXPS and NEXAFS measurements were carried out under UHV conditions at a base pressure lower than 1.5×10^{-9} mbar. The spectra acquisition time was selected in such a way that no noticeable damage by the primary X-rays occurred during the measurements.[30–33] HRXPS experiments were performed at the bending magnet beamline D1011 at the MAX II storage ring of the MAX-lab synchrotron radiation facility in Lund, Sweden. The spectra were collected using normal emission geometry at a photon energy of 350 eV for the S 2p range and 350 and 580 eV for the C 1s range. In addition, Au 4f spectra were acquired and the O 1s range was monitored. The binding energy (BE) scale of every spectrum was individually calibrated using the Au $4f_{7/2}$ emission line of the Au substrate at 83.95 eV.[34] The energy resolution was better than 100 meV, which is noticeably smaller than the full widths at half maximum (fwhm) of the photoemission peaks addressed in this study.

HRXPS spectra were fitted by symmetric Voigt functions using either a Shirley-type or a linear background, depending on the spectral range and primary photon energy. To fit the S $2p_{3/2,1/2}$ doublets we used a pair of such peaks with the same fwhms, a branching ratio of 2 ($2p_{3/2}/2p_{1/2}$) and a spin-orbit splitting (verified by fit) of ~1.18 eV.[35] The fits were carried out self-consistently: the same peak parameters were used for identical spectral regions. The accuracy of the resulting BE/fwhm values in the case of HRXPS is 0.02-0.03 eV.

The thickness of the target films was determined on the basis of the I_{C1s}/I_{Au4f} intensity ratios, assuming a standard exponential attenuation of the photoelectron signal and using the attenuation lengths reported by Wilkes *et al.*.[36] As calibration references, the DDT/Au and HDT/Au samples of known thickness were used, assuming that these samples have comparable packing densities as the target films.

NEXAFS spectroscopy measurements were performed at the same beamline as the HRXPS experiments. The spectra acquisition was carried out at the C and N K-edges in the partial electron yield mode with retarding voltages of -150 and -300 V, respectively. Linear polarized synchrotron light with a polarization factor of 95% was used. The energy resolution was better than 100 meV. The incidence angle of the light was varied from 90° (*E*-vector perpendicular to the surface) to 20° (*E*-vector near surface normal) to determine the orientational order in the SAMs. This approach is based on the dependence of the cross-section of the resonant photoexcitation process on the orientation of the electric field vector of

the synchrotron light with respect to the molecular orbital of interest (so-called linear dichroism in X-ray absorption).[37]

Raw NEXAFS spectra were normalized to the incident photon flux by division through a spectrum of a clean, freshly sputtered gold sample. The photon energy (PE) scale was referenced to the pronounced π* resonance of highly oriented pyrolytic graphite at 285.38 eV.[38] The effect of variable preparation conditions was mostly tested in the home laboratory using conventional XPS spectroscopy. These measurements were performed using a Mg Kα X-ray source and a LHS 11 analyzer. The spectra acquisition was carried out in normal emission geometry with an energy resolution of ≈0.9 eV. The X-ray source was operated at a power of 260 W and positioned ≈1.5 cm away from the samples.

3 Results

3.1 HRXPS

HRXPS spectra provide quantitative information on the composition, chemical identity and thickness of the aromatic films. C 1s HRXPS spectra of **1** - **6** on Au (**1**/Au – **6**/Au) are presented in Figure 3, along with the corresponding fits by several individual components and a background (see Figure S1 in the Supplementary Information for the spectra of DDT/Au and HDT/Au). As expected, the total intensity of the C1s signal increases with increasing length of the SAM precursor. The spectra are dominated by an intense emission at 284.2 – 284.5 eV for **1**/Au – **3**/Au and at 284.4 – 285.0 eV for **4**/Au – **6**/Au which can be assigned to the aromatic backbone and the aliphatic foots of **1** – **6**.[39–41] In the case of **4**/Au – **6**/Au, this emission is accompanied by an additional peak at a BE of 285.2 eV which can be ascribed to the carbon atoms in the ortho and para positions of the pyridine ring.[42] In accordance with the molecular composition (see Figure 2), this peak has a relatively high spectral weight in the spectrum of **4**/Au, less weight in the spectrum of **5**/Au, and even lower relative intensity in the spectrum of **6**/Au. The above two emissions are the only features observed in the spectra of **4**/Au – **6**/Au. The full deprotection of all thiol anchor groups in these monolayers is proven by the absence of a peak at 287.6 eV, which is characteristic of the carbonyl group. Such a peak is however perceptible in the spectra of **1**/Au and **2**/Au, even though very weak. On one hand, it can be associated with the residual protection groups, but, most probably, it can be related to minor contamination. This light contamination may result from remaining carbon dioxide or carbonyl species on gold surface which were not eliminated by the self-cleaning during the SAM formation. Such residual species are frequently observed

in the case of small SAM precursors analogous to **1**.[39] Obviously, the self-cleaning works better for **4**/Au and **5**/Au as compared to **1**/Au and **2**/Au, which underlines the positive role of the nitrogen's lone pair that causes a stronger binding to the gold surface and thus, increases the self cleaning effect.

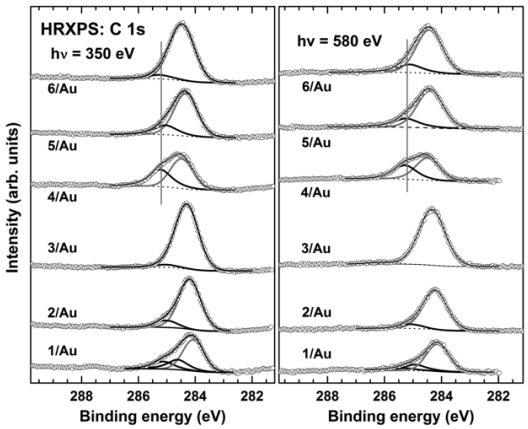

Figure 17. C 1s HRXPS spectra of **1** - **6** on Au acquired at photon energies of 350 eV (left panel) and 580 eV (right panel) along with the corresponding fits by several individual components (see text) and a background. The vertical gray lines are guides for the eye to recognize the weak shoulder.

Along with the major emission, the spectra of **1**/Au – **3**/Au exhibit a weak shoulder at high BE which is typical for thioaromatic SAMs and can be assigned alternatively to the carbon atom bonded to the sulfur anchor group or to shake-up processes in the aromatic matrix.[39] In the case of **1**/Au and, probably, **2**/Au, this shoulder contains also contributions from residual contaminations such as C-O. This is one more evidence that the self-cleaning did not work to the full extent in the case of **1**/Au and **2**/Au.

Along with the analysis of the C 1s HRXPS spectra, they were used to evaluate the effective thickness of the bidentate oligophenylene monolayers. This evaluation was performed on the basis of the C1s/Au4f intensity ratios as described in Section 2. The resulting values of the effective thicknesses are compiled in Table **2** along with the calculated (Spartan 4.1) lengths of the molecules **1** – **6**. In accordance with the molecular composition, the effective thickness of **1**/Au – **3**/Au and **4**/Au – **6**/Au increases with increasing length of the molecular backbone.

Table 2. Estimated molecule lengths of **1**–**6** and film thickness.

	Molecular length, Å[a)]	Film thickness, Å[b)]
1/Au	8	6.6
2/Au	12	9.0
3/Au	16	15.1
4/Au	8	6.6
5/Au	12	9.9
6/Au	16	14.3

[a)] including 2.5 Å for the Au – S bond length; [b)] effective film thickness of **1**/Au – **6**/Au The accuracy of the thickness values is ±1 Å.

The S 2p HRXPS spectra of 1/Au – 6/Au are shown in Figure 4, along with the corresponding fits by the individual components marked as S1 – S3 (see below) and a background. For comparison, the data for DDT/Au and ODT/Au are also presented. The spectra exhibit three distinct S 2p3/2,1/2 doublets S1, S2 and S3 at a BE of ~161.0, ~161.9, and 163.3-162.5 eV (S 2p3/2); the relative weights of these contributions are compiled in Table 3.

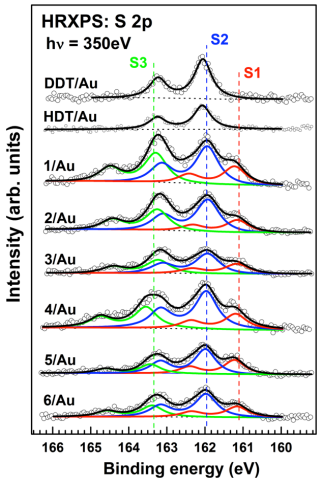

Figure 18. S2p HRXPS spectra of **1**/Au – **6**/Au as well as DDT/Au and HDT/Au (as references). The spectra are decomposed in several individual components, viz. S1 (red), S2 (blue) and, S3 (green); see text for details. The vertical dashed lines are guides for the eye.

No features at higher BE (165.5 – 169.8 eV), characteristic of oxidized sulfur (from SO^- to SO_4^-) were observed. The doublet S2 is typical of thiolate-type bonds which are usually

formed in thiol-derived SAMs as shown here by the example of DDT/Au and HDT/Au.[41] The doublet S1 is frequently observed in the HRXPS spectra of thiol-derived SAMs and can be tentatively assigned to a different type of strong bonding or to atomic sulfur appearing after the cleavage of S-C bond in the SAM constituents (see refs 29 and 31 and references therein). The doublet S3 is typical of physisorbed or disulfide-like sulfur. Whereas S2 is the dominant emission for all the systems under consideration, the presence of S1 and S3 suggests that the SAM-substrate interface is quite heterogeneous and most of the SAM constituents are bound to the substrate by a combination of two different types of bonding.

Table 3. Relative weights of the individual components in the S 2p HRXPS spectra of **1**/Au – **6**/Au

SAM	S1, %	S2, %	S3, %
1/Au	21	45	34
2/Au	18	50	32
3/Au	23	47	30
4/Au	21	51	28
5/Au	30	52	18
6/Au	23	52	25

The character of the S 2p spectra did not change significantly at the different preparation conditions, which are described in Section 2. In particular, we were not able to reproduce the one-component (thiolate) S 2p HRXPS spectrum of 4-methxy-terphenyl-4´´-dimethanethiol monolayer which is very similar to **3**,[15] even if we used the described preparation condition (CH_2Cl_2 , RT). These published data should be considered with care as a quite unusual branching of the S $2p_{3/2}$ and S $2p_{1/2}$ components is displayed in the XPS spectrum. In particular the relative ratios are higher than 2:1 (S $2p_{3/2}$/S $2p_{1/2}$),[15] which is unprecedented in the literature and we cannot think of an explanation for these relative intensities.

The N 1s HRXPS spectra of **4**/Au– **6**/Au, which contain nitrogen, are presented in Figure 5. These spectra display a single emission peak at ~398.7 eV with an intensity similar for all the monolayers under consideration. It is known that for a nitrogen atom in unmodified pyridine molecules the energy can vary from 398.6 to 389.9 eV.[43] Because the value is at the

lower end of the estimated range it can be assumed that the pyridine unit in **4**/Au– **6**/Au is not protonated.

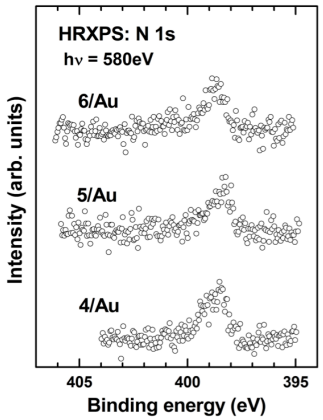

Figure 5. The N 1s HRXPS spectra of **4**/Au– **6**/Au.

Further, a BE of ~398.7 eV is typical for an unbound pyridine which is placed far away from a conductive substrate.[43,44] A gold-bound pyridine is believed to have a higher BE around 399.5 or 400.8 eV[44] following the charge transfer from the lone pair electrons of the pyridine nitrogen atom to the substrate.[44] We believe that such a charge transfer is rather unlikely in the given case since the pyridine nitrogen is presumably placed in the vicinity of the gold substrate and cannot contact directly due to the dimethanethioacetate (or dimethanethiolate) legs. Under such geometry a weaker, presumably electrostatic, interaction between the pyridine ring and the gold substrate can be expected. The respective rise of BE can then be compensated by dynamical screening of the N 1s core hole by the electrons in the closely placed substrate (decrease of BE) resulting in BE values similar to unbound pyridines placed far away from the substrate.

3.2 NEXAFS spectroscopy

NEXAFS spectroscopy provides both chemical and structural information about the target films. The C K-edge NEXAFS data for **1**/Au – **6**/Au are presented in Figure 6: the spectra acquired at a so called magic angle of x-ray incidence of 55º are compiled in the left panel and the differences between the spectra acquired at incidence angles of 90º and 20º are shown in the right panel.

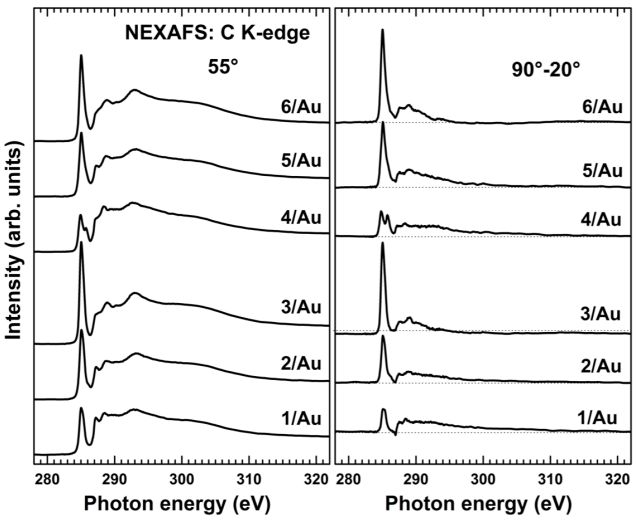

Figure 6. C K-edge NEXAFS spectra of **1**/Au – **6**/Au. Left panel: the spectra acquired at an x-ray incidence angle of 55 º; right panel: the differences between the spectra acquired at x-ray incidence angles of 90º and 20º. The dashed lines in the right panel correspond to zero.

The N K-edge NEXAFS spectra of **4**/Au- **6**/Au are presented in analogous fashion in Figure 7. Note that the 55° spectra are exclusively characteristic of the electronic structure of the target films (unoccupied molecular orbital); these spectra are not affected by any orientational effects.[45] In contrast, the difference spectra are representative of the orientational order and molecular orientation.[45] The 55° C K-edge spectra of **1**/Au **- 3**/Au in Figure 6 (left panel) exhibit characteristic pattern of the adsorption resonances which are typical of aromatic rings and thioaromatic SAMs, a pronounced absorption resonance at ~285.0 eV (π_1^* ring), two weaker resonances at~287.2 eV (mixture of R^* and C-H^*) and ~288.5-288.9 eV (π_2^* ring), and several broader resonances at ~293.0 eV $\sigma(_{1C\text{-}C}{}^*)$ and ~303.6 eV $\sigma(_{2C\text{-}C}{}^*)$.[46,40,47–50] The most characteristic π_1^* resonance becomes more intense with increasing length of the aromatic chain suggesting a successively improving quality of the monolayers. A similar behavior was observed in a series of oligophenyl SAMs with the thiol anchor group.[40] Significantly, the spectra exhibit no characteristic resonances of C=O and COOH moieties which are usually quite pronounced if these species are available. This suggests that the extent of contamination, which could be traced in the C 1s HRXPS spectra (see previous section), is quite low.

The 55° C K-edge spectrum of **4**/Au - **6**/Au exhibit a more complex resonance pattern. As seen by the example of **4**/Au, the π_1^* resonance is accompanied by an additional, weaker π^* -type resonance at ~285.8 eV. Such a resonance pattern is typical for *ortho* substituted pyridine units.[51] According to the theoretical estimates, such a spectral shape and the

resonance branching is typical for the case that the vibrational fine structure does not contribute noticeably into the absorption event.[52] This consideration leads to the conclusion that the vibrations are efficiently quenched in the case of **4**/Au and presumably also for **5**/Au and **6**/Au where the resonance at ~285.8 eV becomes successively weaker in accordance with the molecular structure. The quenching can occur due to the interaction of the nitrogen atom in the pyridine ring with the substrate, which is possible due to the specific adsorption geometry of **4** - **6**.

The 55° N K-edge NEXAFS spectra of **4**/Au – **6**/Au displayed in Figure 7 (left panel) exhibit a strong, characteristic π^* resonance of the pyridine unit at 398.8 eV (N 1s →LUMO) and several less intense π^* and σ^* resonances at higher photon energy. The detailed description and assignments of these resonances can be found in literature.[43,47,52,51]

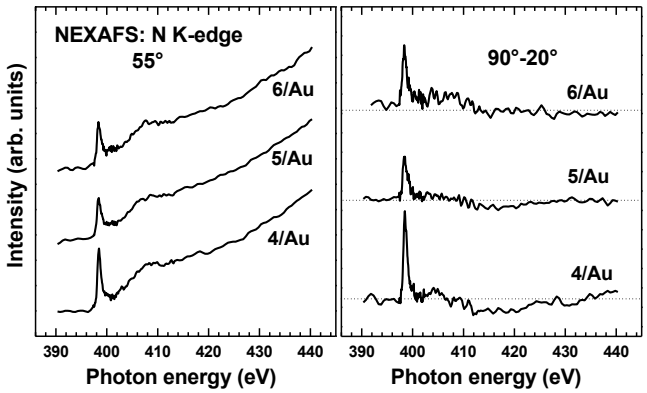

Figure 7. N K-edge NEXAFS spectra of **4**/Au – **6**/Au. Left panel: the spectra acquired at an x-ray incidence angle of 55 º; right panel: the differences between the spectra acquired at x-ray incidence angles of 90º and 20º. The dashed lines in the right panel correspond to zero.

Along with the information on the chemical identity and electronic structure, NEXAFS data provide insight into the molecular order and orientation in the target systems by monitoring linear dichroism effects in x-ray absorptions and taken into account the orientation of the transition dipole moments (TDMs) of the probed molecular orbitals (perpendicular to the bonds for π* and parallel to the bonds for σ*). In the given case, both C and N K-edges spectra of **1**/Au – **6**/Au exhibit significant linear dichroism as evidenced by the 90°-20° difference spectra in Figures 6 and 7 (right panels). The observed reduction in the π* resonance intensity at grazing incidence geometry, manifested as positive peaks at the position of the respective resonances in the difference spectra, suggests an upright molecular orientation in **1**/Au – **6**/Au.

Except for the above qualitative considerations, a quantitative analysis of the angular dependence of the NEXAFS resonance intensities could be performed to estimate the average tilt angle of the aromatic chains in **1**/Au – **6**/Au. For this purpose, the π_1* resonance was selected as the most intense and distinct resonance in the absorption spectra. In addition, the intensities of this resonance could be derived directly from the NEXAFS spectra, without a sometimes ambiguous fitting procedure. As soon as these intensities *I* are known, the average tilt angle α of the π_1* orbitals with respect to the surface normal can be derived from a standard expression for a vector-type orbital[45]

$$I(\alpha,\theta) = A\left\{P \times \tfrac{1}{3}\left[1 + \tfrac{1}{2}\cdot(3\cdot\cos^2\theta - 1)\cdot(3\cdot\cos^2\alpha - 1)\right] + (1-P)\tfrac{1}{2}\sin^2\alpha\right\} \qquad (1)$$

where *A* is a constant, *P* is a polarization degree of the x-rays, and θ is the x-ray incidence angle.

As far as the molecular backbones have a planar configuration typical for densely packed assemblies,[53–55] the tilt angle α of the π_1* orbitals is directly related to the tilt angle φ of the molecular axis with respect to the surface normal and to the twist angle ϑ of the aromatic rings with respect to the plane spanned by the surface normal and the molecular axis[56,57]

$$\cos\alpha = \cos\vartheta\cdot\sin\varphi \qquad (2)$$

This expression allows to estimate the tilt angle of the molecular axis as soon as some assumptions about the value of the twist angle are made. Usually, either the value of the twist angle typical of the bulk aromatic compounds (32°)[58] is assumed or this angle is directly determined, which however required the attachment of a special tail group to the aromatic backbone.[57] The bidentate nature of the compounds **1** – **6** inhibits the free rotation around the molecular axis upon the tilt leading to a twist angle value of 0°.

Both C and N K-edge NEXAFS spectra were processed. The best fits of the angular dependence of the π_1* resonance intensities according to eq. 1 resulted in the values of the average tilt angles, which are compiled in Table 4.

Table 4. Average tilt angle of the molecular backbones in **1**/Au– **6**/Au with respect to the surface normal calculated on the basis of the C and N K-edge NEXAFS spectra. The accuracy of the values is ±3°.

Monolayer	1/Au	2/Au	3/Au	4/Au	5/Au	6/Au
Tilt angle (φ) – C K-edge	31°	29°	26°	29°	25°	24°
Tilt angle (φ) – N K-edge	-	-	-	23°	26°	24°

Two tendencies were observed. First, the tilt angles decreased successively with the increasing length of the aromatic backbone both for the **1**/Au– **3**/Au and **4**/Au– **6**/Au series. Second, the tilt angles for the former series were slightly larger than those for the latter one as far as the monolayers with the similar length of the molecular backbone are compared. Note that values of the average tilt angles calculated on the basis of the C and N K-edge NEXAFS spectra for **5**/Au and **6**/Au agree very well with one another, which supports our assumption about the planar conformation of the molecular backbones in these monolayers. This conclusion can be drawn since the tilt angle derived on the basis of the C K-edge data is representative of the entire backbone while that obtained on the basis of the N K-edge data is representative of the pyridine ring only. These values can only coincide if the pyridine ring and the backbone have the same orientation, which corresponds to the planar conformation. In contrast, the average tilt angles calculated on the basis of the C and N K-edge NEXAFS spectra for **4**/Au are somewhat different. This can be related to the spectra normalization problems in this particular case.

4 Discussion

The HRXPS and NEXAFS data provide complementary information on **1**/Au – **6**/Au and are in good agreement with each other. All SAM precursors form dense and well orientated SAMs on Au(111). The quality of these monolayers, in terms of contamination and orientational order, improves with increasing length of the molecular backbone both for the **1**/Au – **3**/Au and **4**/Au – **6**/Au series. Such a behavior is typical for SAMs.[33,40,41] The presence of contamination is related to the efficiency of the self-cleaning mechanism which is more efficient at a higher driving force for the molecular self-assembly which occurs is the case of a longer molecular backbone. Similarly, the molecular tilt and orientational order depend on the length of the molecular backbone. The longer the molecules are the more upright they are standing on the surface. In the given case, because of the larger conjugated system for the longer backbones, the $\pi - \pi$ stacking effect is stronger and forces the molecules in a more

upright position for a better overlapping of the π systems. The derived average tilt angles are an indirect measurement of the orientational order in the monolayers. Indeed, a totally disordered molecular film exhibits no linear dichroism and can be associated with an average tilt angle of a vector orbital of 54.7° since I(α,θ) does not depend on θ at α = 54.7° (see eq 1). A deviation from this value is a fingerprint of the orientational order. The average tilt angle values presented in Table 4 suggest a higher orientational order increasing from **1**/Au to **3**/Au for the OPBs and from **4**/Au to **6**/Au for the OPPs. The orientational order is always higher for the OPP case as compared to OPB as far as the molecules with the same length of the molecular backbone are compared.

Along with the influence of the molecular length, the effect of terminal pyridine moiety is of particular interest. According to both HRXPS and NEXAFS data **4**/Au – **6**/Au show less contamination, higher orientational order and better homogeneity of the S-Au interface (including a higher percentage of the bound thiol) compared to **1**/Au – **3**/Au as far as monolayers of the corresponding compounds are compared. First, **1**/Au and **2**/Au exhibit some contamination, which is not the case for **4**/Au and **5**/Au (see Section 3.1). This suggests that the self-cleaning mechanism works more efficiently for the OPP films, which can be reasonably associated with the additional interaction between the terminal nitrogen atom of the pyridine ring and the substrate. Second, the molecular inclination is slightly larger in **1**/Au – **3**/Au as compared to **4**/Au – **6**/Au. On one hand, this observation can be explained with less sterical hindrance for the OPP monolayers because no hydrogen atom is pointing to the surface and causing repulsion as it happens in **1**/Au – **3**/Au. On the other hand, the smaller inclination can be associated with the pyridine-substrate interaction acting as the third binding site to the gold surface and providing an additional drive for the upright orientation. An indirect evidence for the interaction is provided by the N 1s HRXPS spectra as discussed at the end of Section 3.1. Another evidence for the coordination is provided by the C K-edge NEXAFS spectra which exhibit the characteristic π^* resonance structure typical of a pyridine unit with distorted vibrational fine structure. The most probable reason for this distortion can be a interaction of the pyridine unit,[51] which, in the given case, can only occur through the pyridine-substrate interaction. This interaction is a quite interesting and potentially useful feature. As shown by Venkataraman et al.[59] in break junction experiments, the conductance of pyridine to gold is optimized in a tilt geometry. That makes the pyridine-2,6-diyldimethanethiol a promising candidate as anchoring group for electronic devices because of their potential bidentate binding and slightly tilted geometry promising good conductivity.

It is however still a challenge to achieve a homogeneous, bidentate binding behavior for the pyridine-2,6-diyldimethanethiol. As demonstrated by the S 2p HRXPS spectra of **1**/Au – **6**/Au in Figure 4, a noticeable amount of the SAM constituents in these monolayers exhibit a heterogeneous binding character with respect to the substrate – one anchor group has a thiolate-type bonding, whereas the other is weakly coordinated, unbound, or participating in a disulfide bridge with the adjacent molecule. We believe that such a bonding heterogeneity is not a result of our specific preparation procedures (see Section 2) but can be associated with the fundamental problems of the molecular arrangement in the given case. Indeed, typical architecture of both aromatic bulk compounds[58,60,61] and aromatic SAMs[62] is a herring-bone arrangement of the individual molecules mediated by the T-shaped interaction.[63,64] Such a most thermodynamically favourable arrangement is hardly possible in **1**/Au – **6**/Au since it involves both molecular tilt and significant twist (32° in the bulk compounds)[58]. The bidentate bonding of the SAM constituents in **1**/Au – **6**/Au excludes any twist at a molecular tilt resulting, potentially, in another structure, which is probably less favorable from the viewpoint of the intermolecular interaction. A way to solve this dilemma is the breaking of a part of the gold-thiolate bonds for one of the molecular foots, which is exactly the situation occurring in **1**/Au – **6**/Au.

An interesting point is the absolute packing density of the SAM constituents in **1**/Au – **6**/Au. This parameter can be coarsely estimated on the basis of the S2p/Au4f intensity ratios of the target films taking the well-known and well-defined DDT and HDT SAMs as reference.[65] This ratio is a direct measure of the molecular packing density. As compared to the S 2p signal itself, this ratio suffers much less from all problems related to the absolute intensity comparison and to the different attenuation of this signal in different films. Due to the quite close binding energies of the Au 4f and S 2p emissions, both signals are attenuated similarly as far as the primary excitation is performed at a high photon energy. Even though this is not the case here (the photon energy for the S 2p spectra was 350 eV), at least a coarse estimation can be made. According to this estimation the packing density of the strongly bound sulfur (S1 + S2, see section 3.1) is close to that of the alkanethiolate SAMs on Au(111) As reported, these films exhibit ($\sqrt{3}\times\sqrt{3}$)R30° and (2$\sqrt{3}\times$3)rect. molecular arrangements and have a molecular density of 4.63×10^{14} cm^{-2}, which corresponds to an area per molecule of 21.6 $Å^2$.[66,67] Interestingly, atomic sulfur is known to pack also into a ($\sqrt{3}\times\sqrt{3}$)R30° lattice on Au(111) corresponding to the same adsorbate density.[68] Thus, the density of the strongly bound S in **1**/Au – **6**/Au corresponds roughly to the characteristic density of S on Au(111)

which means that the interaction between the strongly bound sulfur atoms is an additional factor limiting their density and thus distorting the perfect bidentate bonding for the SAM constituents trying to pack densely within the monolayer.

Whereas the joint intensity of the S1 and S2 doublets is characteristic of the strongly bound sulphur, the total S2p intensity (S1+S2+S3) provides a coarse estimate for the molecular packing density in **1**/Au– **6**/Au. Taking the respective S2p/Au4f intensity ratios and comparing them to the analogous values for the reference DDT and HDT films, we found that the packing density of **1** - **6** is about 70 - 75% of that in DDT/Au and HDT/Au. Presumable reason for such a density reduction is the interaction between the adsorbed (i.e. strongly bound) sulfur atoms at the SAM-substrate interface as described in the previous paragraph. In view of the bidentate character of **1** - **6**, this interaction forces only 50% coverage of **1** - **6** as compared to DDT/Au and HDT/Au, whereas the interaction between the molecular backbones favors 100% coverage. The resulting structure is presumably a compromise between these two factors. Significantly, this compromise can only be achieved by letting some of the anchor groups unbound, which is exactly the situation we observe in the given case.

5 Conclusions

Two series of oligophenylenes comprising 1,3-phenylenedimethanethiol and pyridine-2,6-diyldimethanethiol as anchoring group were synthesized in order to examine their SAM forming abilities and to prove the applicability of the bidentate design. Both series form densely packed monolayers with a high orientational order. The quality of these films improves with increasing length of the molecular backbone. Along with this general tendency, the SAMs with the pyridine-2,6-diyldimethanethiol as anchoring group exhibit significantly lower level of contamination and higher orientational order as compared to their counterparts with the 1,3-phenylenedimethanethiol anchor group. This was explained by a coordination of the terminal nitrogen atom in the pyridine ring with the gold substrate, which provides an additional mechanism for self-cleaning and additional drive for the upright molecular orientation.

Independent of the parameters of the preparation procedure, a noticeable amount of the SAM constituents in the oligophenylene monolayers exhibit a heterogeneous binding character with respect to the substrate – one anchor group has a thiolate-type bonding, whereas the other is weakly coordinated, unbound, or participating in a disulfide bridge with the adjacent molecules. We believe that such a bonding heterogeneity results from the

fundamental problems of the molecular arrangement in the given case. First, bidentate-like bonding makes impossible the molecular twist, which is a prerequisite to achieve a thermodynamically favorable arrangement of the aromatic moieties. Second, the interaction between the strongly bound S species at the SAM/substrate interface governs their density, forcing bond breaking for the superficial atoms as far as the SAM precursors try to pack densely within the monolayer.

The studied SAM precursors, and especially those with pyridine-2,6-diyldimethanethiol as anchoring group, can be considered as prospective nanoparticle stabilizing ligands. With the prove of the proposed gold surface - nitrogen interaction, they are ideal candidates for contacting and stabilizing gold nanoparticles. Especially with the reference to the conductance measurements of molecular wires with pyridine anchoring groups, the presented compounds show very promising characteristics for a good conductance by their tilted geometry to the surface. Also the bidentate design providing potentially very stable junctions of the molecules to metal surfaces and electrodes represents a promising structural motive for next generation SAMs. To gain more insight in the electronic properties of these systems conductance measurements have to be done in the future.

Whereas the joint intensity of the S1 and S2 doublets is characteristic of the strongly bound sulphur, the total S2p intensity (S1+S2+S3) provides a coarse estimate for the molecular packing density in **1**/Au– **6**/Au. Taking the respective S2p/Au4f intensity ratios and comparing them to the analogous values for the reference DDT and HDT films, we found that the packing density of **1**/Au - **6**/Au is about 70-75% of that in DDT/Au and HDT/Au. Presumable reason for such a density reduction is the interaction between the adsorbed (i.e. strongly bound) sulfur atoms at the SAM-substrate interface as described in the previous paragraph. In view of the bidentate character of **1** - **6**, this interaction forces only 50% coverage of **1** - **6** as compared to DDT/Au and HDT/Au, whereas the interaction between the molecular backbones favors 100% coverage. The resulting structure is presumably a compromise between these two factors. Significantly, this compromise can only be achieved by letting some of the anchor groups unbound, which is exactly the situation we observe in the given case.

Acknowledgement

HH and MZ thank L. S. O. Johansson and E. Moons (Karlstad University) for the cooperation at MAX-lab, and MAX-lab staff, including A. Preobrajenski in particular, for the assistance during the spectroscopic experiments. This work has been supported by DFG (ZH 63/9-3 and ZH 63/14-1). FS, JH and MM thank U. Fluch for supporting the synthesis work of the model compounds, the University of Basel and the Karlsruhe Institute of Technology for ongoing support and are grateful for financial support of the Swiss National Science Foundation (SNF),National Center of Competence in Research (NCCR) „Nanoscale Science“ and Swiss Nanoscience Institute (SNI).

Notes and references

[a] University of Basel, Department of Chemistry, St. Johannsring 19, CH-4056 Basel, Switzerland. Fax: +41 (0)61 267 10 16; Tel: +41 (0)61 267 10 06; E-mail: *marcel.mayor@unibas.ch*

[b] Karlsruhe Institute of Technology, Eggenstein-Leopoldshafen, D-76344, Germany. Tel: +49 (0)721 608 26392; E-mail: *marcel.mayor@kit.edu*

[c] Angewandte Physikalische Chemie, Universität Heidelberg, Im Neuenheimer Feld 253, 69120 Heidelberg, Germany. Fax: +49 (0)6221 54 6199 Tel: +49 (0)6221 54 4921; E-mail: michael.zharnikov@urz.uni-heidelberg.de

† Electronic Supplementary Information (ESI) available: Results of NMR-spectroscopic characterization and elemental analyses of **1 - 6** are presented in the Supporting Information.

1. J. J. Gooding, F. Mearns, W. Yang, and J. Liu, *Electroanal*, 2003, **15**, 81–96.

2. N. K. Chaki and K. Vijayamohanan, *Biosens. Bioelectron.*, 2002, **17**, 1–12.

3. V. Balzani, A. Credi, and M. Venturi, *ChemPhysChem*, 2008, **9**, 202–220.

4. J. M. Tour, *Acc. Chem. Res.*, 2000, **33**, 791–804.

5. C. E. D. Chidsey, C. R. Bertozzi, T. M. Putvinski, and A. M. Mujsce, *J. Am. Chem. Soc.*, 1990, **112**, 4301–4306.

6. J.-S. Park, A. N. Vo, D. Barriet, Y.-S. Shon, and T. R. Lee, *Langmuir*, 2005, **21**, 2902–2911.

7. T. Weidner, A. Krämer, C. Bruhn, M. Zharnikov, A. Shaporenko, U. Siemeling, and F. Träger, *Dalton Trans.*, 2006, 2767–2777.

8. T. Weidner, N. Ballav, U. Siemeling, D. Troegel, T. Walter, R. Tacke, D. G. Castner, and M. Zharnikov, *J. Phys. Chem. C*, 2009, **113**, 19609–19617.

9. L. Zobbi, M. Mannini, M. Pacchioni, G. Chastanet, D. Bonacchi, C. Zanardi, R. Biagi, U. D. Pennino, D. Gatteschi, A. Cornia, and R. Sessoli, *Chem. Comm.*, 2005, 1640–1642.

10. M. W. J. Beulen, J. Bügler, B. Lammerink, F. A. J. Geurts, E. M. E. F. Biemond, K. G. C. van Leerdam, F. C. J. M. van Veggel, J. F. J. Engbersen, and D. N. Reinhoudt, *Langmuir*, 1998, **14**, 6424–6429.

11. T. G. Lee, K. Kim, and M. S. Kim, *J. Phys. Chem.*, 1991, **95**, 9950–9955.

12. S. Rifai and M. Morin, *J. Electroanal. Chem.*, 2003, **550–551**, 277–289.

13. J. K. Lim, Y. Kim, O. Kwon, and S.-W. Joo, *ChemPhysChem*, 2008, **9**, 1781–1787.

14. J. K. Lim, O. Kwon, and S.-W. Joo, *J. Phys. Chem. C*, 2008, **112**, 6816–6821.

15. G. Bruno, F. Babudri, A. Operamolla, G. V. Bianco, M. Losurdo, M. M. Giangregorio, O. Hassan Omar, F. Mavelli, G. M. Farinola, P. Capezzuto, and F. Naso, *Langmuir*, 2010, **26**, 8430–8440.

16. F. Sander, T. Peterle, N. Ballav, F. von Wrochem, M. Zharnikov, and M. Mayor, *J. Phys. Chem. C*, 2010, **114**, 4118–4125.

17. S. Casalini, F. Leonardi, C. A. Bortolotti, A. Operamolla, O. H. Omar, L. Paltrinieri, C. Albonetti, G. M. Farinola, and F. Biscarini, *J. Mater. Chem.*, 2012, **22**, 12155–12163.

18. P. Chinwangso, A. C. Jamison, and T. R. Lee, *Acc. Chem. Res.*, 2011, **44**, 511–519.

19. T. Peterle, P. Ringler, and M. Mayor, *Adv. Funct. Mater*, 2009, **19**, 3497–3506.

20. J. P. Hermes, F. Sander, T. Peterle, C. Cioffi, P. Ringler, T. Pfohl, and M. Mayor, *Small*, 2011, **7**, 920–929.

21. R. H. Mitchell and J. Zhang, *Tetrahedron Letters*, 1995, **36**, 1177–1180.

22. A. Operamolla, O. Hassan Omar, F. Babudri, G. M. Farinola, and F. Naso, *J. Org. Chem.*, 2007, **72**, 10272–10275.

23. M.-F. Paugam, J. T. Bien, B. D. Smith, L. A. J. Chrisstoffels, F. de Jong, and D. N. Reinhoudt, *J. Am. Chem. Soc.*, 1996, **118**, 9820–9825.

24. A. V. Rukavishnikov, A. Phadke, M. D. Lee, D. H. LaMunyon, P. A. Petukhov, and J. F. W. Keana, *Tetrahedron Lett.*, 1999, **40**, 6353–6356.

25. J. P. Wolfe, R. A. Singer, B. H. Yang, and S. L. Buchwald, *J. Am. Chem. Soc.*, 1999, **121**, 9550–9561.

26. M. B. Skaddan and J. A. Katzenellenbogen, *Bioconjugate Chem.*, 1999, **10**, 119–129.

27. H. Takalo and J. Kankare, *Acta Chem. Scand., Ser. B*, 1987, 291.

28. H. Takalo, P. Pasanen, and J. Kankare, *Acta Chem. Scand., Ser. B*, 1988, 373.

29. K. Heister, M. Zharnikov, M. Grunze, and L. S. O. Johansson, *J. Phys. Chem. B*, 2001, **105**, 4058–4061.

30. M. Wirde, U. Gelius, T. Dunbar, and D. L. Allara, *Nuclear Instruments and Methods in Physics Research Section B: Beam Interactions with Materials and Atoms*, 1997, **131**, 245–251.

31. B. Jager, H. Schurmann, H. U. Muller, H. J. Himmel, M. Neumann, M. Grunze, and C. Woll, *Z. Phys. Chem.*, 1997, **202**, 263.

32. K. Heister, M. Zharnikov, M. Grunze, L. S. O. Johansson, and A. Ulman, *Langmuir*, 2001, **17**, 8–11.

33. M. Zharnikov and M. Grunze, *J. Vac. Sci. Technol. B*, 2002, **20**, 1793–1807.

34. Surface chemical analysis – X-ray photoelectron spectrometers – Calibration of the energy scales.

35. J. F. Moulder, W. F. Stickle, P. E. Sobol, and K. D. Bomben, *Handbook of X Ray Photoelectron Spectroscopy: A Reference Book of Standard Spectra for Identification and Interpretation of Xps Data*, Physical Electronics, 1995.

36. C. L. A. Lamont and J. Wilkes, *Langmuir*, 1999, **15**, 2037–2042.

37. J. Stohr, *Nexafs Spectroscopy*, Springer-Verlag, 1996.

38. P. E. Batson, *Phys. Rev. B*, 1993, **48**, 2608.

39. A. Shaporenko, A. Terfort, M. Grunze, and M. Zharnikov, *J. Electr. Spectr. Rel. Phenom.*, 2006, **151**, 45–51.

40. S. Frey, V. Stadler, K. Heister, W. Eck, M. Zharnikov, M. Grunze, B. Zeysing, and A. Terfort, *Langmuir*, 2001, **17**, 2408–2415.

41. M. Zharnikov, *J. Electr. Spectr. Rel. Phenom.*, 2010, **178–179**, 380–393.

42. Y. Zubavichus, M. Zharnikov, Y. Yang, O. Fuchs, E. Umbach, C. Heske, A. Ulman, and M. Grunze, *Langmuir*, 2004, **20**, 11022–11029.

43. J. Liu, B. Schüpbach, A. Bashir, O. Shekhah, A. Nefedov, M. Kind, A. Terfort, and C. Wöll, *Phys. Chem. Chem. Phys.*, 2010, **12**, 4459–4472.

44. A. Kim, F. S. Ou, D. A. A. Ohlberg, M. Hu, R. S. Williams, and Z. Li, *J. Am. Chem. Soc.*, 2011, **133**, 8234–8239.

45. J. Stöhr and D. A. Outka, *Phys. Rev. B*, 1987, **36**, 7891–7905.

46. J. Stohr, *Nexafs Spectroscopy*, Springer-Verlag, 1996.

47. J. A. Horsley, J. Stöhr, A. P. Hitchcock, D. C. Newbury, A. L. Johnson, and F. Sette, *J. Chem. Phys.*, 1985, **83**, 6099–6107.

48. T. Yokoyama, K. Seki, I. Morisada, K. Edamatsu, and T. Ohta, *Physica Scripta*, 1990, **41**, 189–192.

49. A. Shaporenko, K. Heister, A. Ulman, M. Grunze, and M. Zharnikov, *J. Phys. Chem. B*, 2005, **109**, 4096–4103.

50. A. Shaporenko, K. Rössler, H. Lang, and M. Zharnikov, *J. Phys. Chem. B*, 2006, **110**, 24621–24628.

51. H. Hamoudi, K. Döring, F. Chesneau, H. Lang, and M. Zharnikov, *J. Phys. Chem. C*, 2012, **116**, 861–870.

52. C. Kolczewski, R. Püttner, O. Plashkevych, H. Ågren, V. Staemmler, M. Martins, G. Snell, A. S. Schlachter, M. Sant'Anna, G. Kaindl, and L. G. M. Pettersson, *J. Chem. Phys.*, 2001, **115**, 6426–6437.

53. H. M. Rietveld, E. N. Maslen, and C. J. B. Clews, *Acta Crystallogr. B*, 1970, **26**, 693–706.

54. J. H. Lii and N. L. Allinger, *J. Am. Chem. Soc.*, 1989, **111**, 8576–8582.

55. H.-J. Himmel, A. Terfort, and C. Wöll, *J. Am. Chem. Soc.*, 1998, **120**, 12069–12074.

56. H.-T. Rong, S. Frey, Y.-J. Yang, M. Zharnikov, M. Buck, M. Wühn, C. Wöll, and G. Helmchen, *Langmuir*, 2001, **17**, 1582–1593.

57. N. Ballav, B. Schüpbach, O. Dethloff, P. Feulner, A. Terfort, and M. Zharnikov, *J. Am. Chem. Soc.*, 2007, **129**, 15416–15417.

58. J. Trotter, *Acta Crystallogr*, 1961, **14**, 1135–1140.

59. M. Kamenetska, S. Y. Quek, A. C. Whalley, M. L. Steigerwald, H. J. Choi, S. G. Louie, C. Nuckolls, M. S. Hybertsen, J. B. Neaton, and L. Venkataraman, *J. Am. Chem. Soc.*, 2010, **132**, 6817–6821.

60. A. Hargreaves and S. H. Rizvi, *Acta Crystallogr.*, 1962, **15**, 365–373.

61. J. L. Baudour, *Acta Crystallogr. B*, 1991, **47**, 935–949.

62. A. Bashir, D. Käfer, J. Müller, C. Wöll, A. Terfort, and G. Witte, *Angew. Chem. Int. Ed.*, 2008, **47**, 5250–5252.

63. H. Brunner and R. Lukas, *Chem. Ber.*, 1979, **112**, 2528–2538.

64. S. E. Garner and A. G. Orpen, *J. Chem. Soc., Dalton Trans.*, 1993, 533.

65. F. Chesneau, B. Schüpbach, K. Szelągowska-Kunstman, N. Ballav, P. Cyganik, A. Terfort, and M. Zharnikov, *Phys. Chem. Chem. Phys.*, 2010, **12**, 12123–12137.

66. F. Schreiber, *Prog. Surf. Sci.*, 2000, **65**, 151–257.

67. F. Chesneau, J. Zhao, C. Shen, M. Buck, and M. Zharnikov, *J. Phys. Chem. C*, 2010, **114**, 7112–7119.

68. C. Vericat, M. E. Vela, G. A. Benitez, J. A. M. Gago, X. Torrelles, and R. C. Salvarezza, *J. Phy.: Condens. Matter*, 2006, **18**, R867–R900.

TOC

Improved SAM properties are observed for S-acetyl protected oligoarylpyridine dithiols compared to the parent oligoaryl-benzene derivatives.

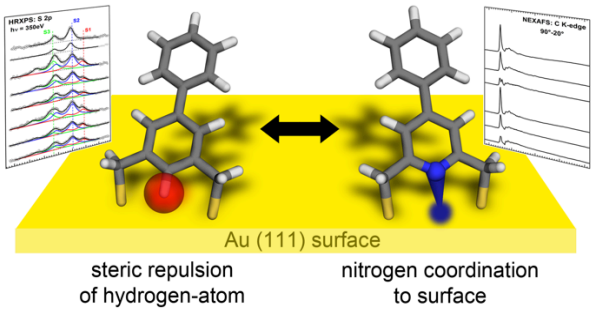

3.2.1 Supplementary Information

Add a Third Hook: S-Acetyl Protected Oligophenylene Pyridine Dithiols as Advanced Precursors for Self-Assembled Monolayers

Fabian Sander,[a)] Jens Peter Hermes,[a)] Marcel Mayor,[a), b)*] Hicham Hamoudi[c)] and Michael Zharnikov[c)*]

[a)] *University of Basel, Department of Chemistry, St. Johannsring 19, CH-4056 Basel, Switzerland. Fax: +41 (0)61 267 10 16; Tel: +41 (0)61 267 10 06; E-mail: marcel.mayor@unibas.ch*

[b)] *Karlsruhe Institute of Technology, Eggenstein-Leopoldshafen, D-76344, Germany. Tel: +49 (0)721 608 26392; E-mail: marcel.mayor@kit.edu*

[c)] *Angewandte Physikalische Chemie, Universität Heidelberg, Im Neuenheimer Feld 253, 69120 Heidelberg, Germany. Fax: +49 (0)6221 54 6199 Tel: +49 (0)6221 54 4921; E-mail: michael.zharnikov@urz.uni-heidelberg.de*

S1. General Methods - Used Reagent, Solvents and Analytical Devices

All commercially available starting materials were of reagent grade and used as received. Absolute tetrahydrofuran (THF) was purchased from *Fluka*, stored over 4 Å molecular sieves, and handled under Argon. Dichloromethane and all other used solvents were of technical grade and distilled prior to use. For microwave reactions a *Biotage Initiator 8* was used. Column chromatography purifications were carried out on *silica gel 60* (particle size 40-63 µm) from *Fluka*. Deuterated solvents were purchased from *Cambridge Isotope Laboratories*. $_1$H and $_{13}$C NMR spectra were recorded with a *Bruker DMX 400* instrument ($_1$H resonance 400 MHz) or a *Bruker DRX 500* instrument ($_1$H resonance 500 MHz) at 298 K. Electron Impact (EI) mass spectra were recorded on a *Finnigan MAT 95Q* by H. Nadig. Elemental analyses were performed by W. Kirsch on a *Perkin-Elmer Analysator 240*.

S2. Synthesis Procedures and Analytical Data for the OPBs 1 - 3 and OPPs 4 - 6

General Procedure for 1 and 4

The reactions were carried out in 3 mmol scale. The corresponding dibromide (1 eq.) was dissolved in 10 mL degassed THF and 3 eq. potassium thoiacetate were added. The mixture was stirred under argon over night. After quenching the reaction with 20 mL water the mixture was extracted three times with 20 mL dichlormethan and the combined organic phases were dried over $MgSO_4$. After removing the solvent in vacuum the product was purified by column chromatography (silica, 6:1, c-hexane:ethyl acetate). The products were yielded as colorless solids.

1 S,S'-(1,3-phenylenebis(methylene)) diethanethioate

Yield: 98%

^{1}H-NMR (400 MHz, $CDCl_3$) δ = 7.25-7.16 (m, 4H, arom-*H*); 4.09 (s, 4H, benz-*H*); 2.35 (s, 6H, C*H*$_3$)

^{13}C-NMR (100MHz, $CDCl_3$) δ = 195.0; 138.0; 129.2; 129.0; 127.8; 33.2; 30.3

MS EI(m/z (%)): 254 (30)[M^+], 211 (95)[M^+-Ac), 179(100) (M^+-SAc)

EA calc C=56.66, H=5.55, N=0.0; found: C=56.68, H=5.65, N=0.0

4 S,S'-(pyridine-2,6-diylbis(methylene)) diethanethioate

Yield: 96%

^{1}H-NMR (400 MHz, $CDCl_3$) δ = 7.56(t, $^{3}J_{HH}$=7.7 Hz, 1H, arom*H*); 7.21(d, $^{3}J_{HH}$=7.7 Hz, 2H, arom*H*); 4.22 (s, 4H, benz-*H*); 2.36(s, 6H, C*H*$_3$)

^{13}C-NMR (100MHz, $CDCl_3$) δ = 209.0; 157.2; 137.5; 121.7; 35.3; 30.3

MS EI(m/z (%)): 255 (1)[M^+], 213 (100)[M^+-Ac), 170 (47)(M^+-Ac_2)

EA calc: C=51.74; H=5.13; N=5.49; found: C=51.77; H=5.12; N=5.49

General Procedure for Suzuki coupling:

The reactions were carried out in 1 mmol scale. A microwave tube containing a magnetic stirrer and purged with argon was charged with phenylboronic acid (1.5 eq.), freshly grounded anhydrous K_3PO_4 (2.0 eq.), and **10**; S,S'-((5-bromo-1,3-phenylene)bis(methylene)) diethanethioate or **16**; (((4-bromopyridine-2,6-diyl)bis(methylene)) diethanethioate) and 2-dicyclohexyl phosphino-2',6'-dimethoxybiphenyl (S-Phos) (12.5 mol%). 5 mL dry toluene were added and the reaction mixture was degassed with argon for 10 min. After adding $Pd(OAc)_2$ (10 mol%) the reaction vessel was closed and the mixture was heat to 180 °C under microwave irradiation for 1.5 hours. After cooling down to room temperature the reaction mixture was filtered through thin silica pad elucidate with ethyl acetate (EE), concentrate under vacuum. The compounds were purified by column chromatography (silica, 6:1, c-hexane:ethyl acetate) and the products yielded as colorless solids.

(2) S,S'-([1,1'-biphenyl]-3,5-diylbis(methylene)) diethanethioate

Yield: 53%

^{1}H-NMR (400 MHz, $CDCl_3$) δ = 7.58-7.56 (m, 2H, arom*H*); 7.46-7.43(m, 2H, arom*H*); 7.41 (m, 2H, arom*H*); 7.38-7.35 (m, 1H, arom*H*); 7.16 (s, 1H), arom*H*); 4.15(s, 4H, benz-*H*); 2.35(s, 6H, CH_3)

^{13}C-NMR (100MHz, $CDCl_3$) δ = 195.0; 142.1; 140.2; 138.6; 128.7; 128.1; 127.6; 127.2; 126.7; 33.3; 30.37.

MS EI(m/z (%)): 330 (79)[M^+], 255 (100)[M^+-Ac), 212 (71) (M^+-SAc)

EA calc: C=65.42; H=5.49; N=0.0 found: C=66.08; H=5.89; N=0.0

(3) S,S'-([1,1':4',1''-terphenyl]-3,5-diylbis(methylene)) diethanethioate

Yield: 51%

^{1}H-NMR (400 MHz, $CDCl_3$) δ = 7.70 – 7.65 (m, 6H, arom*H*); 7.50 – 7.46 (m, 4H, arom*H*); 7.40 - 7,37 (m, 1H, arom*H*); 7.22 (s, 1H), arom*H*); 4.10 (s, 4H, benz-*H*); 2.40 (s, 6H, CH_3).

^{13}C-NMR (100MHz, $CDCl_3$) δ = 195.0; 141.6; 140.6; 140.5; 139,3; 138.7; 128.8; 128.2; 127.6; 127.5; 127.4; 127.1; 126.6; 33.3; 30.4.

MS EI(m/z (%)): 406 (100)[M^+], 331 (63)[M^+-Ac), 288 (42) (M^+-SAc)

EA calc: C=70.90; H=5.45; N=0.0 found: C=70.94; H=5.81; N=0.0

(5) S,S'-((4-phenylpyridine-2,6-diyl)bis(methylene)) diethanethioate

Yield: 54%

^{1}H-NMR (400 MHz, $CDCl_3$) δ =7.61-7.60(m, 2H, arom*H*); 7.47-7.44(m, 5H, arom*H*); 4.28(s, 4H, benz-*H*); 2.37(s, 6H, CH_3)

^{13}C-NMR (100MHz, $CDCl_3$) δ = 195.0; 157.7; 150.2; 137.9; 129.2; 129.0; 127.1; 119.8; 35.4; 30.3.

MS ESI (m/z): 354 (M^++Na)

EA calc: C=61.6; H=5.17; N=4.23 found: C=61.55; H=5.37;N=4.17

(6) S,S'-((4-([1,1'-biphenyl]-4-yl)pyridine-2,6-diyl)bis(methylene)) diethanethioate

Yield: 51%

^{1}H-NMR (400 MHz, $CDCl_3$) δ =7.70(m, 4H, arom*H*); 7.65-7.62(m, 2H, arom*H*); 7.49-7.46(m, 4H, arom*H*); 7.40-7.39(m, 1H, arom*H*); 4.30(s, 4H, benz-CH_2); 2.38(s, 6H, CH_3).

^{13}C-NMR (100MHz, $CDCl_3$) δ = 195.0; 157.8; 149.7; 142.1; 140.2; 136.6; 128.9; 127.8; 127.7; 127.5; 127.1; 119.6; 35.5; 30.3

MS ESI m/z: 430 (M^++Na)

EA calc: C=67.78;H=5.17; N=3.44 found: C=67.45; H=5.35; N=3.50

Figure S1: C 1s HRXPS spectra of **1**-**6** on Au acquired at photon energies of 350 eV (left panel) and 580 eV (right panel) along with the corresponding fits by several individual components and a background. For direct comparison, the spectra of DDT/Au (blue) and HDT/Au (red) are included, overlaying with the spectra of **3**/Au and **6**/Au in both panels. DDT/Au and HDT/Au served as references to determine the thickness and effective packing density of **1**-**6** on Au.

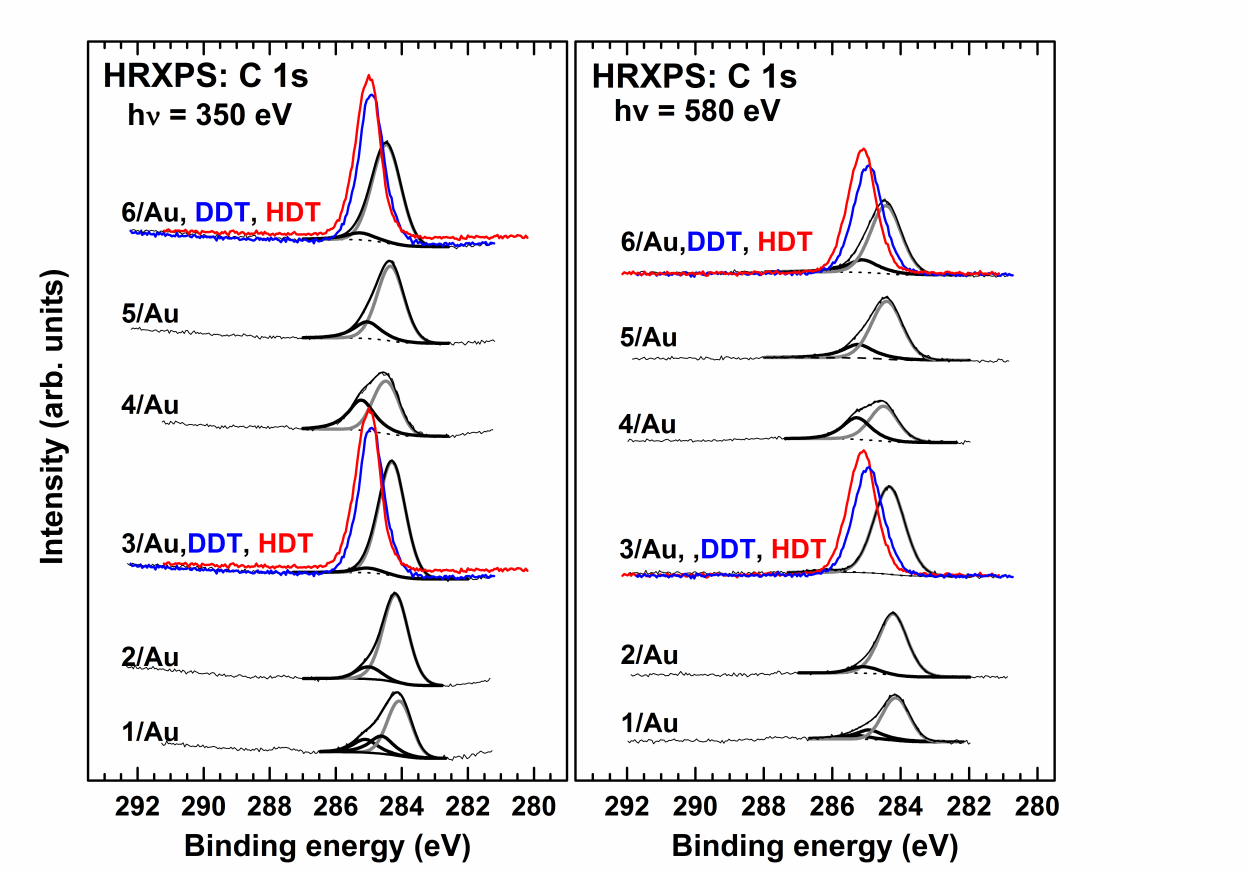

Dumbbells, Trikes and Quads – Organic/Inorganic Hybrid Nanoarchitectures Based on "Clicked" Gold Nanoparticles

*Fabian Sander,[1] Ulrike Fluch[1], Jens Peter Hermes[1] and Marcel Mayor[1,2]**

[*] Prof. Dr. Marcel Mayor, F. Sander, U. Fluch, Dr. J. P. Hermes
University of Basel, Department of Chemistry
St. Johannsring 19, CH-4056 Basel (Switzerland)
E-mail: marcel.mayor@unibas.ch
Prof. M. Mayor
Karlsruhe Institute of Technology (KIT), Institute of Nanotechnology (INT),
P. O. Box 3640, D-76021 Karlsruhe (Germany)

Functionalized gold nanoparticles are interlinked by a click chemistry protocol into defined oligomers. The spatial and geometric arrangement is directed by the size and numbers of functional moieties of the linker molecule. Electron transmission microscopy reveal the formation of dimers, trimers and tetramers.

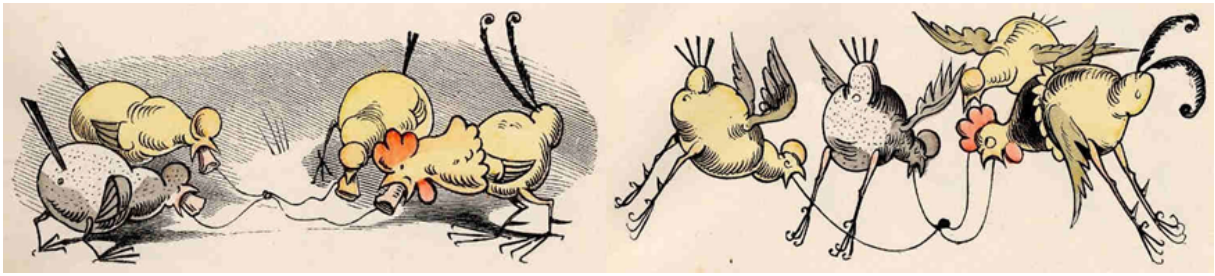

Abstract

The controlled assembly of gold nanoparticles in means of spatial arrangement and number of particles is essential for many future applications like electronic devices, sensors or labeling. Here we present an approach to build up oligomers of mono functionalized gold nanoparticles by the use of 1,3-bipolar azide alkyne cycloaddition click chemistry. The gold nanoparticles of 1.3 nm diameter are stabilized by one dendritic thioether ligand comprising an alkyne function. Together with di-, tri- and tetra-azide linker molecules the gold nanoparticle can be

covalently coupled by a wet chemical protocol. The reaction is tracked with IR and UV/vis spectroscopy and the yielded organic-inorganic hybrid structures are analyzed by transmission electron microscopy. To evaluate the success of this click chemistry reaction statistical analysis of the formed oligomers is performed. The geometric and spatial arrangements of the found oligomers match perfectly the calculated values for the used linker molecules. Dimers, trimers and tetramers could be identified after the reaction with the corresponding linker molecule. The results of this model reaction suggest that the used click chemistry protocol is working well with mono functionalized gold nanoparticles.

1. Introduction

Gold Nanoparticles (Au NPs) are intensively studied as easy accessible model compounds and functional units in various applications. Au NPs are utilized for example in catalysis,[1,2] sensor application,[3] nano electronic devices[4,5] and labeling.[6–9] For most of these applications a controlled assembly of Au NPs into defined architectures is essential and several review articles highlight the importance of this research field.[10–13] Various concepts were developed in order to connect Au NPs into more complex structures by exploiting different binding concepts. The use of $\pi - \pi$ interactions[14], hydrogen bonding,[15–17] charge transfer[18] or coordinative bonds[19] were investigated. The use of host-guest interactions[20–23] and DNA recognition subunits[24–33] were also used to build up well defined assemblies of nanoparticles. Covalent bonds are among the most stable ways to assemble Au NPs into complex structures. A widely used tool to interlinke Au NPs or to decorate their surface is the Cu(I) catalyzed "*Sharpless* click reaction",[34] as the mild room temperature version of the *Huisgen* 1,3-dipolar cycloaddition between azide and an alkyne forming a 1,2,3-triazole. The covalent interlinking of Au NPs has been used for the optical detection of copper by color change of Au NP solutions or by precipitation after forming huge networks.[35–38] The detection of proteins has been achieved by using functional Au NPs, which create large assemblies resulting in an optical response.[39,40] Au NPs were also assembled by click chemistry to form photo responsive networks,[41] liquid crystals,[42] oligomers,[43] chains,[31] combined networks of metal nanoparticles[44,45] and robust nanostructures of different shapes of Au NPs.[46] Furthermore the assembly of Au NPs via click chemistry on functionalized metal and polymer surfaces was performed.[47–51]

These approaches were usually controlled by the maximum number of reactants fitting around one NP or were performed in a statistical fashion. Our goal is to obtain well-defined oligomers of Au NPs in means of spatial arrangement and number of NPs within each assembly. To obtain such structures the ideal Au NP would be characterized by three key features: good chemical stability, narrow size-distribution and well controlled number and spatial arrangement of functional groups exposed at its surface. In 2008 our research group presented the formation of stable Au NPs stabilized by octadentate thioether ligands.[52] It was found that two ligands are coating the NP's surface, leading to bifunctional Au NPs upon introduction of a functional moiety into the ligands backbone.[53] These functional NPs carrying two terminal protected acetylenes were coupled to form organic/inorganic superstructures by applying a wet-chemical oxidative acetylene homocoupling protocol.[54] In order to create monofunctionalized NPs, larger dendritic ligands were designed. Exactly one

second generation dendrimer consisting of 20 thioether moieties was able to stabilize an entire Au NP[55] leading to monofunctionalized Au NPs, which were used to form dumbbell structures by oxidative acetylene coupling.[56] These alkyne-monofunctionalize Au NPs can be considered as artificial molecules and in order to further explore the range of applicable reactions, we became interested in the copper catalyzed mild click reaction between alkynes and azides.

Here we present the assembly of organic/inorganic hybrid architectures by interlinking mono-alkyne functionalized Au NPs with small oligoazide functionalized linker structures using click chemistry. In particular our attempts to assemble dimers, trimers and tetramers are reported.

2. Concept & Strategy

The dendritic thioether ligand **G2** (Scheme 1) efficiently stabilizes Au NPs of a size of about 1.3 nm. The Au NPs are formed by reduction of choloro auric acid in present of the ligand **G2**. While this reduction the growing Au NPs are enwrapped by the dendritic ligand that stabilizes and traps the Au NPs with an almost monodisperse size distribution around 1.3 nm that is given by the size of ligand's cavity. One **G2** dendrimer bearing a triisopropylsilyl (TIPS) protected acetylene moiety is capable to stabilize an entire Au NP (**Au/G2**) and for that reason provides full control over the chemical reactivity of the organic shell surrounding the **Au/G2**.[55,56] The acetylene moiety is attached to an oligo phenylethylene (OPE) rod in order to have the functionality in the NP's periphery. A pyridine moiety was chosen as anchor of the OPE to the NP surface because it is known to provide a fixed perpendicular arrangement of the OPE spacer on the Au NP surface.[54] This rigid arrangement increases the spatial control over the NPs forming the organic/inorganic hybrid structure. Click chemistry seems particularly suited to covalently assemble the monofunctional Au NPs **Au/G2** in well-defined structures. The mild conditions of this well-known azide-alkyne click chemistry reaction make it perfect candidate for this purpose. All reagents used to catalyze this 1,3-bipolar cycloaddition are easily removed after the reaction by aqueous workup. In order to perform click chemistry azide functionalities have to be installed at the periphery of the interlinking structure. By the number of the installed azide moieties, the size of the interlinking structure and their geometric arrangement full control is gained over the number of linked particles and their spatial arrangement. Here benzyl azides are investigated due to the easy synthetic accessability of this functional group and its known reactivity in click

reactions. On the one hand rotational freedom around the benzylic carbon-carbon bond is expected to provide an increased reactivity because the huge particles can evade each other and do not cause sterical hindrance. One the other hand the distance between the particles can differ more if they can form varying arrangements around the linker molecules. However, the difference in the distance should be small enough that a statistical evaluation by transmission electron microscopy (TEM) imaging is still possible. Different numbers of benzylic azides evenly arranged on a central benzene ring are expected to direct the assembly of Au NPs into unique geometric arrangements, which can be observed by TEM investigations. **Figure 1** sketches the concept of controlling the spatial assembly of the interlinked NPs by the azide substitution pattern of the linker.

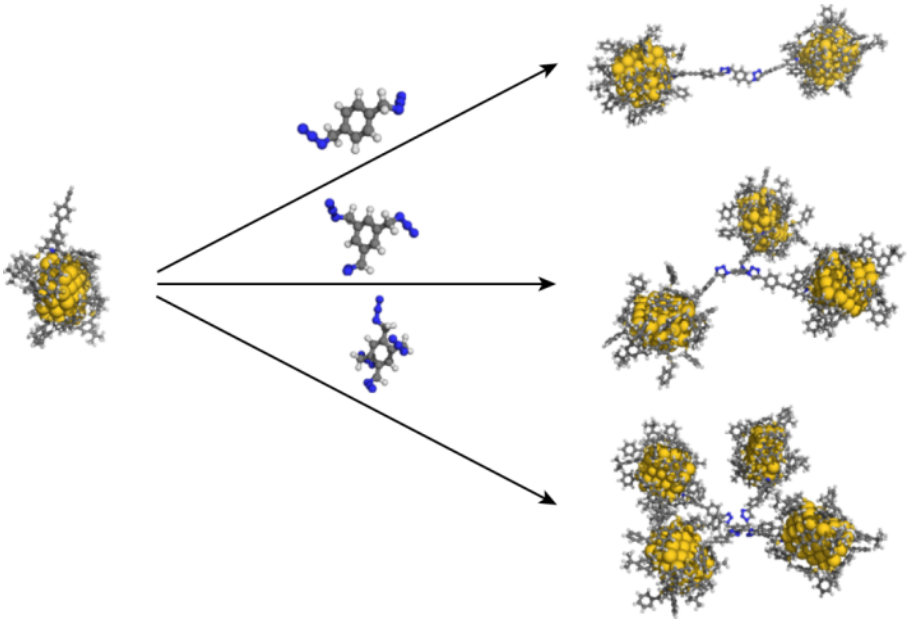

Figure 1. 3D sketch of the click reaction and the resulting oligomers. **G2** stabilized Au NPs (left) are clicked together with benzyl azides (middle) into dimers, trimers and tetramers (right).

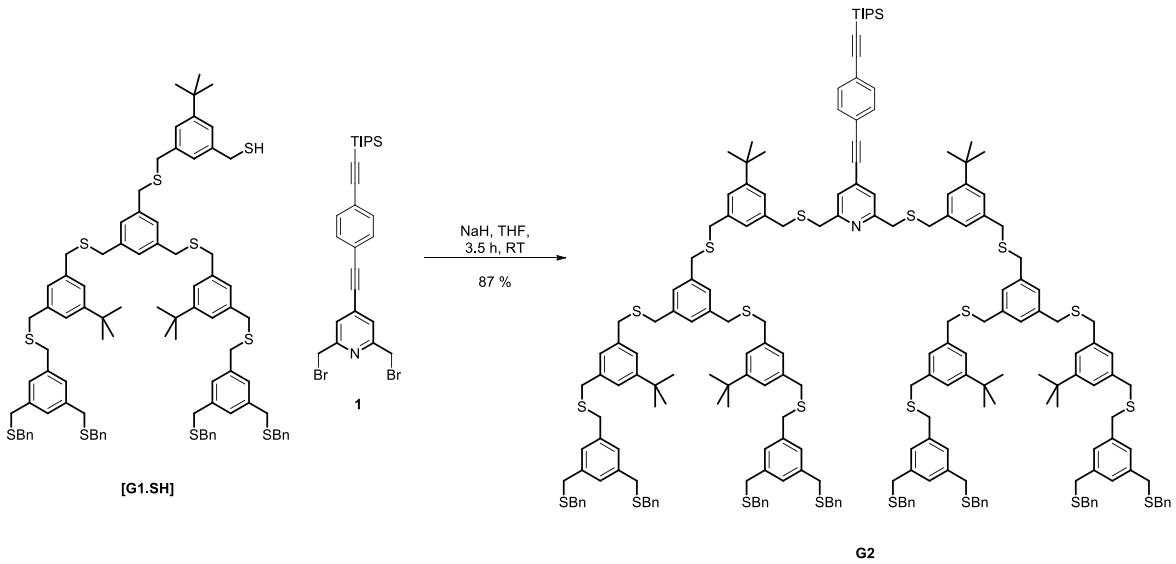

Scheme 1. Synthesis of ligand **G2** using literature known fragments **G1[SH]** and **1**.

3. Synthesis

3.1. Synthesis of the ligand

The **G2** dendrimer, which is used to stabilize the Au NPs, was synthesized from literature known dendron **[G1.SH]** and the functional OPE rod (**1**, see Scheme 1).[56]

To yield **G2** two equivalents of **[G1.SH]** were reacted with one equivalent of the OPE rod (**1**) in tetrahydrofurane (THF) with sodium hydride (NaH) as base. After aqueous workup and purification with silica column chromatography and finally recycling gel permeation chromatography (GPC) the dendritic ligand was obtained as colorless oil in good yields.

3.2. Synthesis of the Multi-Triazide Functionalized Linkers

The azide functionalized linker molecules **2 - 4** were synthesized by a classical S_N2 reaction following a reported protocol. The benzylbromide derivative of interest was treated with an excess of sodium azide (approximately 25 equivalent) as 0.5 M solution in dimethylsulfoxide (DMSO) (Scheme 2).[57] After stirring for 18 h, the reactions were quenched and washed five times with water to remove remaining DMSO. The crude products were purified by column chromatography. Those compounds were obtained in quantitative yields and were stable at ambient conditions for several days. Starting from 1,4-bis(bromomethylene)benzene **5** the 1,4-bis(azidomethylene)benzene **2** was obtained as colorless oil. The 1,3,5-tris(azidomethylene)benzene **3** was synthesized from 1,3,5-tris(bromomethylene)benzene **6** as colorless oil. The 1,2,4,5-tetrakis(azidomethylene)benzene **4** was isolated as colorless solid starting from 1,2,4,5-tetrakis(bromomethylene)benzene **7.** The literature known azides **2 - 4** were characterized by ^{1}H- and ^{13}C NMR, mass spectrometry (MS) and match the reported data.[58–60]

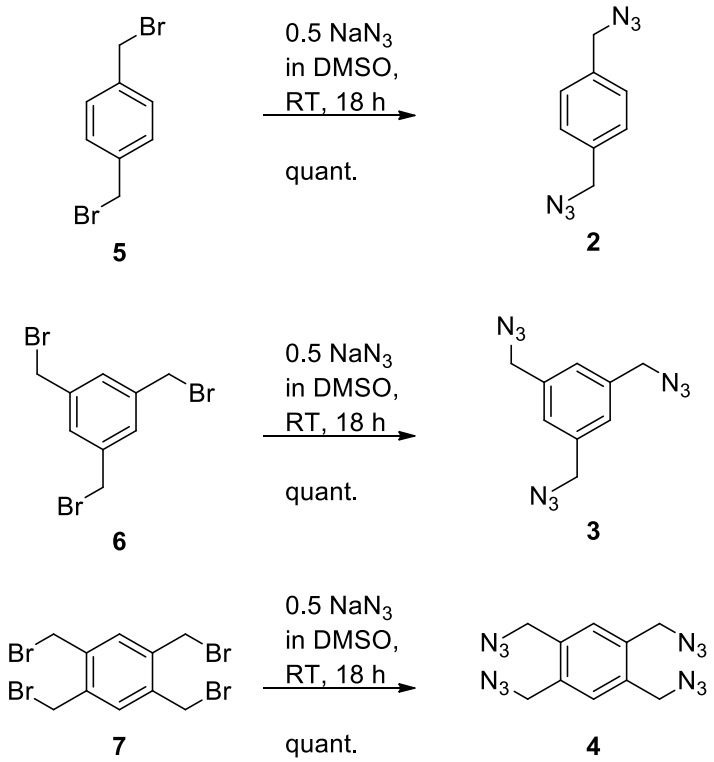

Scheme 2. Synthesis of azide linker molecules **2 - 4**.

3.3. Synthesis of the Au NPs

The Au NPs were synthesized in presence of the dendrimer **G2** in a H_2O/CH_2Cl_2 solvent mixture following a protocol by Brust et al.[61] Hydrochloroauric acid was solved in H_2O and then transferred into the organic phase by adding tetraoctylammonium bromide (TOAB) as phase transfer agent in CH_2Cl_2. The dendrimer **G2** solved in CH_2Cl_2 was added to this mixture and stirred for 15 minutes. Subsequently a solution of sodium borohydride in H_2O was added as reducing agent leading to an immediate color change to dark brown indicating the formation of Au NPs. This mixture was stirred additional 30 min. After aqueous workup and removal of ligand excess by gel permeation chromatography (GPC) the size of the Au NPs was determined by UV/vis and TEM. The UV/vis was measured in CH_2Cl_2 and showed a very weak plasmon band at 520 nm, indicating Au NPs with a size below 2 nm. The features of the OPE rod were observed at 280 nm **(Figure 2).** A diluted sample was transferred on a carbon coated copper grid (CCCG) to determine the particle size by TEM images. Small Au NPs with a narrow dispersity were observed on the TEM pictures from which the size was measured by an automatic investigation method using the software *imageJ*.[62] As recently published, the yielded Au NPs show narrow size distribution with a mean diameter of 1.3 nm ± 0.4 nm.[56] Similar diameters were found for related ligand-stabilized NPs systems based

on unfunctionalized thioether dendrimers or linear thioether ligands.[52–54,63] The 1/1 ratio of stabilizing ligand per Au NPs was corroborated by thermogravimetry. As only one ligand is coating the entire Au NP, only one functional group is exposed per Au NP. It is noteworthy that similar monofunctionalized NPs formed exclusively dimers upon oxidative coupling conditions, further supporting the hypothesis of monofunctionalized Au NPs.[56,64]

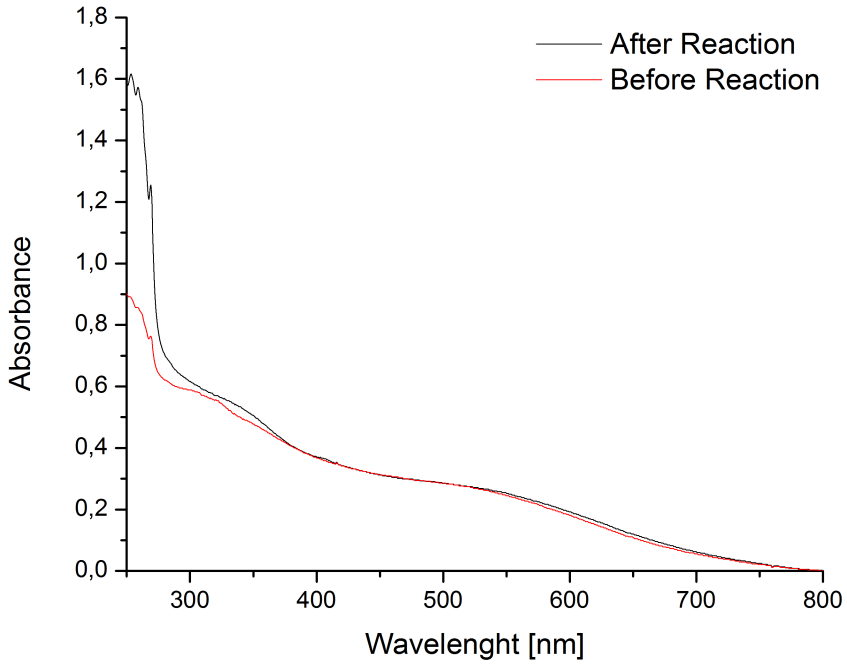

Figure 2. UV/vis spectra to monitor the click reaction.

3.4. Interlinking of the monofunctionalized Au NPs

The oxidative homocoupling of the acetylene functionalized particles in recent publications was conducted with Cu(I) as catalyst in stoichiometric amounts. In order to favor the cycloaddition and avoid homocoupling as competing reaction, a protocol was used with a low concentration of Cu(I) as active catalytic species which was formed in situ by reduction of Cu(II) by sodium ascorbate. As test reaction the Au NPs were exposed to all reagents in CH_2Cl_2 and CH_2Cl_2/H_2O mixtures in order to investigate the stability of the NPs under the reaction conditions. No precipitation or changes in the UV/vis spectra were observed during this treatment. Also subsequent TEM investigations showed a similar size distribution as the initial sample, pointing at the stability of the particles under the reaction conditions of interest.

The synthesis of NP oligomers by interlinking the ethynyl-exposing NPs with the oligoazides **2-4** is displayed in **scheme 3**. First the Au NPs were dissolved in CH_2Cl_2 and the TIPS protection group of the ethynyl function was removed by fluoride ions coming from

subsequently added tetrabutylammonium fluoride (TBAF). The reaction was quenched after 1 hour and washed with water. After these deprotected AuNPs exposing a free ethynyl group were dried and redissolved in CH_2Cl_2, an equivalent of triazides was provided by adding the required amounts of the multi-triazide linker dissolved CH_2Cl_2. Thus 1/2 equivalent **2**, 1/3 equivalent **3** and 1/4 equivalent **4** were added respectively. Subsequently a 1 M $CuSO_4$ solution in followed by 25 mol % sodium ascorbate as 1 M solution in water were added to the vigorously stirred reaction mixture. For the reactions of all linker molecules a similar analytical procedure was applied. First a sample of the CH_2Cl_2 phase was taken and investigated by UV/vis spectroscopy to monitor the Au NPs size (Figure 2). No increase in intensity or shift of the plasmon band was observed pointing at the structural integrity of the Au NPs under the applied reaction conditions. In contrast to that the signal of the OPE structure around 280 nm displayed a pronounced increase in intensity together with a slight shift to longer wavelength. These spectral changes point at an increased delocalization of the π-system, as it is expected by the formation of the triazole heterocycles as products of the "click-chemistry".

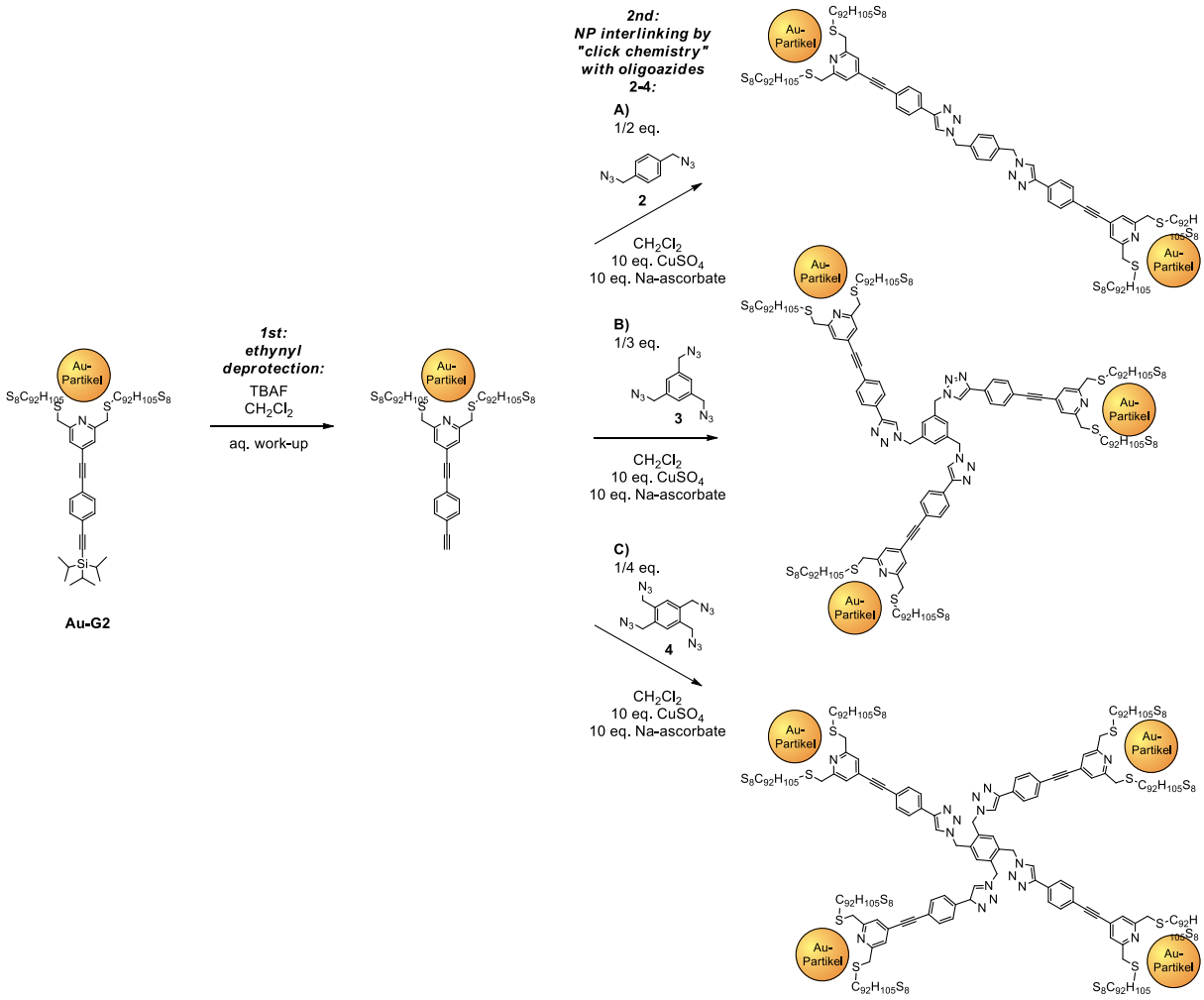

Scheme 3. Synthesis of nano-scale objects by wet-chemical assembly of mono-ethynyl functionalized nano-particles and the azide linkers **2** – **4** under "click-chemistry" conditions. Synthesis of a "dumbbell" dimer A), a trimer B) and a tetramer C); (the particle coating dendritic ligand is only sketched as formula to increase clarity).

The click reaction was further monitored by attenuated total reflectance infrared spectroscopy (ATR-IR) where mainly the consumption of the azide linker was observed (**Figure 3**). The triazide band at 2100 cm^{-1} decreased to a very small remaining trace showing the almost complete transformation of the triazide group during the course of the "click" reaction.

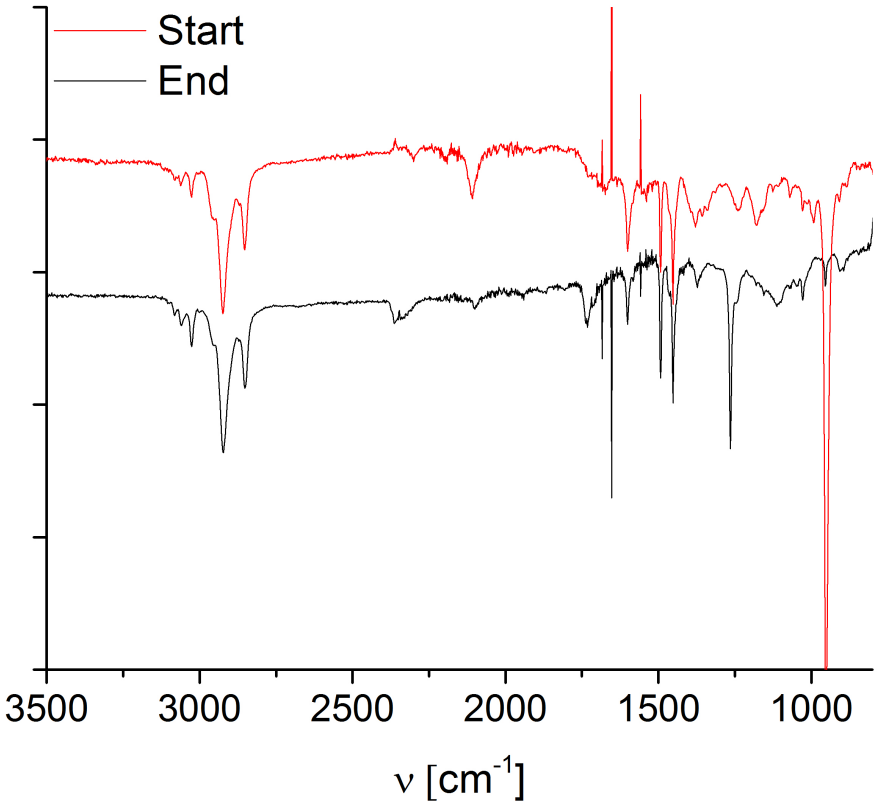

Figure 3. Normalized ATR-IR Spectra to monitor the decrease of azide groups (2100 cm^{-1}).

Finally the reaction was stopped by allowing the two phases to separate and the dark brown reddish colored CH_2Cl_2 phase was dried over $MgSO_4$.

4. TEM Analysis

The solved coupled Au NPs were further diluted by approximately a factor of 1000. This diluted solution was spotted on a CCCG in order to investigate structural features of the

reaction products by TEM. Of particular interest are sizes, distances and spatial arrangements of Au NPs. While the first parameter mainly allows analyzing the NPs' stability, the latter two reflect dimensional details of the hybrid architecture. Thus TEM analyses were ideally suited to investigate the nature and the ratios of the formed hybrid oligomers. In all three samples of the reactions with the respective linker molecules the NP sizes maintained pointing at their stability in the applied reaction conditions. The yield of the obtained NP oligomers was counted on randomly recorded TEM pictures of very diluted solutions. High dilution was chosen to minimize wrong hits eventually emerging from agglomerating hybrid objects and/or NPs, which might result in similar inter NP spacing as the desired hybrid objects. On these diluted micrographs all particles where counted and the amount of oligomeric architectures was determined manually. A set of NPs was considered as a hybrid architecture if their lateral separation was within the distances d_{max} given by the following considerations. In order to determine d_{max} the maximal expansion of the interlinking molecular structure was analyzed. These structures combine the functional units of the NPs fused to the corresponding linker molecule and were created with the software SPARTAN V4.1.1 and shown as simplified drawing in **Figure 4**. The modeled structures are called ***ms*2**, ***ms*3** and ***ms*4**. To determine their maximal extensions d_{max} the OPE structures were rotated around the benzylic C – C bond until the maximum possible distance between two terminal N atoms of the structure was found (Figure 4).

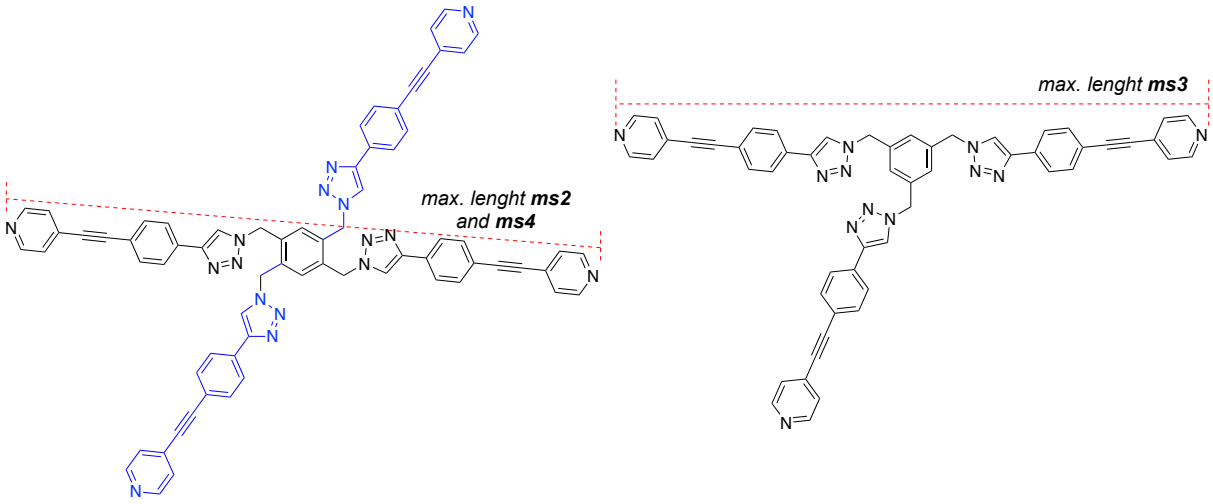

Figure 4. Schematic drawing of model structures ***ms*2**, ***ms*3** and ***ms*4** to determine maximum possible distance d_{max} between two NP

In order to consider potential imprecision of the TEM images, the obtained maximum distance between both terminal nitrogen's was increased by 0.4 nm, which is the size of almost two pixels. So two particles were considered as connected if their distance d_{max} was

within the calculated value d_{max} = 3.9 nm for ***ms2***, d_{max} = 3.8 nm for ***ms3*** and d_{max} = 3.9 nm for ***ms4***. For the statistical evaluation all distances of Au NPs fitting this selections rule were counted. Also the ratio of different oligomers was investigated for each sample.

4.1. Dimer Structures

The linker molecule **2** carrying two benzylic azide functions assembles NP with a maximum interparticle distance of d_{max} = 3.9 nm. To yield as many desired dimers as possible 0.5 eq. of **2** were reacted with 1 eq. Au NPs. On TEM images 249 particles were counted. 94 NPs were found as single structures, 128 NPs assembled as dimers, 12 NPs as trimers and 16 NPs within higher oligomers (**Figure 5**A). Trimers and tetramers can occur because of aggregation of the Au NPs. The found trimers can be the aggregation product of three single Au NPs or more likely because of the high dilution one dimer and a monomer. The tetramers are also aggregates of either a dimer with two monomers on each side or two dimers. Over all about 51 % of the counted particles show the expected formation of dimers (Figure 5C). The high amount of single structures points at particles lacking an exposed and reactive acetylene group. As NMR studies document the completeness of the deprotection reaction, potential hypotheses are either sterical shielding by the large NP or competing degradation of the acetylene during the course of the coupling reaction.

The interparticle distance *d* measured of the oligomers display mean value of 2.9 nm calculated by a Gaussian fit (Figure 5B). All distances of particles matching the selection rule mentioned above are taken in account.

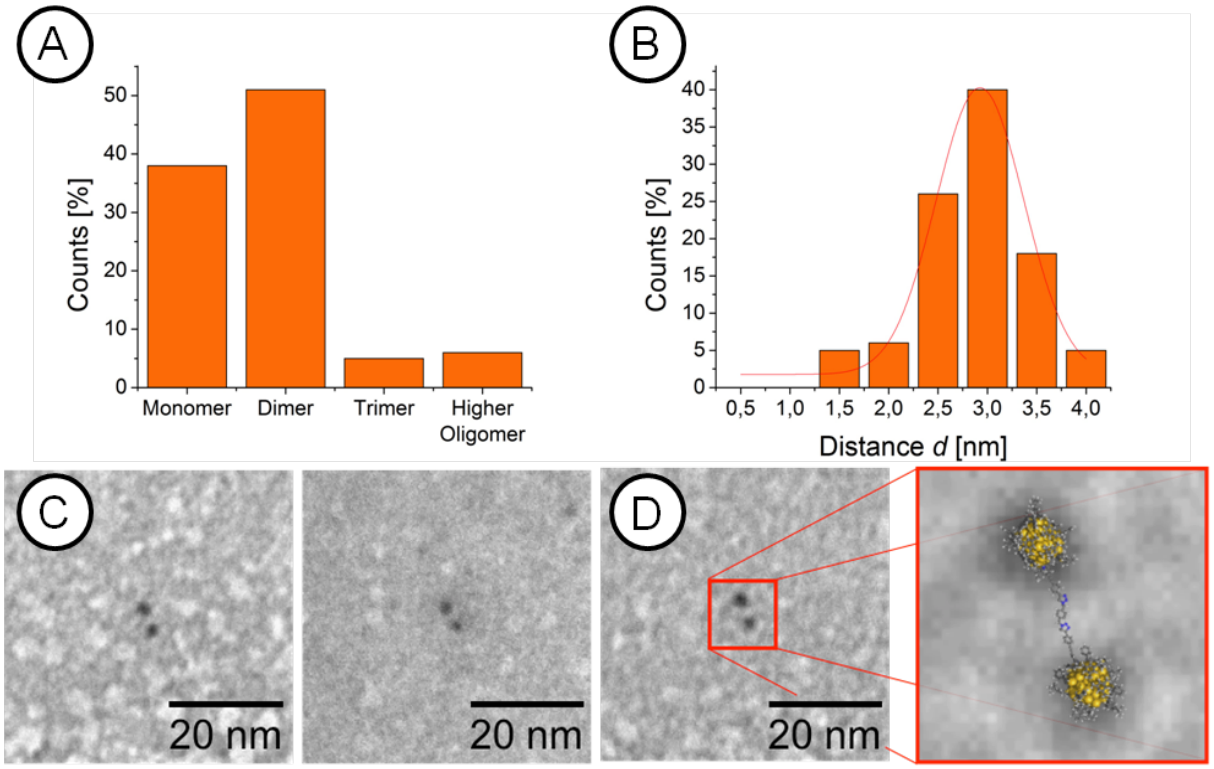

Figure 5. A) Distribution of the formed oligomers, B) Distance distribution between the oligomer forming particles with *Gaussian* fit (red curve), C) Representative TEM pictures of formed dimer with linker molecule, more pictures are displayed in the supporting information (S3, S4), D) Zoom with overlayed 3D sketch of proposed structure

4.2. Trimer Structures

The evaluation of the click reaction with linker molecule **3** was performed following the same procedure. To yield the desired trimers equimolar ratios of azide groups in linker molecule **3** and Au NPs were mixed together under click conditions. The calculated maximum distance d_{max} = 3.8 nm of the clicked triangular structure ***ms*3** is just slightly shorter than the distance of the clicked assembly formed by ***ms*2**. For this arrangement the third NP would form an isosceles triangle if the other two are in a stretched arrangement. Therefore smaller distances are expected as three NPs should form an equilateral triangle for less sterical repulsion. A total of 264 NPs were evaluated, of whom 104 were present as monomers, 22 arranged in dimers, 117 connected to trimers (**Figure 6A**) and 21 lying together as higher oligomers. The found dimers are probably linkers that only reacted with two Au NP, which seems the more likely scenario than two aggregated Au NPs, considering the high dilution deposition protocol. The found tetramers are supposed to be aggregates of trimers with a single Au NP. Again a reasonable amount of monomers could be observed. Because of the low ratio of dimers a passivation of the linking structure during the reaction must occur. If only sterical

reasons would cause this distribution a higher amount of dimers would be expected. The coupling reaction is relatively fast as no further increase in the yield of oligomers is observed after 2 h. This observation further favors the hypothesis of competing side reactions over solely sterical arguments.

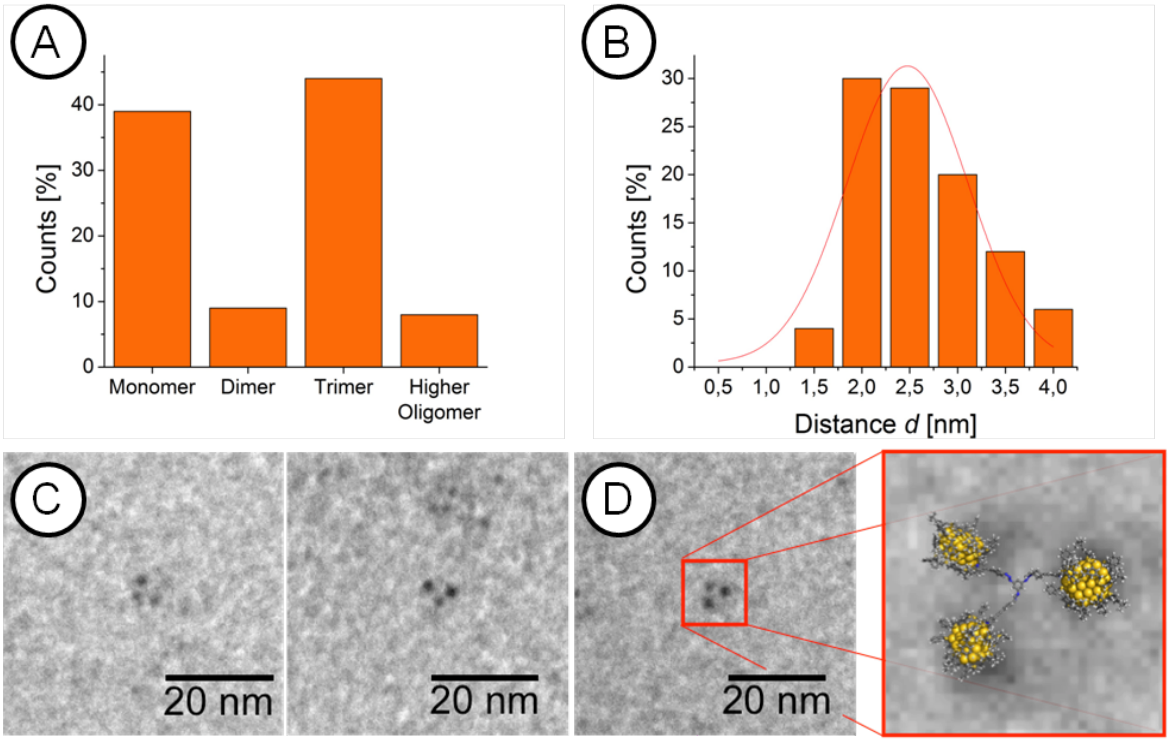

Figure 6. A) Distribution of the formed oligomers, B) Distance distribution between the oligomer forming particles comprising a *Gaussian* fit (red curve), C) Representative TEM pictures of formed trimers with linker molecule **3**, additional TEM records are displayed in the supporting information (S5, S6), D) Zoom with overlayed 3D sketch of the proposed structure.

A clear trend can be observed as about 44 % of the nanoparticles were found in triangular assemblies (Figure 6C). The distance distribution measured from TEM is broader than the first sample and shows a smaller mean interparticle distance of 2.4 nm (Figure 6B). The broadening can be explained by the higher flexibility of three possible rotations around the benzylic C – C bond leading to a larger variety of NPs spacing.

4.3. Tetramer Structure

Subsequently the click reaction of an equimolar amount deprotected NPs with linker molecule **4** was examined. The maximum length d_{max} of ***ms*4** was calculated to be 3.9 nm, which is the same as the stretched conformation of the interlinking structure ***ms*2**. For interlinked

substructure ***ms*4** a rectangular shape with two different sides (Figure 8) is expected. Just the four sides were measured for the evaluation of the interparticle distance; the diagonals were not taken in account. This procedure was applied because also dimers and trimers where measured. In the case of the trimers it cannot be distinguished whether a edge or diagonal distance is measured. To measure a equal representative amount of distances all four edges of a tetramer structure were considered without the diagonals. For a dimer one distance is measured, for a trimer three distances and four distances for a tetramer. The diluted TEM images of the clicked samples displayed nanoparticles present as monomers, dimers, trimers and tetramers without a clear peak for the desired oligomer as in the first experiments (**Figure 7A**). Again about 30 % of the Au NPs were present as monomer structures what is in analogy with the previous reactions. One difference in this case is the decreasing number of found oligomers that is a hint for additional restraining effects. Our hypothesis is that this might be due to the limited space around the linker molecule **4**. This is leading to a higher yield of undesired dimers and trimers instead of tetramers. The first two NPs probably react in the same manner as for linker molecule **2** because the additional benzylic azides are not very sterical demanding. As soon as two NP are attached to linker **4** both remaining azides are already shielded by the present NPs hindering the next reaction step to the trimer. The reaction of the trimer to the tetramer is even more hindered, as the linker molecule is rather small compared to the particles. Therefore, the formation of tetramers is not favored and an equal distribution of oligomers was obtained. Of 299 NPs that were evaluated for the investigation 131 of them were present as monomers. 98 NPs were present as dimers, 93 as trimers and 64 NPs were reacted to tetramers (Figure 7CA). Extended duration of the click reaction could not improve the ratio of the oligomers towards more tetramers. The mean distance for all oligomers stated as connected to each other is 2.4 nm (Figure 7B).

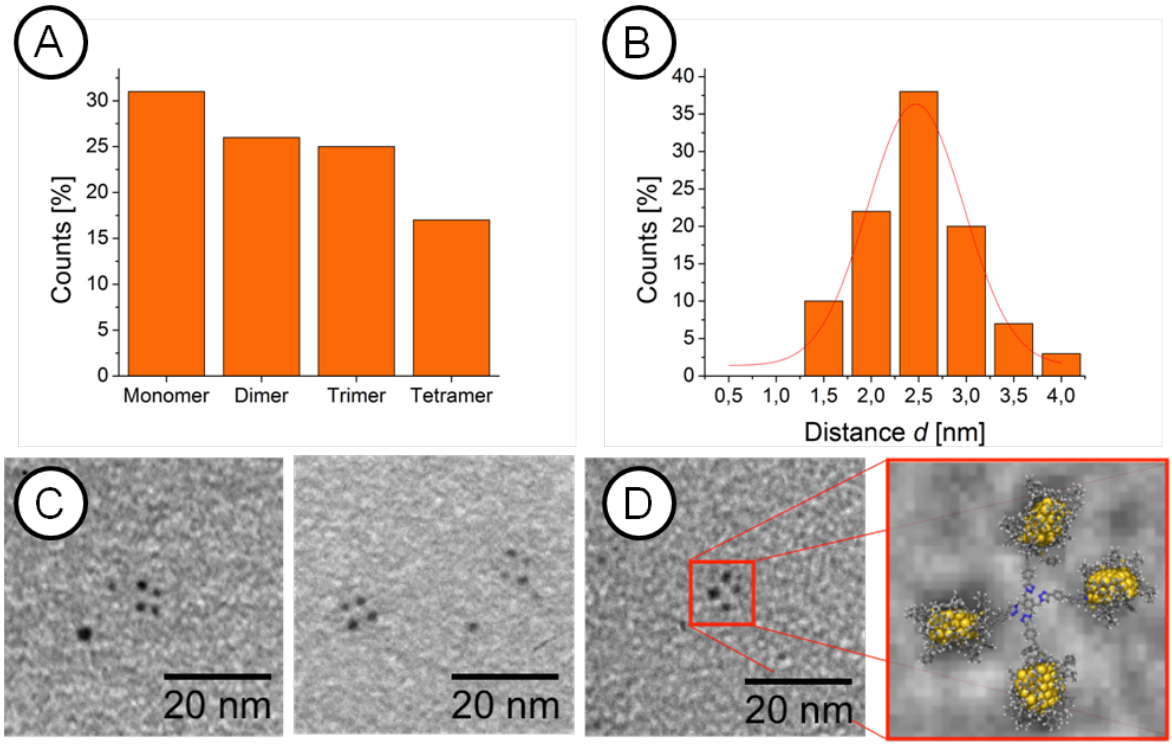

Figure 7. A) Distribution of the formed oligomers, B) Distance distribution between the oligomer forming particles with a *Gaussian* fit (red curve), C) Representative TEM pictures of formed tetramers with linker molecule **4**, more TEM pictures are displayed in the supporting information (S7 - S9), D) Zoom with overlayed 3D sketch of proposed structure.

4.4. Discussion of the measured Distances

All found interparticle distances are all considerably shorter than the calculated maximum possible spacing. This behavior was expected because the maximum distances d_{max} were calculated to define a selection rule in order to determine particles as coupled to each other. In reality the spacing between the particles must be shorter because the interlinking structure will arrange in a more folded geometry (**Figure 8**).

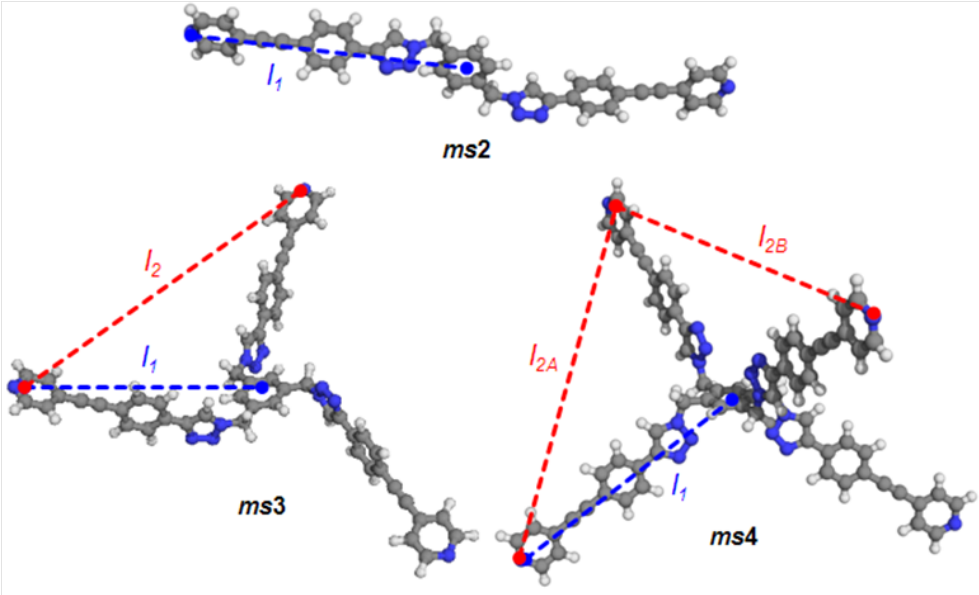

Figure 8. Energy minimized model (MMFF94) structures ***ms*2**, ***ms*3**, and ***ms*4** in stretched out geometry representing the expected maximum spacing between Au NPs interlinked by the molecules **2**, **3**, and **4** respectively.

An approximate value to evaluate the experimental found distances was calculated for each click reaction. The dimer structure ***ms2*** is able to rotate around both benzyl C - C bounds what leads to various stretched and folded conformation of interlinked particles. The minimum distance for the folded conformation is calculated to be $l_{1\,fold}$ = 1.3 nm for the stretched conformation a maximum value of $l_{1\,stre}$ = 3.2 nm is calculated. The mean diameter of all found dimers show a nice distribution from 1.3 nm to d_{max} = 3.9 nm with its mean value at 2.9 nm. Because of the huge size and the resulting repulsion of the Au NPs a stretched assembly is more probably. That is reflected in the found distance d = 2.9 nm which is at the upper end of the possible calculated value matching nearly calculated distance for a stretched assembly.

In contrast to the above discussed stretched dimers, the measured interparticle distances in trimers and tetramers is no longer directly reflecting the interlinking structure and its correlation must thus be corrected. For the trimer structure a flat arrangement like an equilateral triangle is expected. This arrangement would provide a maximum of space for each coupled Au NP. From a MM2 relaxed planar fixed model of structure ***ms3*** the distance d_{calc} for an equilateral triangle is calculated with equation (1).

$$d_{calc} = \frac{l_2 \cdot (l_1 + r)}{l_1} - 2r \qquad (1)$$

The value l_1 is measured form the coupled structures center ***ms3*** to the nitrogen atom of the clicked OPE rod of the ligand **G2** and l_2 from one nitrogen atom to the next neighbored in

this structure (Figure 8). With the radius *r* of the Au NPs the distance *d* can be calculated by applying the intercept theorem as displayed in **Figure 9** using equation (1). The found mean distance *d* of 2.4 nm matches the calculated value d_{calc} of 2.4 nm perfectly. Of course the distances can vary when the structure is rotated around the benzylic C - C bounds from a minimum value of 1.3 nm to a maximum value of 3.1 nm that is well reflected in the distance distribution (Figure 6B). The perfect matching of the calculated value d_{calc} with the measured distances *d* fully supports the hypothesis of formed trimers and their flat relaxed arrangement as equilateral triangle on the CCCG of the TEM.

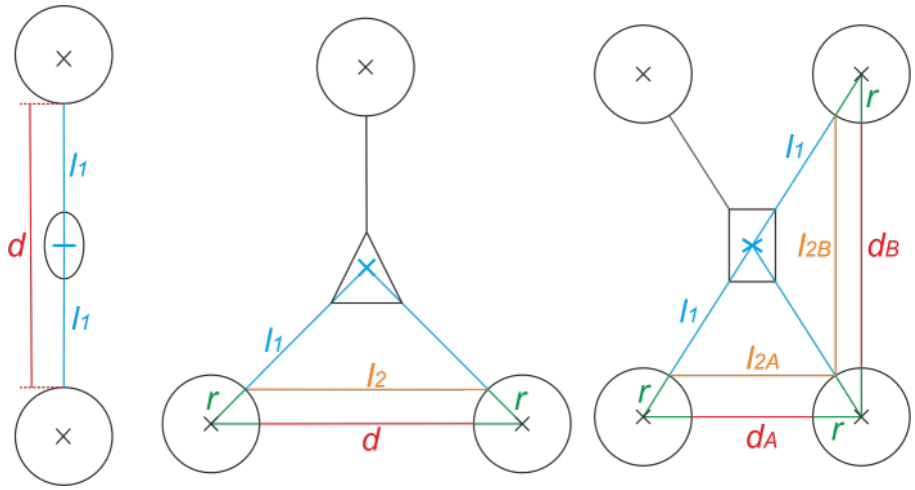

Figure 9. Sketch to visualize calculations for Au NP inter particle distances. Left side dimer structure, middle trimer structure and right tetramer structure. All lengths are calculated by using molecular mechanics (MMFF94) from ***ms*2, *ms*3,** and ***ms*4** (see Figure 8).

In similarity to the trimers above, a flat arrangement is also assumed for the tetramer structures on the CCCG. For the rectangular structures ***ms4*** the two different sides l_{2A} and l_{2B} must be taken into account. The calculated inter particle distances d_A and d_B are calculated from the values l_{1A}, l_{2A}, l_{1B}, l_{2B} and *r* (Figure 8) with formula (1) in the same manner as for the triangle structures (Figure 9). The measured mean distance of 2.4 nm matches calculated mean distance 2,4 nm of $d_A = 2.2$ and $d_B = 2.7$ for a flat assembly perfectly (Table 2). The fact that the measured distances of the reaction to tetramers matches the calculated values supports the hypothesis that also the found dimers and trimers arise from not completely reacted linker molecules, because they assemble in similar distances to each other. These results reflect the flat arrangement of the tetramer structures as well as the hypothesis of the high amount of dimers and trimers caused by sterical repulsion of the Au NPs during the click reaction. All values for the calculation are listed in Table 1.

In table 2 the experimental found and calculated distances are summarized for all synthesized Au NP oligomers.

In summary, the observed nanoparticle oligomers reflecting the numbers and spatial orientation of the functional groups of the oligoazide precursors, the interparticle distance analysis in the obtained organic/inorganic hybrid architectures, and the disappearance of the azide bands in the IR spectra are corroborating the successful interlinking of the ethynyl functionalized particles by "click chemistry". The UV/Vis spectra further support the formation of triazole linkers and corroborate the stability and homogeneity of the ligand coated gold nano-particles under the applied reaction conditions.

5. Conclusion

The formation of Au NPs into defined organic/inorganic hybrid nanoarchitectures in means of quantity and spatial arrangement utilizing a wet click chemistry protocol is successfully demonstrated with mono acetylene functionalized Au NPs. A series of azide linker molecules was used to build up dimer, trimer and tetramer structures reflecting the linker's geometry. Our current attempts are geared towards optimizing the reactive sites for the *Huisgen* 1,3-dipolar cycloaddition in order to improve the efficiency of the coupling reaction. We are searching also for ligand structures providing larger monofunctionalized metallic particles displaying plasmon resonance bands which are of interest for a variety of optical experiments and devises. Finally strategies to improve the stability of the particles are very appealing as the diversity of applicable reactions scales with the stability of the reacting species.

The proof of concept to use Au NPs as artificial molecules engaged in click reactions is appealing for numerous applications ranging from labels to functional units in electronic and optical devises. The future success of the approach however will depend strongly on the nature, variety, and quality of available particles.

Acknowledgements

We are grateful to the University of Basel and the Karlsruhe Institute of Technology for ongoing support. Financial support by the EU through the project FUNMOL (no. 213382 of the call FP7-NMP-2007-SMALL-1), the Swiss National Science Foundation (SNF), the Swiss Nanoscience Institute (SNI) and the National Research Program 62 "smart materials" is gratefully acknowledged.

[1] A. Corma, H. Garcia, *Chem. Soc. Rev.* **2008**, *37*, 2096–2126.

[2] C. Della Pina, E. Falletta, L. Prati, M. Rossi, *Chem. Soc. Rev.* **2008**, *37*, 2077–2095.

[3] X. Zhang, Q. Guo, D. Cui, *Sensors* **2009**, *9*, 1033–1053.

[4] M. Homberger, U. Simon, *Phil. Trans. R. Soc. A* **2010**, *368*, 1405–1453.

[5] G. Schmid, *Chem. Soc. Rev.* **2008**, *37*, 1909–1930.

[6] I. Willner, B. Willner, *Nano Lett.* **2010**, *10*, 3805–3815.

[7] R. D. Powell, J. F. Hainfeld, *Micron* **2011**, *42*, 163–174.

[8] J. I. Cutler, E. Auyeung, C. A. Mirkin, *J. Am. Chem. Soc.* **2012**, *134*, 1376–1391.

[9] L. Dykman, N. Khlebtsov, *Chem. Soc. Rev.* **2012**, *41*, 2256.

[10] F. Westerlund, T. Bjørnholm, *Curr. Opin. Colloid Interface Sci.* **2009**, *14*, 126–134.

[11] K. J. M. Bishop, C. E. Wilmer, S. Soh, B. A. Grzybowski, *Small* **2009**, *5*, 1600–1630.

[12] C. L. Choi, A. P. Alivisatos, *Annu. Rev. Phys. Chem.* **2010**, *61*, 369–389.

[13] M. Grzelczak, J. Vermant, E. M. Furst, L. M. Liz-Marzán, *ACS Nano* **2010**, *4*, 3591–3605.

[14] K. Naka, H. Itoh, Y. Chujo, *Langmuir* **2003**, *19*, 5496–5501.

[15] C. R. van den Brom, P. Rudolf, T. T. M. Palstra, B. Hessen, *Chem. Commun.* **2007**, 4922.

[16] H. Ozawa, M. Kawao, H. Tanaka, T. Ogawa, *Langmuir* **2007**, *23*, 6365–6371.

[17] C.-P. Chak, S. Xuan, P. M. Mendes, J. C. Yu, C. H. K. Cheng, K. C.-F. Leung, *ACS Nano* **2009**, *3*, 2129–2138.

[18] K. Naka, H. Itoh, Y. Chujo, *Langmuir* **2003**, *19*, 5496–5501.

[19] H. Ozawa, M. Kawao, H. Tanaka, T. Ogawa, *Langmuir* **2007**, *23*, 6365–6371.

[20] R. Klajn, M. A. Olson, P. J. Wesson, L. Fang, A. Coskun, A. Trabolsi, S. Soh, J. F. Stoddart, B. A. Grzybowski, *Nat. Chem.* **2009**, *1*, 733–738.

[21] M. A. Olson, A. Coskun, R. Klajn, L. Fang, S. K. Dey, K. P. Browne, B. A. Grzybowski, J. F. Stoddart, *Nano Lett.* **2009**, *9*, 3185–3190.

[22] M. A. Olson, A. Coskun, R. Klajn, L. Fang, S. K. Dey, K. P. Browne, B. A. Grzybowski, J. F. Stoddart, *Nano Lett.* **2009**, *9*, 3185–3190.

[23] Q. Zeng, R. Marthi, A. McNally, C. Dickinson, T. E. Keyes, R. J. Forster, *Langmuir* **2010**, *26*, 1325–1333.

[24] A. P. Alivisatos, K. P. Johnsson, X. Peng, T. E. Wilson, C. J. Loweth, M. P. Bruchez, P. G. Schultz, *Nature* **1996**, *382*, 609–611.

[25] C. A. Mirkin, R. L. Letsinger, R. C. Mucic, J. J. Storhoff, *Nature* **1996**, *382*, 607–609.

[26] Z. Deng, Y. Tian, S.-H. Lee, A. E. Ribbe, C. Mao, *Angew. Chem., Int. Ed.* **2005**, *44*, 3582–3585.

[27] F. A. Aldaye, H. F. Sleiman, *Angew. Chem., Int. Ed.* **2006**, *45*, 2204–2209.

[28] F. Huo, A. K. R. Lytton-Jean, C. A. Mirkin, *Adv. Mater.* **2006**, *18*, 2304–2306.

[29] S. E. Stanca, R. Eritja, D. Fitzmaurice, *Faraday Discuss.* **2006**, *131*, 155.

[30] J. H. Lee, D. P. Wernette, M. V. Yigit, J. Liu, Z. Wang, Y. Lu, *Angew. Chem., Int. Ed.* **2007**, *46*, 9006–9010.

[31] M. Fischler, A. Sologubenko, J. Mayer, G. Clever, G. Burley, J. Gierlich, T. Carell, U. Simon, *Chem. Commun.* **2008**, 169.

[32] M. H. S. Shyr, D. P. Wernette, P. Wiltzius, Y. Lu, P. V. Braun, *J. Am. Chem. Soc.* **2008**, *130*, 8234–8240.

[33] M. H. S. Shyr, D. P. Wernette, P. Wiltzius, Y. Lu, P. V. Braun, *J. Am. Chem. Soc.* **2008**, *130*, 8234–8240.

[34] V. V. Rostovtsev, L. G. Green, V. V. Fokin, K. B. Sharpless, *Angewandte Chemie Int. Ed.* **2002**, *41*, 2596–2599.

[35] Y. Zhou, S. Wang, K. Zhang, X. Jiang, *Angew. Chem., Int. Ed.* **2008**, *47*, 7454–7456.

[36] X. Xu, W. L. Daniel, W. Wei, C. A. Mirkin, *Small* **2010**, *6*, 623–626.

[37] C. Hua, W. H. Zhang, A. De, S. Ciampi, D. Gloria, G. Liu, J. B. Harper, J. J. Gooding, *Analyst* **2012**, *137*, 82–86.

[38] Z. Lin, S. Gao, J. Lin, W. Lin, S. Qiu, L. Guo, B. Qiu, G. Chen, *Anal. Methods* **2012**, *4*, 612–615.

[39] M.-X. Zhang, B.-H. Huang, X.-Y. Sun, D.-W. Pang, *Langmuir* **2010**, *26*, 10171–10176.

[40] K. Zhu, Y. Zhang, S. He, W. Chen, J. Shen, Z. Wang, X. Jiang, *Anal. Chem.* **2012**, *84*, 4267–4270.

[41] A. Kimoto, K. Iwasaki, J. Abe, *Photochem. Photobiol. Sci.* **2010**, *9*, 152–156.

[42] S. Mischler, S. Guerra, R. Deschenaux, *Chem. Commun.* **2012**, *48*, 2183–2185.

[43] M. Homberger, S. Schmid, J. Timper, U. Simon, *J. Cluster Sci.* **2012**, *23*, 1049-1059.

[44] W. Maneeprakorn, M. A. Malik, P. O'Brien, *J. Am. Chem. Soc.* **2010**, *132*, 1780–1781.

[45] E. Locatelli, G. Ori, M. Fournelle, R. Lemor, M. Montorsi, F. Comes, *Chem. Eur. J.* **2011**, *17*, 9052–9056, S9052/1–S9052/14.

[46] M. Xie, L. Ding, Z. You, D. Gao, G. Yang, H. Han, *J. Mater. Chem.* **2012**, *22*, 14108–14118.

[47] T. Zhang, Z. Zheng, X. Ding, Y. Peng, *Macromol. Rapid Commun.* **2008**, *29*, 1716–1720.

[48] H. Gehan, L. Fillaud, M. M. Chehimi, J. Aubard, A. Hohenau, N. Felidj, C.

Mangeney, *ACS Nano* **2010**, *4*, 6491–6500.

[49] H. Gehan, L. Fillaud, N. Felidj, J. Aubard, P. Lang, M. M. Chehimi, C. Mangeney, *Langmuir* **2010**, *26*, 3975–3980.

[50] S. A. Krovi, D. Smith, S. T. Nguyen, *Chem. Commun.* **2010**, *46*, 5277–5279.

[51] M. Guerrouache, S. Mahouche-Chergui, M. M. Chehimi, B. Carbonnier, *Chem. Commun.* **2012**, *48*, 7486–7488.

[52] T. Peterle, A. Leifert, J. Timper, A. Sologubenko, U. Simon, M. Mayor, *Chem. Commun.* **2008**, 3438–3440.

[53] T. Peterle, P. Ringler, M. Mayor, *Adv. Funct. Mater.* **2009**, *19*, 3497–3506.

[54] J. P. Hermes, F. Sander, T. Peterle, C. Cioffi, P. Ringler, T. Pfohl, M. Mayor, *Small* **2011**, *7*, 920–929.

[55] J. P. Hermes, F. Sander, T. Peterle, R. Urbani, T. Pfohl, D. Thompson, M. Mayor, *Chem. Eur. J.* **2011**, *17*, 13473–13481.

[56] J. P. Hermes, F. Sander, U. Fluch, T. Peterle, D. Thompson, R. Urbani, T. Pfohl, M. Mayor, *J. Am. Chem. Soc.* **2012**, *134*, 14674-14677.

[57] S. G. Alvarez, M. T. Alvarez, *Synthesis* **1997**, *1997*, 413–414.

[58] J. R. Thomas, X. Liu, P. J. Hergenrother, *J. Am. Chem. Soc.* **2005**, *127*, 12434–12435.

[59] Y. Song, E. K. Kohlmeir, T. J. Meade, *J. Am. Chem. Soc.* **2008**, *130*, 6662–6663.

[60] H. E. Montenegro, P. Ramírez-López, M. C. de la Torre, M. Asenjo, M. A. Sierra, *Chem. Eur. J.* **2010**, *16*, 3798–3814.

[61] M. Brust, M. Walker, D. Bethell, D. J. Schiffrin, R. Whyman, *Chem. Commun.* **1994**, 801–802.

[62] M. D. Abramoff, P. J. Magalhães, S. J. Ram, *Biophotonics int.* **2004**, *11*, 36–42.

[63] J. P. Hermes, F. Sander, T. Peterle, M. Mayor, *Chimia* **2011**, *65*, 219–222.

[64] D. Thompson, J. P. Hermes, A. J. Quinn, M. Mayor, *ACS Nano* **2012**, *6*, 3007–3017.

Supporting Information

Dumbbells, Trikes and Quads - Click Gold Nanopartricles together

Fabian Sander,[1] Jens Peter Hermes,[1] Ulrike Fluch[1], Marcel Mayor,[1,2]

[1] *University of Basel, Department of Chemistry, St. Johannsring 19, CH-4056 Basel, Switzerland*

[2] *Karlsruhe Institute of Technology (KIT), Institute of Nanotechnology (INT), P. O. Box 3640, D-76021 Karlsruhe, Germany*

S1. General Methods - Used Reagent, Solvents and Analytical Devices

All commercially available starting materials were of reagent grade and used as received. Absolute tetrahydrofuran (THF) and Dichloromethane used as solvent for reactions was purchased from *Fluka*, stored over 4 Å molecular sieves, and handled under Argon. All other used solvents were of technical grade and distilled prior to use. For microwave reactions a *Biotage Initiator 8* was used. Column chromatography purifications were carried out on *silica gel 60* (particle size 40-63 μm) from *Fluka*. Deuterated solvents were purchased from *Cambridge Isotope Laboratories*. ^{1}H and ^{13}C NMR spectra were recorded with a *Bruker DMX 400* instrument (^{1}H resonance 400 MHz) or a *Bruker DRX 500* instrument (^{1}H resonance 500 MHz) at 298 K. Electron Impact (EI) mass spectra were recorded on a *Finnigan MAT 95Q* by H. Nadig. Elemental analyses were performed by W. Kirsch on a *Perkin-Elmer Analysator 240*. Gel Permeation Chromatography (GPC) was performed on a Shimadzu Prominence System with SDV preparative columns from Polymer Standards Service (two columns in series, 60 cm each, operating range: 100 – 30,000 g mol^{-1}) using chloroform as eluent. Size exclusion chromatography (SEC) was performed using Bio-Rad Bio-Beads S-X1 Beads (operating range 600 – 14000 g mol^{-1}) with toluene as eluent.

General Procedure for Preparation of Benzyl Azides 2 - 4

Note: Safety and in Handling of Azides:

During our experiments we did not experienced any problems in handling these compounds, however some organic azides have been reported to be explosive and toxic. Therefore precaution should be taken. Be aware that sodium azide is toxic and can be absorbed through the skin.

To 5 mL of a 0.5 M solution of NaN_3 in DMSO were added 1 mmol of the corresponding benzyl bromide. The mixture was stirred for 18 h and then quenched with water and extracted with dichloromethane. The organic phase was then washed five times with water to remove DMSO, dried over $MgSO_4$. After the solvent was removed in vacuum the crude product was purified by column chromatography (cyclohexane : ethylacetate 4 : 1).

(2) 1,4-bis(azidomethylene)benzene[1]

colorless oil, yield 97 %.

^{1}H-NMR (400 MHz, $CDCl_3$): δ = 7.35 (s, 4H), 4.36 (s, 4H).

^{13}C-NMR (125 MHz, $CDCl_3$): δ = 133.9, 130.2, 129.0, 52,3.

MS EI(m/z (%)):188.1 (32%)[M^+], 146.1 (100%)[M^+-N_3], 118.1 (43%)[M^+-N_3,N_2], 91.1 (34%)[M^+-N_3,-CH_2N_3).

(3) 1,3,5-tris(azidomethylene)benzene[2,3]

colorless oil, yield 98 %.

^{1}H-NMR (400 MHz, $CDCl_3$): δ = 7.22 (s, 3H), 4.36 (s, 6H).

^{13}C-NMR (125 MHz, $CDCl_3$): δ = 137.2, 127.7, 54.5.

MS EI(m/z (%)): 243.1 (27%)[M^+], 201 (100%)[M^+-N_3], 117.1 (19%)[M^+-3xN_3].

(4) 1,2,4,5-tetrakis(azidomethylene)benzene[3]

colorless solid, yield 96 %

^{1}H-NMR (500 MHz, $CDCl_3$): δ = 7.40 (s, 2H), 4.47(s, 8H).

^{13}C-NMR (135 MHz, $CDCl_3$): δ = 134.6, 131.3, 51.7.

MS EI(m/z (%)): 255.1 (2%)(M^+-N_3), 228.1 (39%)[M^+-N_3,-N_2], 170,1(41%)[M^+-3xN_3], 130.1 (85%)[M^+-3xCH_2N_3], (117.1 (100%)[M^+-CH_2,-4xN_3,].

Preparation of Ligand G2

[G1.SH] (1036 mg, 0.709 mmol, 2.25 eq) and 2,6-bis(bromomethyl)-4-((4-((triisopropylsilyl)ethynyl)phenyl)ethynyl)pyridine (172 mg, 0.315 mmol, 1 eq) were dissolved in dry tetrahydrofuran (15 ml) under an atmosphere of argon. The mixture was

degassed by bubbling argon through the solution to avoid disulfide formation during the reaction. After this procedure, sodium hydride (60 % in mineral oil, 51 mg, 1.26 mmol, 4 eq) was added and the mixture was left stirring at room temperature for 3 h. The reaction was quenched with water and extracted with methyl-*tert*-butylether three times. The combined organic fractions were washed with brine, dried over magnesium sulfate and evaporated to dryness. Purification of the crude product was achieved by column chromatography (cyclohexane:dichloromethane 1:4 with 1% triethylamine) followed by recycling GPC (8 cycles) to yield G2 (987 mg, 0.298 mmol, 95%) as colorless very viscous oil.

^{1}H-NMR (400 MHz, $CDCl_3$): δ = 7.45 (m, 4H, aryl-H), 7.32 – 7.03 (m, 78H, aryl-H), 3.71 (s, 4H, CH_2), 3.67 (s, 4H, CH_2), 3.59 – 3.54 (m, 72H, CH_2), 1.28 (s, 54H, $C(CH_3)_3$), 1.14 (s, 21H, iPr-H);

^{13}C-NMR (125 MHz, $CDCl_3$): δ = 158.6, 151.6, 151.5, 138.7, 138.4, 138.0, 137.9, 137.8, 137.7, 132.1 (2×), 131.7, 131.6, 129.0, 128.5, 128.3, 127.0, 126.9, 126.8, 125.1, 124.9, 124.8, 124.3, 123.0, 121.9, 93.6, 93.3, 88.6, 37.3, 36.1, 35.9, 35.7, 35.6, 35.4, 34.6, 31.4, 16.7, 11.3;

MS (MALDI-TOF, m/z): broad peak around 3416 [M^+];

Elemental analysis calculated for $C_{208}H_{237}NS_20Si$: C 73.04, H 6.98, N 0.41; found: C 72.49, H 7.00, N 0.68.

Preparation of Au NPs

Gold nanoparticle (Au NP) syntheses were carried out on a 2.5–3.5 mmol scale with respect to the ligand G2. Tetrachloroauric acid (20 eq.) was dissolved in deionized water (2.5 mL). One equivalent of gold precursor was used per thioether moiety of the respective dendrimer. A solution of TOAB (32 eq.) in dichloromethane (2.5 mL) was added, and the two-phase mixture stirred until the aqueous phase became colorless. The G2 (1 equivalent) was dissolved in dichloromethane (2.5 mL) and then added to the reaction mixture, followed by a freshly prepared solution of sodium borohydride (132 eq) in water (2.5 mL). After 15-20 min stirring, the resulting strongly colored CH_2Cl_2 phase was separated, and the aqueous phase was washed twice with CH_2Cl_2. The combined organic fractions were dried over magnesium sulfate, filtered, and concentrated to a volume of ca. 2 mL. Ethanol (20 mL) was added to precipitate the NPs, which were then centrifuged. The supernatant was discarded, and the procedure was repeated twice. After this procedure, the NPs were subjected to SEC or GPC. The colored, NP-containing fractions were collected, the removal of excess ligand checked by UV/vis and the solvent was removed by a N_2-stream and finally dried at room temperature in high vacuum.

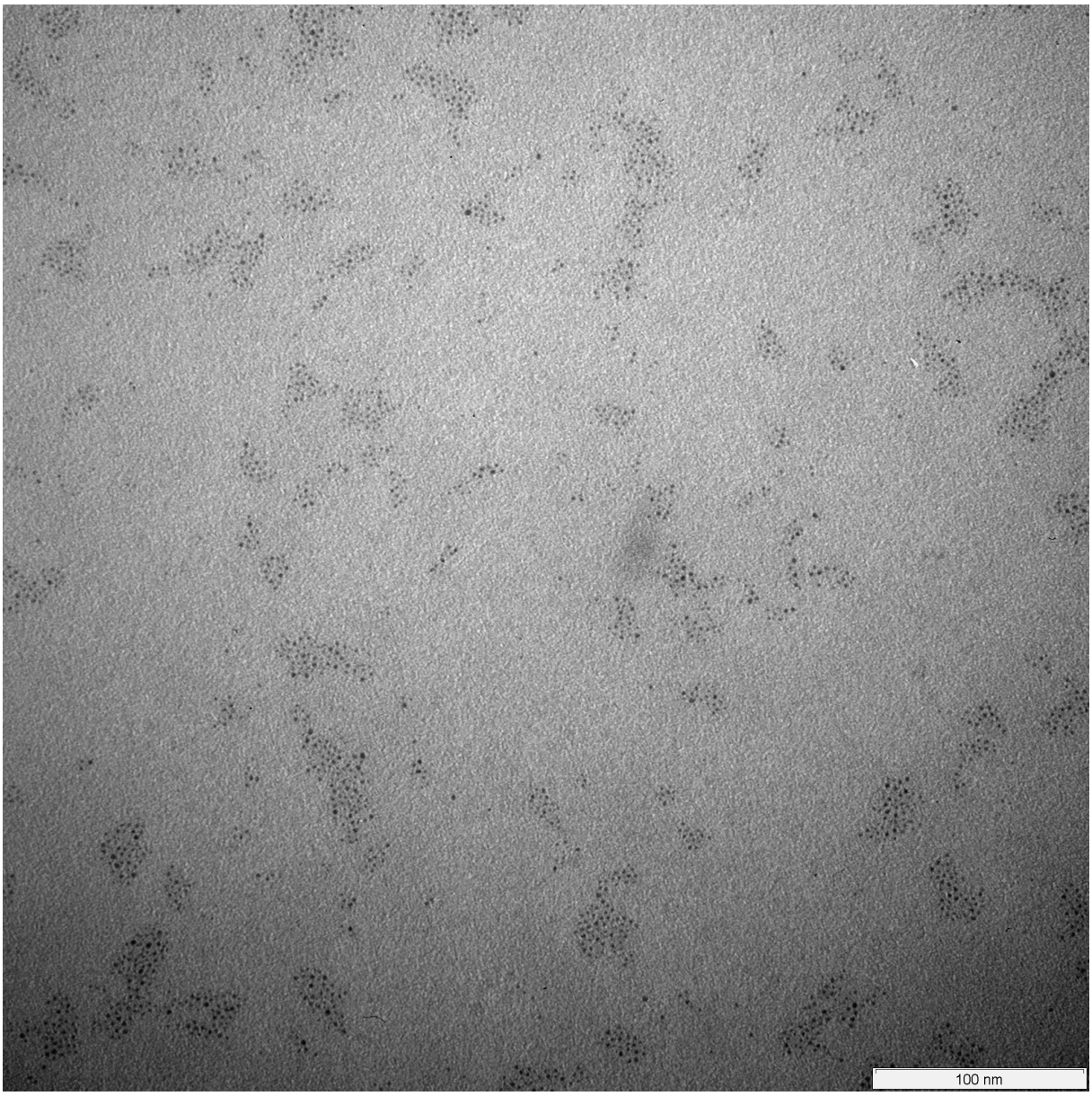

S 1. G2 stabilized Au NPs on CCCG after preparation for size measurement.

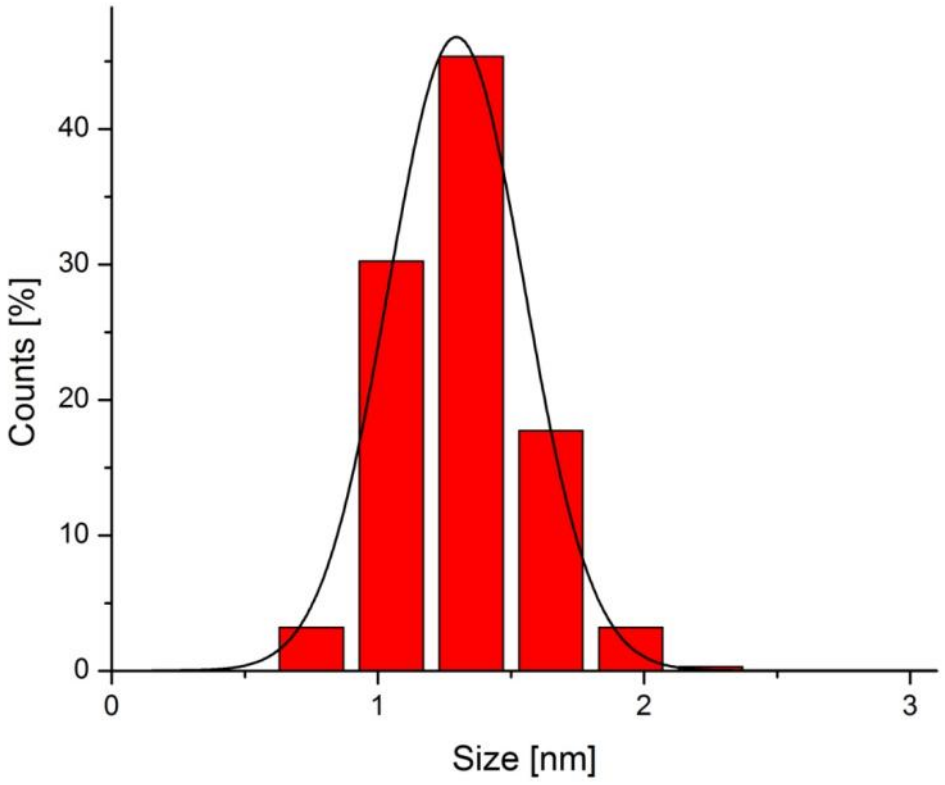

S 2. G2 stabilized Au NPs size distribution over 344 counts with Gaussian fit to determine mean diameter of 1.3 nm.

Coupling of Au NPs with Azides

The Au NP coupling reactions were carried out with 3 - 5 mg Au NPs (MW 14253,5 g/mol [one ligand G2 with 55 Au atoms]). The acetylene functionalized Au NPs were dispersed in dichloromethane (200 µl) and tetra-n-butylammonium fluoride (1M in tetrahydrofuran, 50 µl) was added. The mixture was left stirring for 1 hour, and quenched with water, extracted with dichloromethane and dried with $MgSO_4$. After filtration the solution was concentrated first in N_2 stream followed by vacuum at room temperature.

The dry deproctected Au NPs were dissolved in 50 µl dichloromethane. Corresponding to the amount of azide moieties 0.5 eq. for **2** 0.33 eq. for **3** and 0.25 eq. for **4** were dissolved in 50 µl dichloromethane and added to the solution followed by 20 mol % of $CuSO_4$ in 20 µl water. While intense stirring 30 mol % sodium ascorbate in 20 µl water were added. After 2 h reaction time the mixture was extracted with dichloromethane and dried over $MgSO_4$ to yield the coupled Au NPs that were used for UV/vis, IR and TEM measurements.

Representative raw TEM Pictures

Transmission Electron Microscopy (TEM) TEM was performed on a Philips CM100 transmission electron microscope at 80 kV. Electron micrographs where recorded on a 2000 by 2000 pixel charge-coupled device camera Veleta from Olympus. The micrographs were recorded with a magnitude of 180kx leading to micrographs with 520 nm by 520 nm and a size of 0.26 nm per pixel. Therefore the column width of the histograms was chosen to be 0.5 nm. One NP has a diameter of four pixels and an area of ten to twelve pixels. The NPs were deposited by carefully placing a drop of the NP dispersion on top of a thin carbon film that spanned a perforated holey carbon support film covering a gold-plated copper microscopy grid. The remaining solvent was directly blotted with filter paper and the grid was air dried.

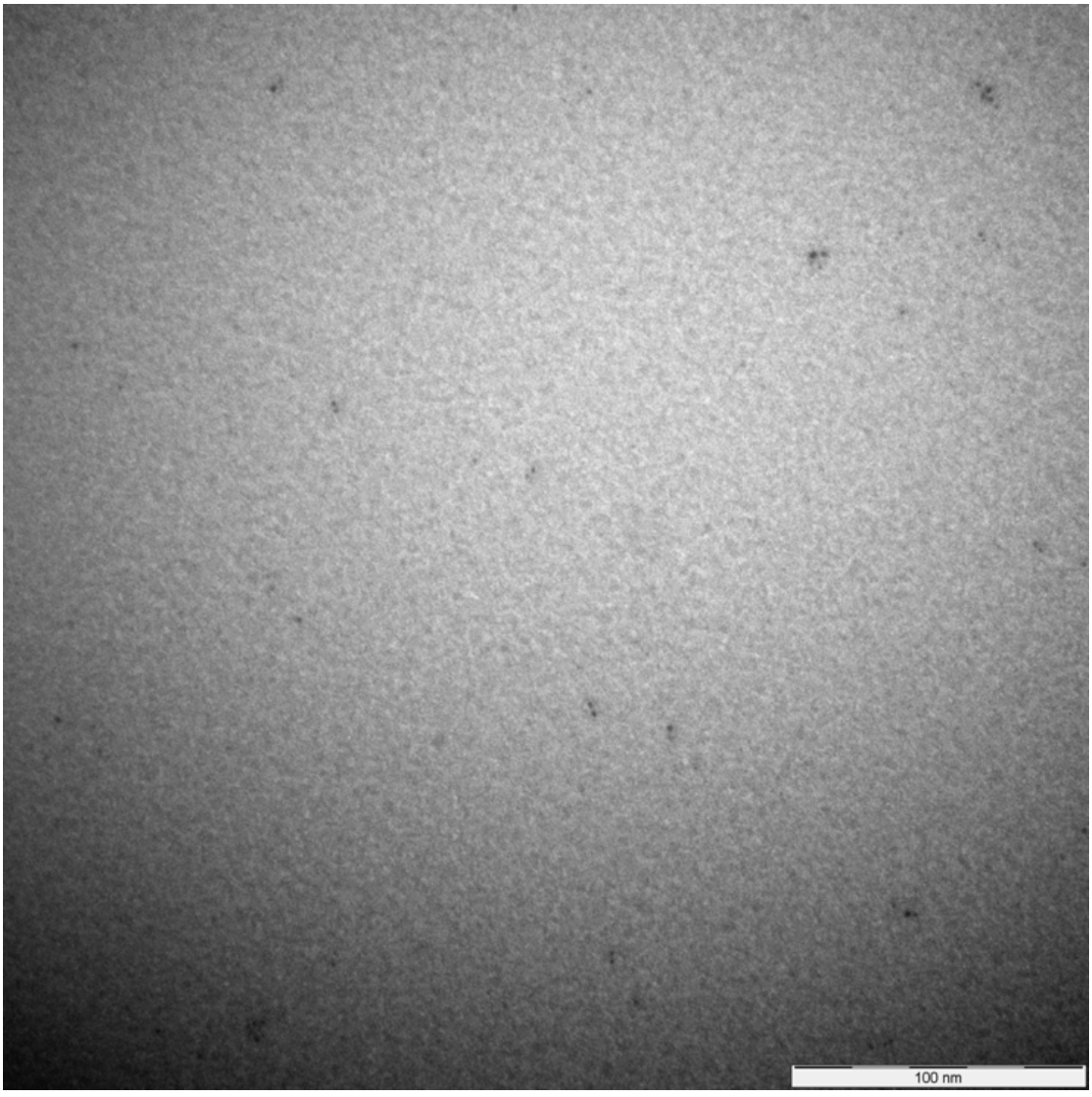

S 3. Raw picture of reaction with linker molecule **2**.

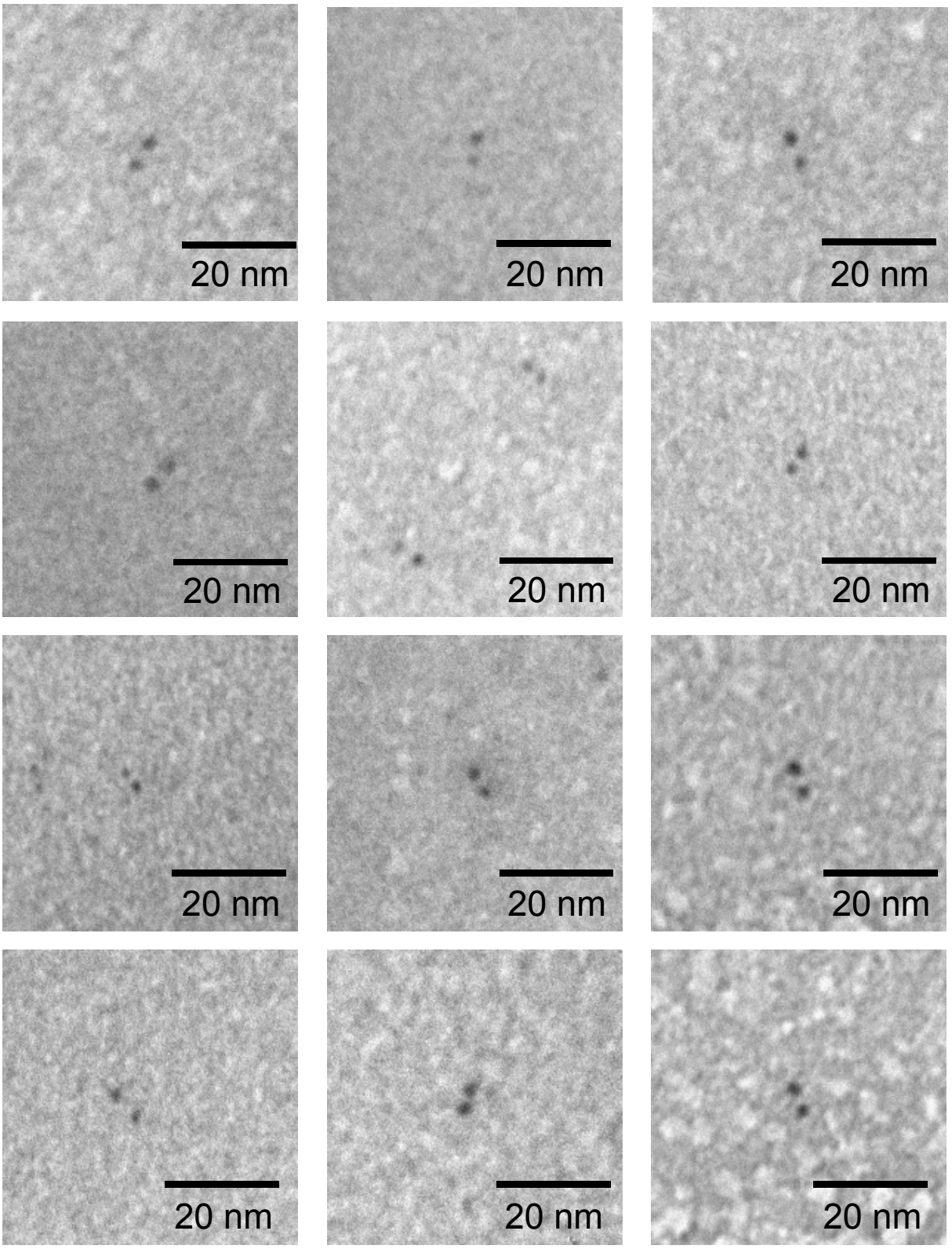

S 4. Cropped pictures showing coupling to dimers with molecule **2**.

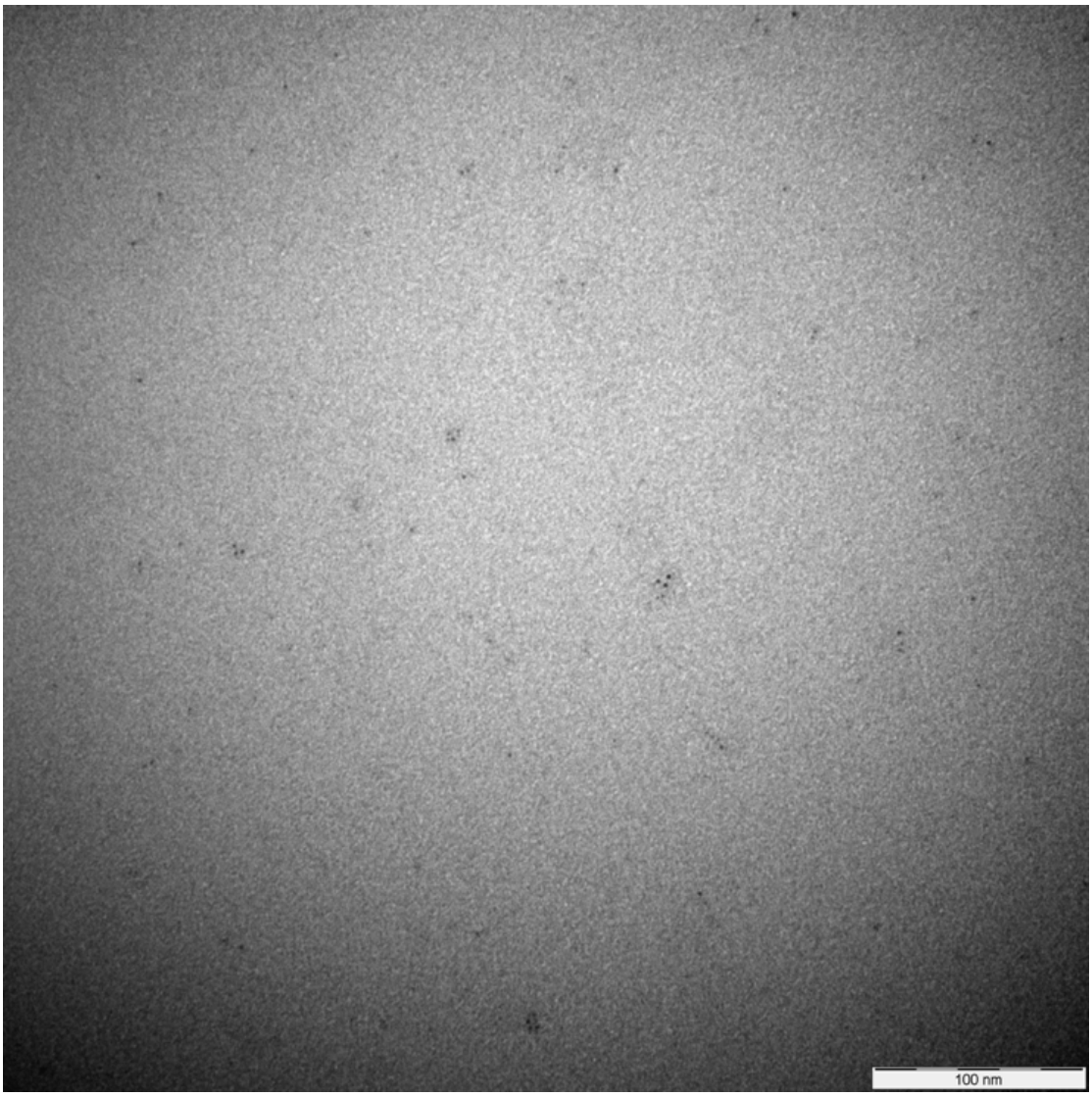

S 5. Raw picture of click reaction with linker **3**.

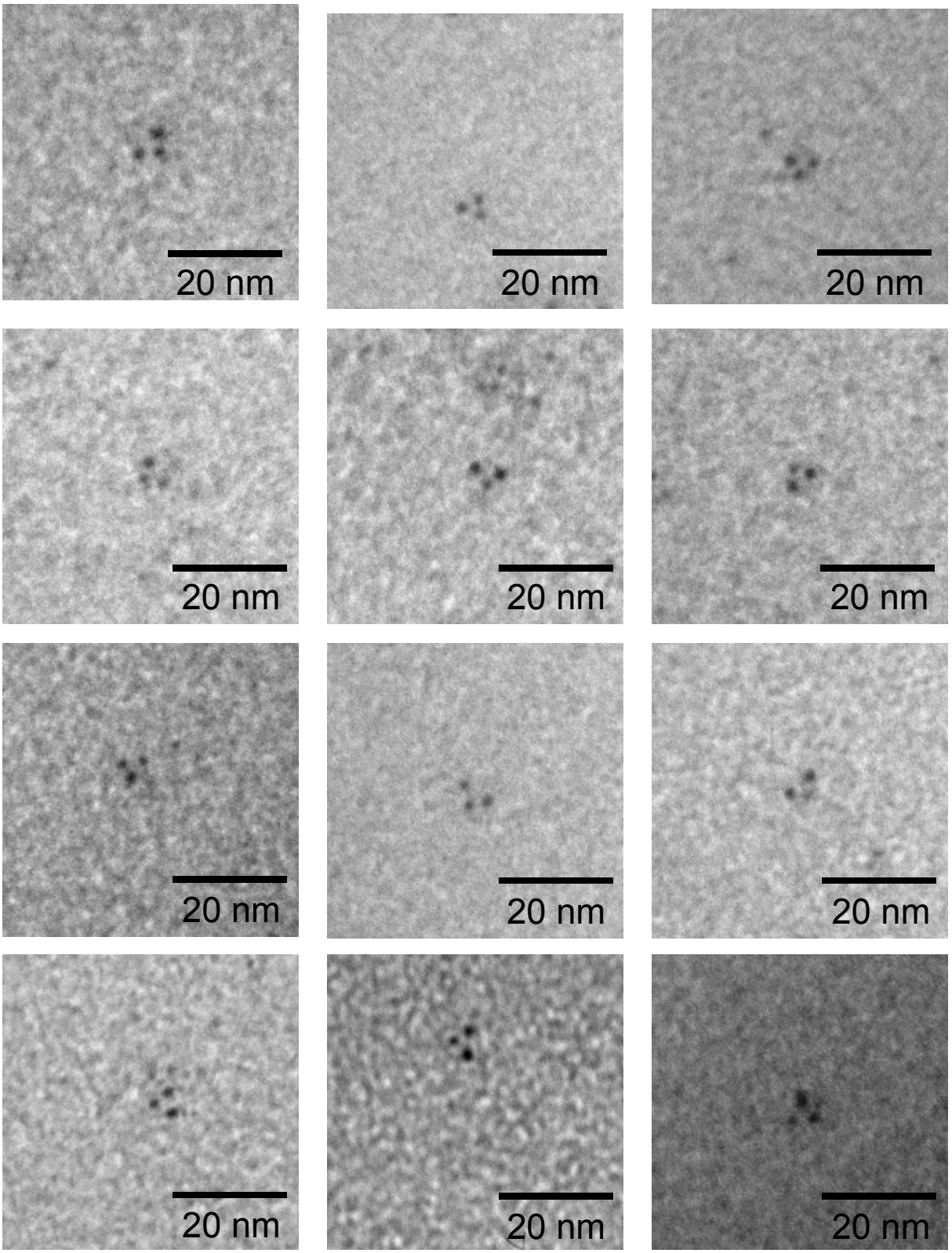

S 6. Cropped pictures showing coupling to trimers with molecule **3**.

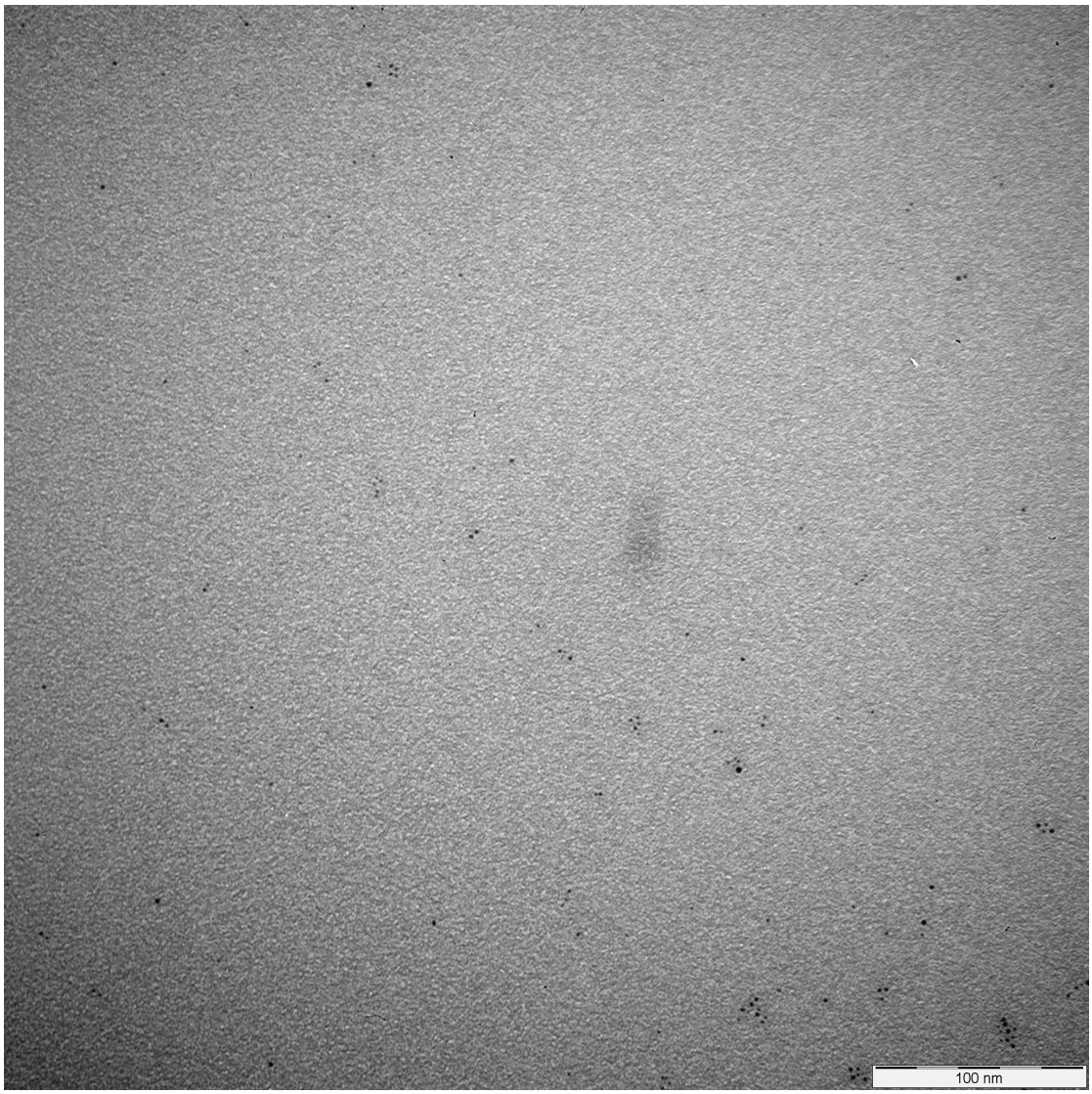

S 7. Raw picture of click reaction with linker **4**.

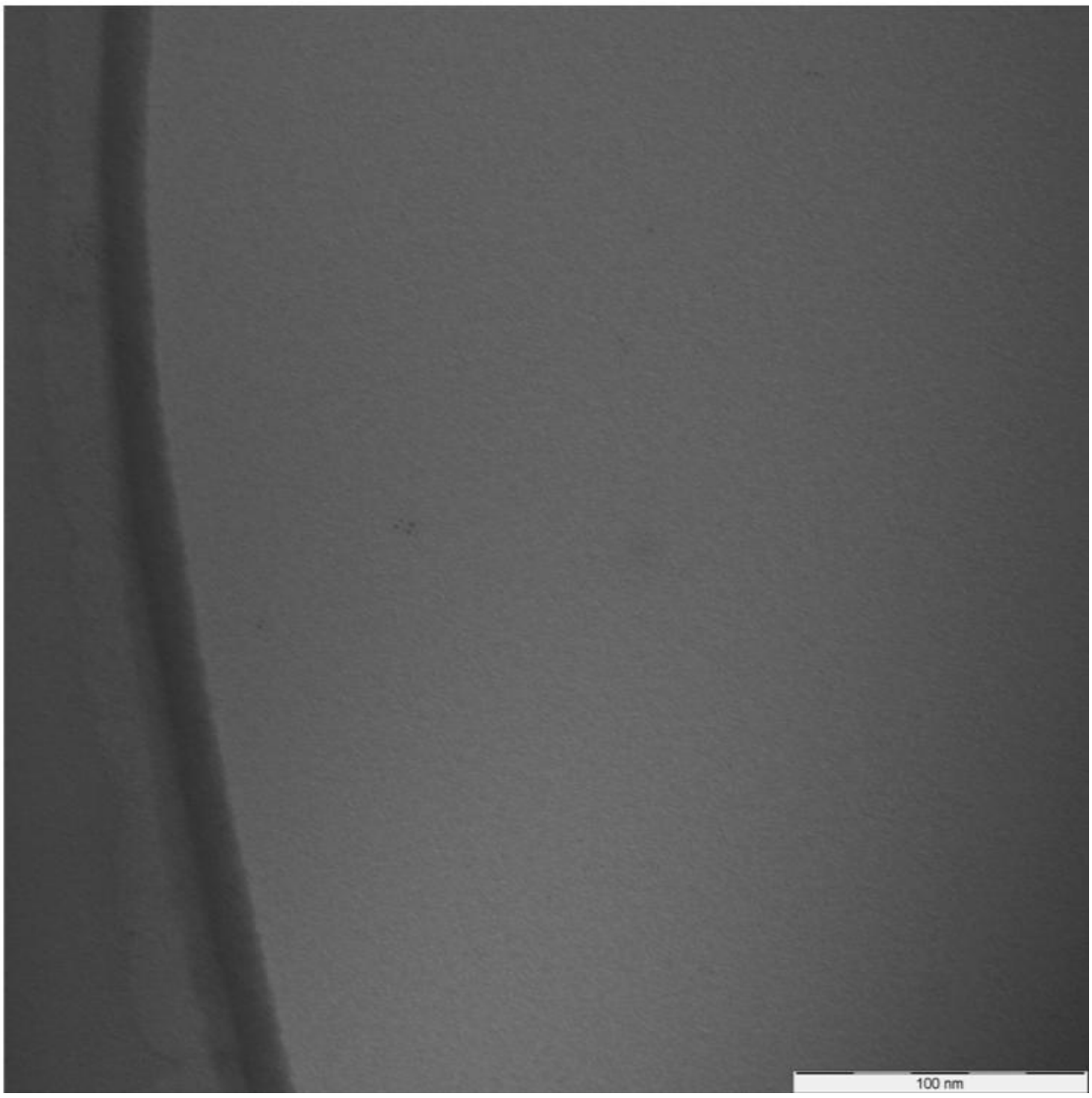

S 8. Raw picture of very high diluted sample of linker molecule **4**.

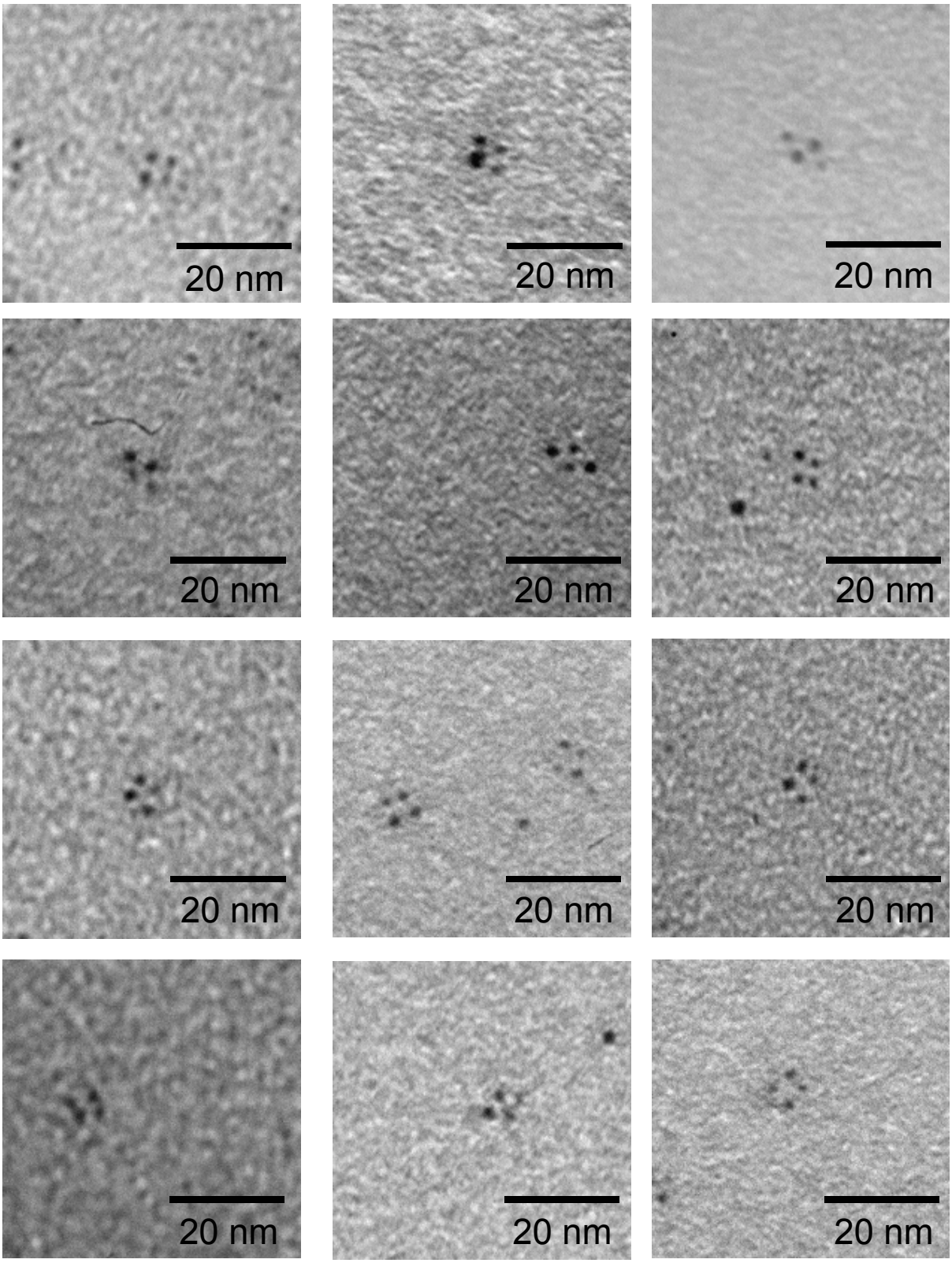

S 9. Cropped pictures showing coupling to tetramers with molecule **4**.

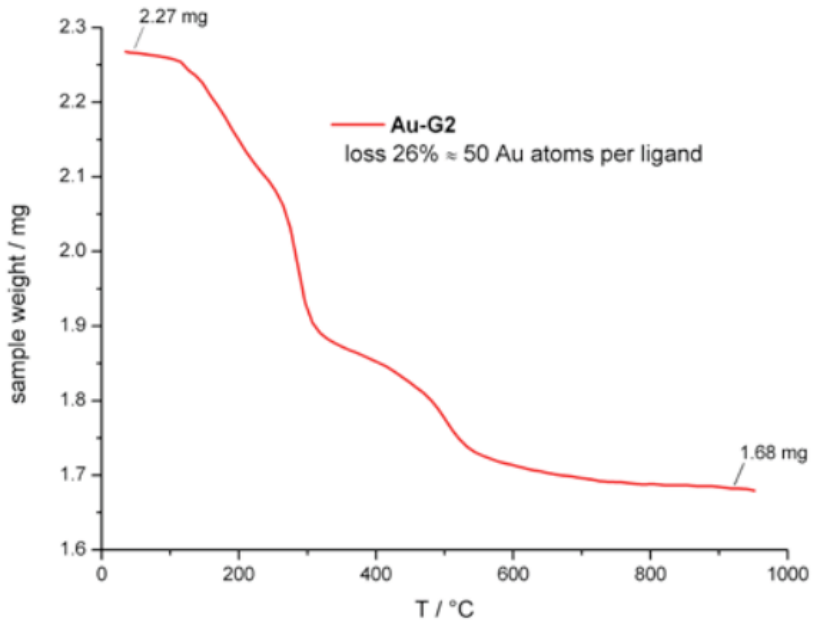

S 10. Thermogravimetric analyses of Au-G2. To remove the organic shell in the TGA experiments, the dry NPs were heated to 950 °C. The amounts of weight loss was 26% for Au-G2. The number of gold atoms stabilized per dendrimer was calculated from this value. We found that on average one G2 ligand coats 50 atoms. The dimensions of Au-G2 NPs determined by TEM suggest an average number of ~55 gold atoms per NP. In analogy to the parent ligand structure, a single G2 dendrimer is required to stabilize one Au NP.[4]

Literature

[1] J. R. Thomas, X. Liu, P. J. Hergenrother, *J. Am. Chem. Soc.* **2005**, *127*, 12434–12435.

[2] Y. Song, E. K. Kohlmeir, T. J. Meade, *J. Am. Chem. Soc.* **2008**, *130*, 6662–6663.

[3] H. E. Montenegro, P. Ramírez-López, M. C. de la Torre, M. Asenjo, M. A. Sierra, *Chem. Eur. J.* **2010**, *16*, 3798–3814.

[4] J. P. Hermes, F. Sander, U. Fluch, T. Peterle, D. Thompson, R. Urbani, T. Pfohl, M. Mayor, *J. Am. Chem. Soc.* **2012**, *134*, 14674–14677.

Click Chemistry with Gold Nanoparticles – A Tool for Functionalization, Interlinking and Labeling

Fabian Sander and Marcel Mayor

Manuscript prepared for submission

Gold Nano Particles

Gold Nanoparticles (Au NPs) are a heavily investigated over the last decades because of their usefulness in medicine, catalysis and electronics.[1–3] The first known utilization of Au NPs was far back in the late Greco-Roman times.[4] Freshly precipitated colloidal gold solutions were already known agents to colorize glass. A famous example is the Lycurgus cup that appears green when the light is reflected by the cup and red when you observe the transmitting light. The minute metallic particles of the used gold-silver alloy to colorize the glass have the right size to scatter the blue end of the spectrum more efficiently than the red end, resulting in a red transmission. Faraday was the first in 1857 who discovered the dependence on particle size in color and started to systematical investigate Au NPs.[5] In the mid of the 20th century the development of Au NPs attracted more and more notice. Turkevich et al. demonstrated the synthesis and analysis of citrate stabilized Au NPs and along with this breakthrough more work was performed to synthesize well defined Au NPs.[6] With the discovery of the Schmid-cluster ($Au_{55}(PPh_3)Cl_6$[7] the first steps towards quantum electronics[8] with NPs and applications like labeling[9] were done. In the 80's the developed protocol of Burst et al. for rapid and simple synthesis of thiolate stabilized Au NPs was a milestone.[10,11] In a two phase system of tetrachloroauric acid solved in water, which was transferred into the organic phase (toluene) using tetraoctylammonium bromide (TOAB) as phase transfer agent, the gold salt was reduced by sodium borohydride ($NaBH_4$) in presence of alkanethiols yielding stable Au NPs wither a narrow size distribution around 3 nm.

Since the end of the last century Au NPs moved in the focus of researchers because of their outstanding stability of Au NPs among metal nanoparticles. Their shape and size depended properties made them suitable for various applications.[12] They are used in medicine[13], bio- and macromolecule labeling[14–17] or in chemistry for catalytic applications[18,19]. Also for current and future sensor applications Au NPs are of great interest.[20–23] Au NPs are also of interest for their use in nanoelectronics[24] as potential future storage device.[25]

Click Chemistry as Tool for Au NP Assembly

Over the last decades the development of metal nano particles is a fast growing research field and a considerable interest has arisen in their chemistry and physics.[26] A large variety of functional Au NPs are now known,[26–38] but many families of Au NPs are still resistant to direct synthesis,[27] ligand exchange reactions[30] or functionalization using high-temperature or other incompatible processes. Thus, in view of multiple possible applications, it is essential to reconsider the problem of the efficiency of Au NP functionalization and their assembly. Click chemistry is meanwhile an often-used concept and opened new routes in organic synthesis under mild conditions.

Sharpless and coworkers introduces in 2001 the concept of click chemistry[39] and set their focus not on production of new compounds but on production of new properties. The concept is to provide the whole range of chemical transformations in a set of processes with a high thermodynamic driving force usually higher than 20 kcal mol^{-1}. These "spring-loaded" starting materials allow an easy and efficient transformation into new substances with useful properties. This concept is very appealing to interlink Au NPs to each other or with other molecules in order to create new functional structures.

The exponential increasing number of hits, from 5 in 2004 to 153 in 2012, for term "click nano particle" demonstrates the arising importance of this research field. The concept of click chemistry allows the creation of complex organic shells around NPs and further opens the route to new assembly and labeling strategies exploiting the size dependent physical and electronic properties of these nano objects.

Composite Materials created by click chemistry

Williams *et al.* introduced in 2006 the concept of functionalization of Au NPs by click chemistry.[40] To avoid the synthesis of individual thiolate ligands for stabilizing Au NPs with special function, click chemistry was used to tailor the stabilizing organic shell. Therefore redox active, fluorescent, and solubilizing species are used to show click chemistry as a facile route toward functionalization of monolayer-protected Au nanoparticles (Figure 1).

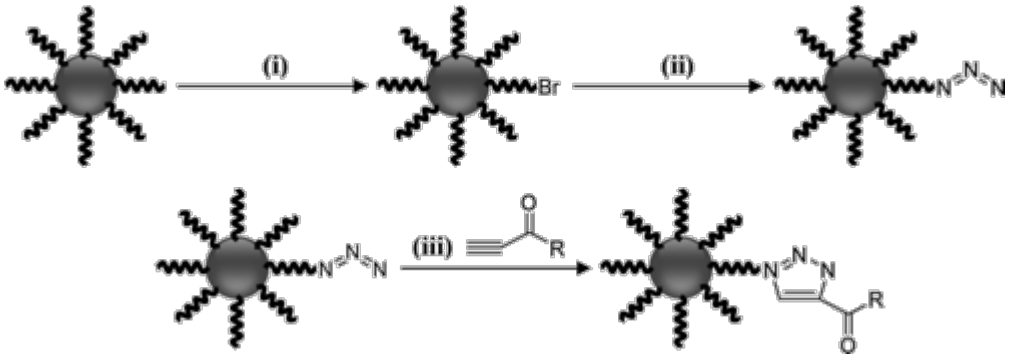

Figure 1. Schematic drawing of Au NPs shell functionalization. (i) ligand exchange: $Br(CH_2)_{11}SH$ in DCM, 60 h at room temperature; (ii) 0.25 M NaN_3 in DCM/DMSO solution, 48 h; (iii) R = propyn-1-one derivatized, 24−96 h in dioxane or 1:1 hexane/dioxane. Reprinted from Williams et al.[40]

After synthesizing thiolate stabilized Au NPs according to the method of Brust et al.[10] and ligand exchange azide groups were established at the Au NPs periphery. Finally the Au NPs successfully decorated with alkynyl substituted derivatives of ferrocene, nitrobenzene, pyrene, anthracene, poly(ethylene glycol), and aniline. The mild conditions at room temperature allow this protocol to be applied to several other compounds. Also work to optimize this reaction type is done.[41]

Burst and coworkers were one of the first who tried to interlink azide functionalized Au NPs by click chemistry with enzymes.[42] Citrate stabilized Au NPs were treated with thiol terminated ligand bearing an azide group to yield thiol capped, azide functionalized Au NPs. The size of 14 nm remained the same after the ligand exchange. Acetylene labeled lipase (*Thermomyces lanuginosus*) was clicked to the Au NP by incubating an excess of lipase and Cu(I) catalyst with the nanoparticle suspension at room temperature for 3 days. The fact that no by produces occurred while this long incubation time makes this reaction very appealing. This approach to combine biomaterials with metal nano particles is general very independent of the chemical nature of the starting materials. Therefore this reaction set the basis for similar composite materials.

With the increasing focus on bottom up approaches to assemble nano electronic devices DNA is a promising structure due to its well-defined chemical structure and the multitude of electrostatic and chemical binding sites utilizable for modification with molecules, metal ions or metal nanoparticles.

However, the fabrication of DNA-based circuit elements requires the spatially defined immobilization of chemical building blocks to the DNA strand that, because of their electronic structure, are capable of electrical switching or charge storage. The use of metal

nanoparticles with diameters below 2 nm, which allow the exploitation of single electron tunneling effects, appears very promising in this context. Therefore Simon et al. demonstrated the DNA template chain like assembly of glutathione functionalized Au NPs to artificial alkyne modified DNA duplexes by Cu(I) catalyzed Huisgen cycloaddition.[43] This approach to covalently immobilize Au NPs on a highly customizable template holds great potential for a controlled assembly of Au NPs in a defined spatial arrangement.

The previous concepts to add functions by click chemistry to azide functionalized Au NPs can be used to build up responsive nanocomposite materials. Peng and coworkers modified Au NPs by click chemistry to yield pH and temperature responsive nanocomposites.[44] Via a ligand exchange procedure mono-azide poly(ethylene glycol) (SS-PEG-N_3) functionalized Au NPs were synthesized. By subsequent coupling with alkyl-terminated poly(4-vinylpyridine) under click conditions pH responsive Au NPs were yielded (Figure 2).

With a pH blow 4 the pyridyl groups are protonated and the repulsing electrostatic forces prevent the particles from agglomeration resulting in a transparent solution. If the pH is higher than 5 the pyridyl groups are deprotonated and the particles start to agglomerate resulting in a intransparent solution. The whole process was shown to be reversible.

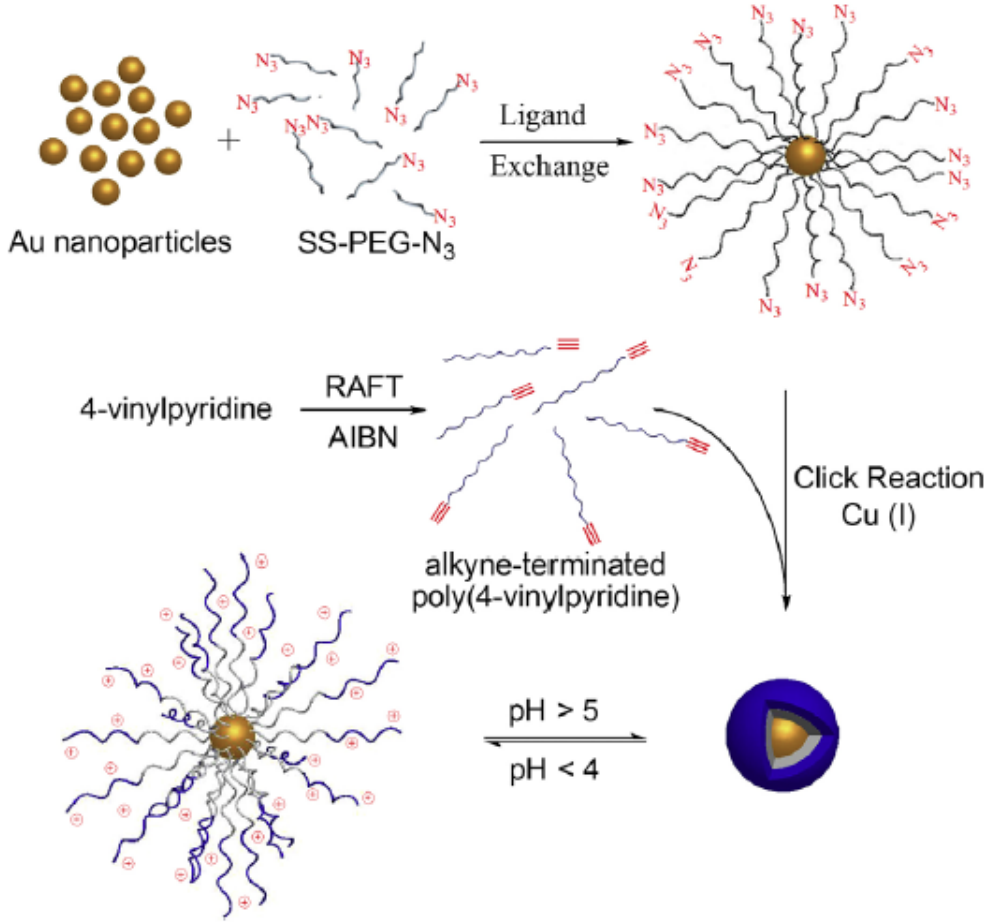

Figure 2. Synthesis of pH responsive Au NP nanocomposits. Reprinted from Peng et al.[44]

With altered polymers clicked to the Au NPs ligand shell also thermoresponsive behavior could be achieved.[45] With alkyne-terminated poly(N-isopropylacrylamide) clicked to the (SS-PEG-N_3) stabilized Au NPs also the transparency of the Au NP solution changed. This time the change was induced by temperature resulting in an intransparent solution at temperatures higher than 40 ºC and transparent solutions at lower temperatures. The whole process was again reversible (Figure 3).

Also for medicine applications click chemistry protocols to modify Au NPs are used.[46] Recently a new prostate cancer treatment is under development where bio compatible polyethylene glycol stabilized Au NPs are used as carrier for antigens causing cancer cells death and tumor label.

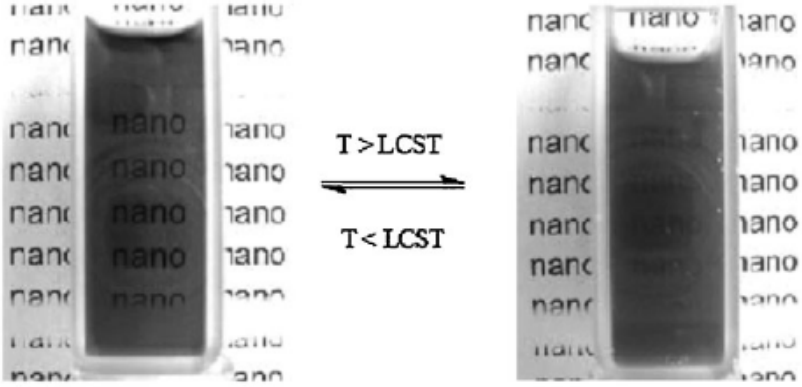

Figure 3. Picture of transparency change at the lower critical solution temperature (LCST). Reprinted from Peng et al.[45]

Also the assembly of different metal NPs utilizing click chemistry was demonstrated. For example the assembly of small alkynyl Au NPs with the size of about 20 nm as satellites around 70 nm azide functionalized Au NPs.[47] However, gold nano rods and silver nano particles could be interlinked by click chemistry as well.[48]

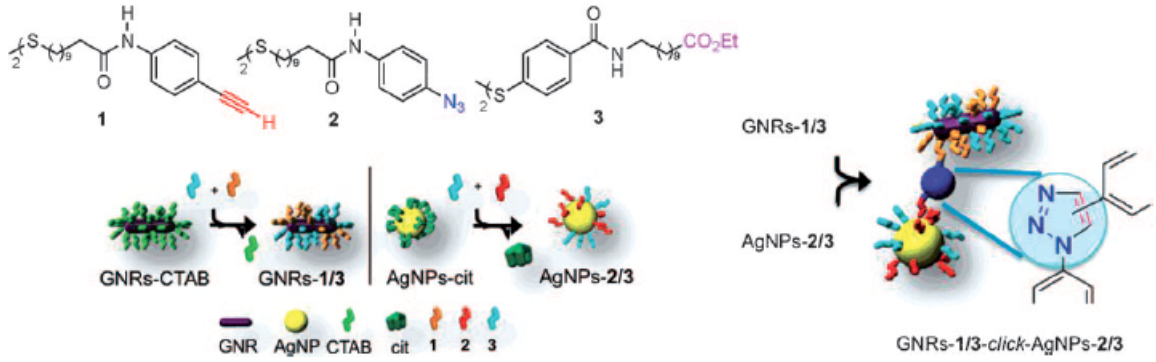

Figure 4. Left: schematic presentation of ligand exchange for Au NP and Ag NP functionalization. Right: assembly of Au NP and Ag NP after click reaction. Reprinted from Franchini et al.[48]

Therefore the gold nanorods were functionalized with terminal alkines and the Ag NPs with terminal azides (Figure 4). After applying click conditions to a solution of both reactants the desired assembly could be observed.[48] Such nanoassemblies can find important applications in numerous biomedical applications including biosensing and bioimaging.[49,50] Facile fabrication of such complex assemblies can be easily extended to different shape-controlled plasmonic nanostructures and other functional inorganic nanostructures such as magnetic nanoparticles, semi-conducting quantum dots and up-conversion nanocrystals.

Au NP Enhanced Metal Ion Sensing by Click Chemistry

Au NPs are very interesting for any kind of sensor application because of their size dependent color. In any system were the size of Au NPs can be change by agglomeration or interlinking with other structures an optical read out is possible. In 2008 mixed alkine / azide functionalized Au NPs were used for colorimetric copper(II) detection.[20] The concept is as simple as effective. The fact that the extinction coefficient of 13 nm diameter nano particles is by several magnitudes of order higher than those of traditional chromophores[51] allows the naked eye to observer color in nanomolar concentrations. Since copper is used as catalyst in azide alkine click chemistry based on the Huisgen's reaction low concentrations of copper allows completing this reaction. Therefore terminal azide and alkyne functionalized thiols were used to functionalize Au NPs. In a ligand exchange citrate stabilized Au NPs were mixed with the respective t hiols (Figure 5). The yielded functionalized Au NPs showed a reddish purple color.

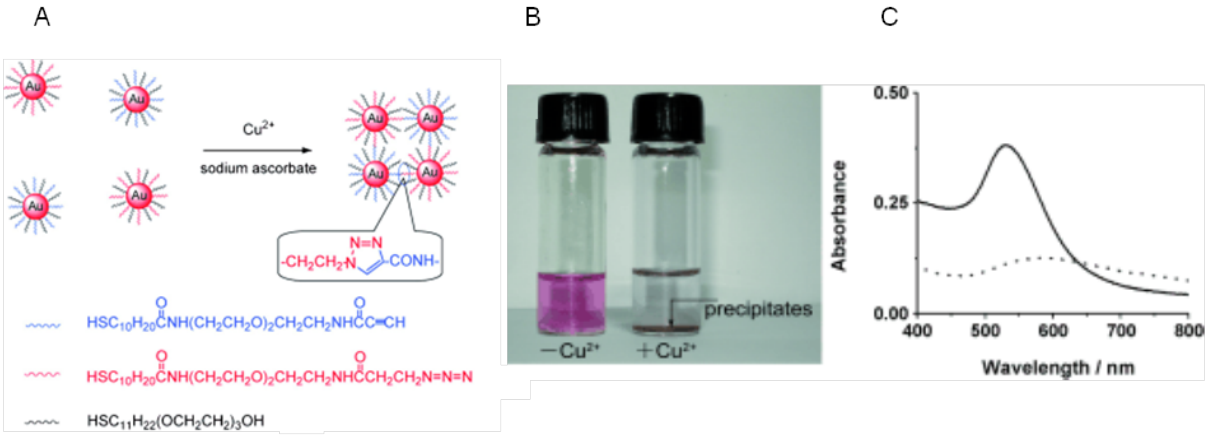

Figure 5. A) The detection of Cu^{2+} ions using click chemistry between two types of gold NPs, each modified with thiols terminated in an alkyne or an azide functional group; B) Color change after cross-linked visible by the naked eye; C) UV/Vis spectra before (black line) and after (dotted line). Reprinted from Jiang et al.[20]

In presence of Cu(II) and a reducing agent, here sodium ascorbate is used, the nano particles start to agglomerate and the color is fading. This process can be monitored by the naked eye without any instruments.

Based on this work several new systems for an optical copper detection based on Au NPs as signal reporter were developed. In a very similar system the generation of Cu(I) out of Cu(II)acetate by bulk electrolysis to promote the click reaction turned out to be very efficient.[52]

As most examples used mixed azide alkyne functionalize particles Gooding *et al*.[53] used 3-azidopropylamie functionalized Au NPs that undergoes the click reaction with 1,4-diethynylbenzene. An advantage of this protocol is the minimal synthetic work to prepare the interface for Cu(II) detection

DNA functionalized Au NPs showed a faster click reaction and provides the additional advantage of an quantitative Cu(II) detection due to the dependence of the DNAs melting points to the degree of cross linking.[54] The more copper found in the sample the more cross linked DNA strands were received resulting in a higher melting point direct correlating the Cu(II) concentration. This method hits the Environmental Protecting Agency-defined limits for the maximum Cu(II) contamination limit of 20 μM in drinking water making it relevant for testing drinking water.

Also unmodified Au NPs were recently used to establish a colorimetric copper detection.[55] By a Cu(I) induced azide-alkyne click ligation caused structural change of single-stranded DNA to double-stranded DNA. This structural change of probe can be monitored by the unmodified AuNPs via mediating their aggregation with a red-to-blue colorimetric read-out because of the differential ability of ssDNA and dsDNA to protect AuNPs against salt-induced aggregation. Under the optimum conditions, this biosensor can sensitively and specifically detect Cu^{2+} with a low detection limit of 250 nM and a linear range of 0.5–10 μM.[55] In contrast to the previous sensing systems this bio sensors do not rely on inter particle cross linking but on the novel design using noncrosslinking aggregation mediated by electrostatic stabilization.

Beside copper, lead is also a very toxic transition metal that cause a lot of environmental pollution because of it's use in batteries, gasoline and paints. Propargylamin functionalized Au NPs where further reacted by click chemistry with azide terminated triethylene glycol in order to detect Pb^{2+} ions.[56] The achieved ligand shell can than act as chelating substrate able to trap Pb^{2+}. The selective response to Pb^{2+} is attributed to the size-fitting effect of the pseudo-crown ethers. The Au NPs are interlinked by the Pb^{2+} due to the coordination process and change color because auf the aggregations (Figure 6).

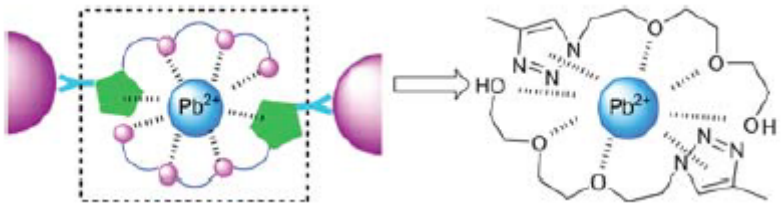

Figure 6. Schematic drawing of the chelating interaction of the functionalized Au NPs to detect lead ions. Reprinted from Han et al.[56]

Not only the detection of metal ions is realized by click reactions with Au NPs also a system for the detection of ascorbic acid is established using azide and alkyne functionalized particles in present of Cu(II).[57] In presence of ascorbic acid Cu(I) is generated hat catalyzes the click reaction resulting in interlinked particles that change color. This method has been proven to be robust against the presence of other reducing organic compounds such as glucose, cysteine, dopamine, uric acide and thiamine.

Proteins can be detected as well using the Cu(I) catalyzed click reaction.[58] Basically the classical Biuret test is combined with the enhanced optical readout by Au NPs. The Biuret reagent is an aqueous mix of potassium hydroxide and a Cu(II) salt. The formed solution proteins are capable to reduce Cu(II) to Cu(I). The change in color by the crosslinked Au NPs enhance the sensitivity of the protein detection dramatically.

In an extended system also the improved detection of toxic organophosphate pesticides (OPs) could be realized.[59] Detection of OPs based on the direct stimulation of Au NPs aggregation or growth by the acetylcholineesterase – acetylthiocholine system (AChE–ATCl) has been reported. However, high amounts of OPs are usually required to initiate detectable color change of Au NPs because of the direct dependence of nanoparticle aggregation on the AChE–ATCl system, limiting the colorimetric sensitivity. Therefore a click reaction as an intermediate colorimetric signal amplification process has been used.

All this concepts are using the superior extinction coefficient of Au NPs to enhance the optical detection of targets like metal ions, ascorbic acid, proteins or organophosphate pesticides.

Outlook

The various concepts to interlink Au NPs by click chemistry and the potential applications in medicine, labeling and sensing demonstrate the importance of this research field. The replacement of coloring agents for sensing applications by Au NPs will set new standards for detections limits by the naked eye or in lab on a chip devices. The on going development of Au NPs click reactions as signal amplifier for conventional sensing systems show the high potential of these applications. Also the possibility to add molecules to Au NPs by simple click reactions to tailor their functionality holds a big future potential for applications. Thermo- and pH responsive probes could be achieved via click chemistry functionalized Au NPs. Also the assembly by DNA templating as bottom up approach for future nano electronic applications is possible.

One drawback is still the control over the number of functional groups around a particle. For a controlled assembly without aggregation into huge networks it is necessary to synthesize Au NPs with only one available moiety for click reaction. Recently the synthesis of a dendritic ligand and subsequent stabilization of Au NPs fulfilling this requirement is reported in literature.[60] These Au NPs will give access many new approaches for labeling, surface functionalization, sensors and future molecular electronic devices.

References

1. R. Sardar, A. M. Funston, P. Mulvaney, and R. W. Murray, *Langmuir*, 2009, **25**, 13840–13851.
2. M. Homberger and U. Simon, *Phil. Trans. R. Soc. A*, 2010, **368**, 1405–1453.
3. M.-C. Daniel and D. Astruc, *Chem. Rev.*, 2004, **104**, 293–346.
4. H. Goesmann and C. Feldmann, *Angew. Chem. Int. Ed.*, 2010, **49**, 1362–1395.
5. M. Faraday, *Phil. Trans. R. Soc. Lond.*, 1857, **147**, 145–181.
6. J. Turkevich, P. C. Stevenson, and J. Hillier, *Discuss. Faraday Soc.*, 1951, **11**, 55.
7. G. Schmid, R. Pfeil, R. Boese, F. Bandermann, S. Meyer, G. H. M. Calis, and J. W. A. van der Velden, *Chem. Ber.*, 1981, **114**, 3634–3642.
8. G. Schmid, *Chem. Rev.*, 1992, **92**, 1709–1727.
9. J. F. Hainfeld and F. R. Furuya, *J Histochem Cytochem*, 1992, **40**, 177–184.
10. M. Brust, M. Walker, D. Bethell, D. J. Schiffrin, and R. Whyman, *J. Chem. Soc., Chem. Commun.*, 1994, 801–802.
11. M. Brust, D. J. Schiffrin, D. Bethell, and C. J. Kiely, *Adv. Mater.*, 1995, **7**, 795–797.
12. H. Häkkinen, *Chem. Soc. Rev.*, 2008, **37**, 1847–1859.
13. L. B. Bangs, *Pure Appl. Chem.*, 1996, **68**, 1873–1879.
14. I. Willner and B. Willner, *Nano Lett.*, 2010, **10**, 3805–3815.
15. R. D. Powell and J. F. Hainfeld, *Micron*, 2011, **42**, 163–174.
16. J. I. Cutler, E. Auyeung, and C. A. Mirkin, *J. Am. Chem. Soc.*, 2012, **134**, 1376–1391.
17. L. Dykman and N. Khlebtsov, *Chem. Soc. Rev.*, 2012, **41**, 2256.
18. C. Della Pina, E. Falletta, L. Prati, and M. Rossi, *Chem. Soc. Rev.*, 2008, **37**, 2077–2095.
19. A. Corma and H. Garcia, *Chem. Soc. Rev.*, 2008, **37**, 2096–2126.
20. Y. Zhou, S. Wang, K. Zhang, and X. Jiang, *Angew. Chem. Int. Ed.*, 2008, **47**, 7454–7456.
21. R. Wilson, *Chem. Soc. Rev.*, 2008, **37**, 2028–2045.
22. Z. Wang and Y. Lu, *J. Mater. Chem.*, 2009, **19**, 1788.
23. X. Zhang, Q. Guo, and D. Cui, *Sensors*, 2009, **9**, 1033–1053.
24. G. Schmid, *Chem. Soc. Rev.*, 2008, **37**, 1909–1930.
25. S.-J. Kim and J.-S. Lee, *Nano Letters*, 2010, **10**, 2884–2890.
26. M.-C. Daniel and D. Astruc, *Chem. Rev.*, 2004, **104**, 293–346.

27. M. Brust, M. Walker, D. Bethell, D. J. Schiffrin, and R. Whyman, *J. Chem. Soc., Chem. Commun.*, 1994, 801–802.
28. P. Mulvaney, *Langmuir*, 1996, **12**, 788–800.
29. R. Elghanian, J. J. Storhoff, R. C. Mucic, R. L. Letsinger, and C. A. Mirkin, *Science*, 1997, **277**, 1078–1081.
30. A. C. Templeton, W. P. Wuelfing, and R. W. Murray, *Acc. Chem. Res.*, 2000, **33**, 27–36.
31. R. M. Crooks, M. Zhao, L. Sun, V. Chechik, and L. K. Yeung, *Acc. Chem. Res.*, 2001, **34**, 181–190.
32. R. W. J. Scott, O. M. Wilson, and R. M. Crooks, *J. Phys. Chem. B*, 2005, **109**, 692–704.
33. J. Kim, S. Park, J. E. Lee, S. M. Jin, J. H. Lee, I. S. Lee, I. Yang, J.-S. Kim, S. K. Kim, M.-H. Cho, and T. Hyeon, *Angew. Chem. Int. Ed.*, 2006, **45**, 7754–7758.
34. C. L. Johnson, E. Snoeck, M. Ezcurdia, B. Rodríguez-González, I. Pastoriza-Santos, L. M. Liz-Marzán, and M. J. Hÿtch, *Nature Mater.*, 2007, **7**, 120–124.
35. G. Han, P. Ghosh, and V. M. Rotello, *Nanomedicine*, 2007, **2**, 113–123.
36. S. J. Son, X. Bai, and S. B. Lee, *Drug Discov. Today*, 2007, **12**, 657–663.
37. S. E. Skrabalak, L. Au, X. Lu, X. Li, and Y. Xia, *Nanomedicine*, 2007, **2**, 657–668.
38. S.-Y. Shim, D.-K. Lim, and J.-M. Nam, *Nanomedicine*, 2008, **3**, 215–232.
39. H. C. Kolb, M. G. Finn, and K. B. Sharpless, *Angew. Chem. Int. Ed.*, 2001, **40**, 2004–2021.
40. D. A. Fleming, C. J. Thode, and M. E. Williams, *Chem. Mater.*, 2006, **18**, 2327–2334.
41. E. Boisselier, L. Salmon, J. Ruiz, and D. Astruc, *Chem. Commun.*, 2008, 5788–5790.
42. J. L. Brennan, N. S. Hatzakis, T. R. Tshikhudo, V. Razumas, S. Patkar, J. Vind, A. Svendsen, R. J. M. Nolte, A. E. Rowan, and M. Brust, *Bioconjugate Chem.*, 2006, **17**, 1373–1375.
43. M. Fischler, A. Sologubenko, J. Mayer, G. Clever, G. Burley, J. Gierlich, T. Carell, and U. Simon, *Chem. Commun.*, 2007, 169–171.
44. T. Zhang, Y. Wu, X. Pan, Z. Zheng, X. Ding, and Y. Peng, *Eur. Polym. J.*, 2009, **45**, 1625–1633.
45. T. Zhang, Z. Zheng, X. Ding, and Y. Peng, *Macromol. Rapid Commun.*, 2008, **29**, 1716–1720.

46. E. C. Dreaden, B. E. Gryder, L. A. Austin, B. A. Tene Defo, S. C. Hayden, M. Pi, L. D. Quarles, A. K. Oyelere, and M. A. El-Sayed, *Bioconjugate Chem.*, 2012, **23**, 1507–1512.
47. N. Gandra and S. Singamaneni, *Chem. Commun.*, 2012, **48**, 11540–11542.
48. E. Locatelli, G. Ori, M. Fournelle, R. Lemor, M. Montorsi, and M. Comes Franchini, *Chemistry*, 2011, **17**, 9052–9056.
49. T. Vo-Dinh, H.-N. Wang, and J. Scaffidi, *J. Biophotonics*, 2010, **3**, 89–102.
50. D. M. Beal and L. H. Jones, *Angew. Chem. Int. Ed.*, 2012, **51**, 6320–6326.
51. R. Jin, G. Wu, Z. Li, C. A. Mirkin, and G. C. Schatz, *J. Am. Chem. Soc.*, 2003, **125**, 1643–1654.
52. Z. Lin, S. Gao, J. Lin, W. Lin, S. Qiu, L. Guo, B. Qiu, and G. Chen, *Anal. Methods*, 2012, **4**, 612–615.
53. C. Hua, W. H. Zhang, S. R. M. D. Almeida, S. Ciampi, D. Gloria, G. Liu, J. B. Harper, and J. J. Gooding, *Analyst*, 2011, **137**, 82–86.
54. X. Xu, W. L. Daniel, W. Wei, and C. A. Mirkin, *Small*, 2010, **6**, 623–626.
55. Q. Shen, W. Li, S. Tang, Y. Hu, Z. Nie, Y. Huang, and S. Yao, *Biosens. Bioelectron.*, 2013, **41**, 663–668.
56. H. Li, Q. Zheng, and C. Han, *Analyst*, 2010, **135**, 1360–1364.
57. Y. Zhang, B. Li, and C. Xu, *Analyst*, 2010, **135**, 1579–1584.
58. K. Zhu, Y. Zhang, S. He, W. Chen, J. Shen, Z. Wang, and X. Jiang, *Anal. Chem.*, 2012, **84**, 4267–4270.
59. G. Fu, W. Chen, X. Yue, and X. Jiang, *Talanta*, 2013, **103**, 110–115.
60. J. P. Hermes, F. Sander, U. Fluch, T. Peterle, D. Thompson, R. Urbani, T. Pfohl, and M. Mayor, *J. Am. Chem. Soc.*, 2012.

4 Conclusion and Outlook

Model compounds were synthesized and assembled on Au 111 surfaces to analyze their ability to stabilize Au NPs. It was shown that thioether oligomers suitable to stabilize gold nano particles can assemble on gold surfaces. The results of the SAM forming properties on gold surfaces of the analyzed compounds may lead to a more stable ligand design. The investigations showed the superior binding of a free thiol over thioethers to gold resulting in only thiolate anchored SAMs. Adding masked thiol groups to an Au NP stabilizing ligand that can be liberated after the NP formation by reducing the gold salt with $NaBH_4$, could result more stable ligand-Au NP junction. The resulting higher tolerance to higher temperatures and harsher processing steps would be very welcome.

The final prove of the supposed pyridine-gold interaction by investigating a set of model compounds helped the fundamental understanding of the superior properties of pyridine ligand derivatives over benzene ones. Of additional interest is the bidentate binding concept to generate a higher stability by more binding sites for future single molecular applications.

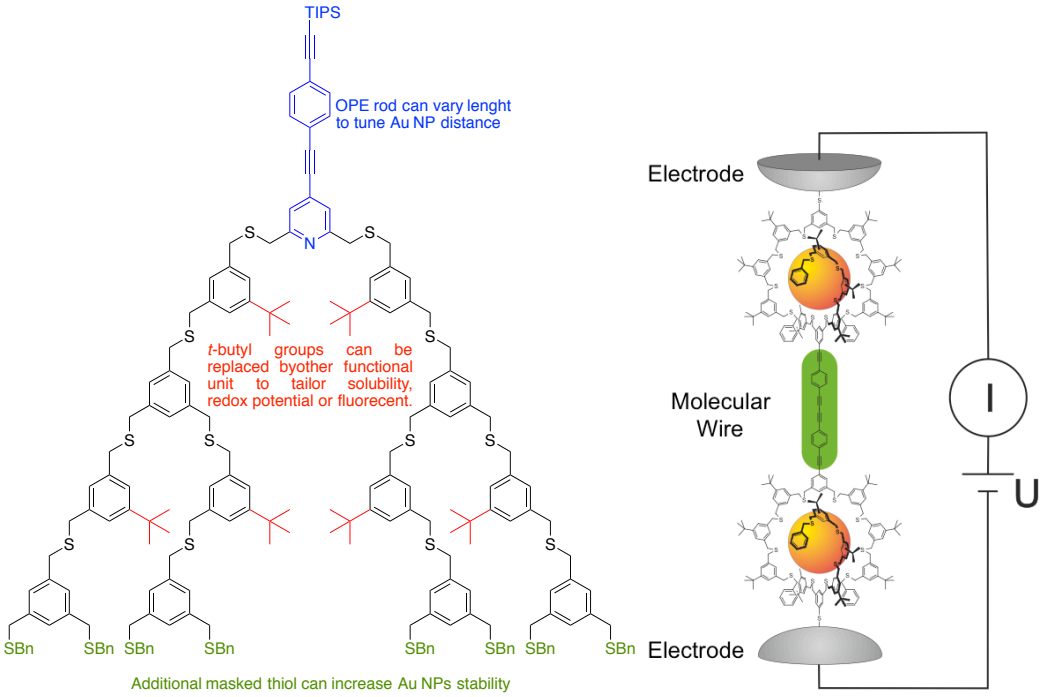

Figure 28. Left schematic drawing of ligand **G2** with color tagged moieties that can be varied for a tailored organic shell for future applications; right possible assembly of Au NPs as single molecular contact.

Gold Nanoparticles stabilized by one dendritic thioether ligand with a OPE rod as functional unit were used to perform azide acetylene click chemistry. Linker molecules with two, three and four azide moieties led to the formation of dimers, trimers and tetramers,

which could be visualized by TEM. Due to the rigid design of the OPE and the linker molecules the spatial arrangement could be controlled. The monofuctional NPs demonstrated a variety of potential utilizations. By clicking them to other compounds they can be used as TEM label to visualize for example carbon nanotubes or for sensing applications making nano scale concentrations visible to the naked eye. Also the assembly in 2D- and 3D-networks depending of the geometry of the linking molecule are possible. With these results of the synthesis, functionalization and further interlinking of the described Au NPs our research group created a basic developer kit.

Further research can open access to many more applications. By exchanging the *t*-butyl groups with other sterical demanding and functional units the NP's properties can be tuned in means of solubility, redox activity, fluorescence, bio capability or additional functional moieties for further coupling reactions.

Curriculum Vitae – Fabian Sander

Personal Data: Born: September 1st, 1982, Ulm, Germany

Adress (Privat): Zweerdeneiland 33

9766 VA, Eelderwolde, Nederland

Phone: +31 (0) 63 3351604

e-Mail: fbnsndr@gmail.com

Work Experience:

Since 12/2013	Development Scientist at Foseco Nederland B. V. (Enschede)
5/2013 – 11/2013	Research Chemist at Syncom B. V. (Groningen)

Education:

2/2009 – 3/2013	Dissertation in Organic Chemistry; *"From Self Assembled Monolayers to Clickable Gold Nanoparticles"* Advisor: Prof. Dr. Marcel Mayor; University of Basel graded *"magna cum laude"*
11/2008	Diploma in Chemistry at University of Stuttgart with the grade 1.9 (very good)
4/2008 – 10/2008	Diploma thesis 1.3 (excellent); advisor: Prof. Dr. Sabine Laschat; University of Stuttgart: "*Synthesis of Asymmetric Discotic Liquid Crystals with Amide Groups"*
10/2003 – 4/2007	Diploma study at the University of Stuttgart
1993 – 2002	German Abitur, Kolleg der Schulbrüder Illertissen, Germany

Publications:

"*Loops versus Stems: Benzylic Sulfide Oligomers Forming Carpet Type Monolayers"* F. Sander, T. Peterle, N. Ballav, F. Wrochem, M. Zharnikov, M. Mayor *J. Phys. Chem. C*, **2010**, *114*, 4118

"Direct Control of the Spatial Arrangement of Gold Nanoparticles in Organic–Inorganic Hybrid Superstructures" J. P. Hermes, F. Sander, T. Peterle, C. Cioffi, P. Ringler, T. Pfohl, M. Mayor *Small* **2011**, *7*, 920.

"*From ligand-stabilized gold nanoparticles to hybrid organic-inorganic superstructures"* J. P. Hermes, F. Sander, M. Mayor *Chimia*, **2011**, *65*, 219.

"Wedge-shaped 1,2-diamidobenzenes forming columnar mesophases via hydrogen bonding" F. Sander, S. Tussetschläger, S. Sauer, M. Kaller, K. V. Axenov, S. Laschat *Liquid Crystals* **2012**, *39*, 303.

"*Gold Nanoparticles Stabilized by Thioether Dendrimers"* J. P. Hermes, F. Sander, T. Peterle, R. Urbani, T. Pfohl, D. Thompson, M. Mayor *Chem. Eur. J.* **2011**, *17*, 13473.

"Optically switchable organic field-effect transistors based on photoresponsive gold nanoparticles blended with poly(3-hexylthiophene)" C. Raimondo , N. Crivillers , F. Reinders , F. Sander , M. Mayor , P. Samori PNAS **2012,** *109***,** 12375**.**

"*Monofunctionalized Gold Nanoparticles stabilized by a Single Dendrimer form Dumbbell Structures upon Homo-coupling"* J. P. Hermes, F. Sander, U. Fluch, T. Peterle, D. Thompson, R. Urbani, T. Pfohl, M. Mayor *JACS* **2012**, *134*, 14674.

"*Add a Third Hook: S-Acetyl Protected Oligophenylene Pyridine Dithiols as Advanced Precursors for Self-Assembled Monolayers*" F. Sander, J. P. Hermes, M. Mayor, H. Hamoudi, M. Zharnikov PCCP, **2013**, *15*, 2836.

"Dumbbells, Trikes and Quads – Organic/Inorganic Hybrid Nanoarchitectures Based on "Clicked" Gold Nanoparticles" F. Sander, U. Fluch, J. P. Hermes, M.Mayor Small, **2014**, *10*, 349.

Poster Presentations:

3/2009	Oligomer thioether ligands for better control of functionalization of gold nanoparticles
8/2009	Optimization of gold nanoparticle stabilizing ligands
1/2010	Loops versus Stems: Benzylic Sulfide Oligomers Forming Carpet Type Monolayers
8/2011	Controlled Synthesis of Organic – Inorganic Hybrid Structures
9/2011	Gold Nanoparticles - Novel Building Blocks for Molecular Electronics

Relevant Experiences:

6/2012 – 7/2012	Teaching assistant: introductory organic chemistry course for pharmacist (4 week block course)
9/2010 – 12/2010	Teaching assistant: advanced organic chemistry course (1 semester),
2/2010 – 7/2010	Teaching assistant: introductory organic chemistry course (1 semester)
2005 – 2007	Member of the executive board of the GDCh Jungchemikerforum Stuttgart (regional youth association of the GDCh)
2005 – 2006	Teaching assistant: introduction inorganic chemistry of engineers (2 semesters)
9/2002 – 4/2003	Civilian Service: Caritas Centrum Illertissen

Analytical Skills:	IR, UV/Vis, Mass Spectroscopy (EI, ESI, MALDI-TOF), LC/MS, Liquid Chromatography (HPLC, GPC), Gas Chromatography, GC-MS, NMR, Transmitting Electron Microscopy, Scanning Tunneling Microscopy, X-Ray Photoelectron Spectroscopy, Near Angle X-Ray Absorption Fine Structure Spectroscopy, Small and Wide Angle X-Ray Scattering, Thermogravimetric Analysis, Elemental Analysis, Differential Scanning Calorimetry, Polarization Microscopy, Dynamic Light Scattering, Cyclic Voltammetry.
PC Skills:	Windows, MS Office, OS X, iWorks, ChemOffice, Scifinder, Reaxys, Linux, Apache Server, Windows Server.
Languages:	German: native speaker; English: fluent spoken and written; Dutch: basic knowledge.
Interests:	Sailing, Guitar and Bass Guitar, Photography
Affiliation:	Gesellschaft Deutscher Chemiker (GDCh), Swiss Chemical Society (SCS)